THE UNIVERSITY OF CALGARY

Computer Simulation of Rhythm-Generating Neuronal Networks

by

Eugene Igras

A THESIS

SUBMITTED TO THE FACULTY OF GRADUATE STUDIES

IN PARTIAL FULFILLMENT OF THE REQUIREMENTS FOR THE

DEGREE OF MASTER OF SCIENCE

DEPARTMENT OF NEUROSCIENCE

CALGARY, ALBERTA

SEPTEMBER, 1999

Abstract

Despite the diversity of repetitive or rhythmic activities in different species, the neuronal control of these activities appears to rely on some general organizational and functional principles. Furthermore, a small number of neuronal mechanisms involved in the generation of rhythmic output have been identified. These building blocks, when linked together, are thought to generate complex patterns. This research focuses on the development of theoretical and computational models of the building blocks and the study of the dynamics of the elementary rhythm-generating networks. Four classes of network architectures capable of generating rhythmic output, along with models of the underlying cellular and synaptic mechanisms, were implemented. The interactions between network, synaptic and membrane properties were investigated, and their contribution to the characteristics of rhythmic output were studied. The necessity of cellular and synaptic building block candidates, and the sensitivity of model output to changes in model variables, were investigated.

Acknowledgements

Throughout the past three years during my M.Sc. studies I have received limitless support and assistance from those I wish to thank below. I would like to thank Dr. M. Hulliger for providing an intellectually stimulating environment and for his guidance. I am grateful for the effort and support to my supervisory committee Drs. R. French, S. Lukasiewicz, and D.A. Syme. A large note of gratitude is forwarded to Drs. J. Foweraker and A. Ware for taking the time to review and provide helpful comments about the results of simulation experiments. I would also like to express my appreciation to Drs. A. Bulloch and R.W. Turner for their encouragement and direction. I would like to thank Christopher, my son-in-law, for helpful suggestions and stimulating discussions and to my grandchildren, Alexander and Monica, for being grandchildren. Above all, I would like to thank my wife Wanda and my children Dorothy and Darius for their endless support, encouragement and devoted love for which I am deeply indebted.

To my Wife.

To my Children.

To my Mother.

In memory of my Father.

Table of Contents

List of Figures

List of Tables

List of Abbreviations and Symbols

Symbol	Description	Units
AP	Action potential	mV
AP/B	Number of action potentials per burst	
BF	Burst frequency	1/sec
BFR	Burst frequency rate	1/sec
c_m	Specific membrane capacitance per unit length	μF/cm
C	Total capacitance	nF
C_m	Specific membrane capacitance	$\mu F/cm^2$
$[ion]_i$	Concentration of free intracellular ions (ion=Na^+, K^+, Ca^{2+})	μM
d	Diameter	μm
E_{ion}	Ionic reversal potential (ion=Na, K, Ca)	mV
EPSP	Excitatory postsynaptic potential	mV
g_{ion}	Ionic conductance (ion=Na, K, Ca)	nS
g_{pas}	Passive (leak) conductance	nS
g_{syn}	Maximal synaptic conductance	nS
$\bar{g}_{current}$	The maximum specific ionic conductance (current=Na, K, A, M, AHP, T, etc.). This notation is used in mathematical equations included in this thesis.	S/cm^2
gmax_ icurrent	Equivalent notation for the maximum specific ionic conductance used in the NEURON software (current=Na, K, A, M, AHP, T, etc.).	mho/cm^2 = S/cm^2
h(t)	Inactivation variable	
$h_\infty(V)$	Steady-state inactivation variable	

I_{ion}	Ionic current (ion=Na, K, Ca)	nA/cm^2
IPSP	Inhibitory postsynaptic potential	mV
L	Length	μm
m(t)	Activation variable	
$m_\infty(V)$	Steady-state activation variable	
n(t)	Activation variable	
$n_\infty(V)$	Steady-state activation variable	
PSP	Postsynaptic potential	mV
r_a	Intracellular resistance per unit length	Ω/cm
r_m	Specific membrane resistance per unit length	Ω·cm
R_∞	Input resistance in a semi-finite cable	MΩ
R_i	Intracellular resistance	$\Omega \cdot cm^2$
R_{in}	Input resistance	MΩ
SC	Stimulation current	nA
t	Time	msec
V(x, t)	Transmembrane potential relative to V_{rest}	mV
$V_m(x, t)$	Absolute transmembrane potential	mV
V_{rest}	Resting potential	mV
x	Position	μm

1 INTRODUCTION

In the nervous system rhythm-generating networks are a phenomenon of fundamental importance. They are thought to control repetitive or rhythmic activities (such as walking, running, swimming, chewing, digesting, flying, scratching, breathing, and pumping blood) and play an important part in cortical sensory processing. This research focuses on the rhythm-generating or oscillatory neuronal networks. It is based on the notion that different forms of rhythm-generating networks rely on some general principles of neuronal organization. Furthermore, only a relatively small number of rhythm generation mechanisms are thought to exist. It is thought that these 'building block' mechanisms can be linked together in different combinations to generate complex patterns of rhythmic output.

Experimental studies of the neuronal organization of rhythm-generating networks involved in locomotion in invertebrates (such as the marine mollusk *Tritonia*) and vertebrates (such as the *lamprey* and the frog *Xenopus*) have proven that these networks are complex and the research is laborious and time consuming. Similarly detailed studies of these networks in the complex mammalian nervous system are beyond the reach of current experimental techniques. Little is known about the localization and specific characteristics of the neurons and interconnections making up such systems. As a result of these difficulties, researchers have resorted to using modeling and computer simulation techniques to learn the possible functional organization of these networks. In the case of

relatively simple nervous systems, computer-based models have proven to be an invaluable neurophysiological tool and created new possibilities in understanding intricate networks involved in the generation of locomotion. However, for the more complex mammalian nervous systems only a few detailed modeling studies have so far been carried out. To understand how the rhythm-generating networks operate, and therefore how they might fail due to disease or injury, requires knowledge of the principles of network organization and function, and how these principles are implemented by cells and synapses.

1.1 Previous Work in Rhythm-Generating Networks

The study of rhythmic movements has provided significant insight into rhythm-generating circuits. In almost all species studied to date, these movements can be generated, in the absence of afferent inputs, by neuronal networks called central pattern generators (CPGs). Because these networks generate measurable outputs, they serve as excellent model systems not only for understanding the neural basis of behaviour in general, but also for understanding the principles of network function within the nervous system.

Early investigations of rhythmic locomotion were aimed at demonstrating experimentally that these circuits exist, that is, that simple rhythmic behaviour can be generated entirely within the central nervous system. In 1914 Graham Brown demonstrated that spinal animals are capable of rhythmic stepping after transection of their spinal cord, indicating

that spinal circuits alone generate sustained rhythmic output, without requiring rhythmic input from supraspinal structures. He further proposed that a half-center organization of neurons in the spinal cord could account for the rhythmic stepping.

Subsequent research attempted to understand the neuronal organization and underlying mechanisms of CPGs. Early successes in the experimental studies of CPGs in invertebrates and lower vertebrates raised expectations in terms of understanding their organization and computational principles of their operation. Studies of the marine mollusc *Tritonia* (Getting, 1981-1983), the lobster stomatogastric ganglion (Rowat and Selverston, 1993), and the heart of the leech (Calabrese and Schutter, 1992; Hooper, 1995) revealed complex connectivity of the CPG networks. It was hoped that knowledge of the connectivity would explain how these neuronal networks operate, and that for each neuronal function there would be a limited number of ways to implement the function in neuronal circuitry. It was also hoped that similar functions might be provided by similar neuronal networks. The lessons learned from these initial studies in invertebrates were quite surprising. They showed that the neuronal networks involved in the generation of locomotion patterns were complex and diverse, with multiple levels of feed-forward and feedback pathways embedded in complicated arrays of connections and cells (Grillner, 1981; Getting, 1983). They also showed that networks with similar connectivity can produce dramatically different activity patterns and, conversely, similar activity patterns can be produced by dramatically different neuronal networks. Furthermore, it was

demonstrated that knowledge of connectivity alone does not explain the operation and capabilities of neuronal networks (Getting, 1988).

The lamprey has successfully been used in studies of vertebrate CPGs. These organisms propel themselves through water by a sequence of rhythmic body undulations caused by travelling waves of contractions that progress down the axial muscles from head to tail. Their swimming patterns have led to the development of models of locomotion composed of coupled oscillators. These models represent the oscillatory networks that occur in segments along the spinal cord and control the sequence of muscle contractions along the body during locomotion (Grillner et al., 1988 and 1991; Cohen et al., 1992; Wallen et al., 1992).

A substantial body of knowledge has been accumulated about the structure and function of spinal neuronal circuits in mammals. The notion that neuronal networks in the spinal cord play an essential role in locomotion generation and coordination has been widely accepted in neuroscience. Experiments conducted by Grillner and his coworkers provided evidence that CPG circuits in mammals are located in the spinal cord. During these experiments on cats, the thoracic part of the spinal cord was transected, isolating the part of the spinal cord that controls the hindlimbs from descending signals. Under these conditions the cat was able to walk with a near normal stepping pattern confirming that the CPGs are located in the spinal cord (Grillner, 1981). However, complexity of the spinal neuronal circuitry in mammals has caused practical difficulties in identifying the

component neurons, in mapping the synaptic connectivity within the circuit comprehensively, and in measuring the intrinsic membrane properties of functionally identified neurons in the mammalian CPGs. As a result, little is known about the specific localization and characteristics of the neurons and networks making up such systems. The CPG for mammalian locomotion is most likely distributed among a large population of neurons.

Studies of the oscillatory networks involved in information transmission in the thalamus conducted in the last two decades revealed additional details of the rhythm-generating networks. With the exception of olfaction, all sensory systems access cortex by projecting through the thalamus. The ability of the thalamus to relay information to the cortex is controlled by specialized neuronal circuitry – the relay cells. Rhythm-generating properties of the relay cells strongly influence the nature of the thalamic relay (Sherman and Koch, 1998).

1.2 Building Blocks

Studies of locomotion have led to the definition of requirements for a CPG to produce self-sustaining oscillations i.e., rhythmic activity not requiring phasic external input. These requirements are *action reversal* and *time delay*. Action reversal occurs when one type of action is followed by its antagonistic action. Thus, excitation of a neuron within a CPG must be followed by inhibition of the same neuron, and likewise, inhibition must

lead to excitation. There also must be a delay between an initial action and its antagonist. It allows one process (excitation or inhibition) to be expressed before the onset of the opposite process. These studies have also led to more generalized theoretical research that is focused on understanding how the neurons in a CPG interact and influence one another, how the underlying circuitry of the network produces the collective behaviour, and what mechanisms allow the network to switch between various patterns of activity. The hope has been that, by analyzing the CPGs for different rhythmic systems, a relatively small number of mechanisms for pattern generation would emerge. If, during evolution, these mechanisms were conserved from species to species or behaviour to behaviour, then perhaps similar mechanisms would be involved in the generation of rhythmic motor responses in more complex systems such as those of the mammals.

This approach led to the development of the concept of common pool of 'building block' mechanisms linked together in different combinations. Each combination could generate a different pattern thereby explaining the diversity of rhythmic behaviour (Getting, 1989). It has proven convenient to divide the building block mechanisms into three categories:

a) *network*, describing the assembly of cells and synapses into neuronal circuits,

b) *cellular*, associated with properties intrinsic of single cells, and

c) *synaptic*, governing the action of single synapses.

The ability of a CPG to generate rhythmic activity arises from the specific building block mechanisms used, and the manner in which they are assembled and interact. Thus,

network operation depends upon the "cooperative interactions" among multiple network, synaptic, and cellular properties. Calling these properties 'building blocks' does not imply that all CPGs can be either constructed from, or reduced to, several schemes. Nor should it be interpreted that network function can be considered as the simple summation of the action of these components. The properties of these elementary circuits may be modified when embedded in larger networks. Further, large networks may display properties not found in smaller ones. These 'building blocks' are, however, commonly encountered and appear to form a basis for network function in many diverse CPG systems.

1.2.1 Network Properties

Certain patterns of connectivity between neurons have been recognized as potentially important for the generation of rhythmic behaviour (Getting, 1989).

Reciprocal Inhibition. A network formed by two or three neurons that inhibit each other (Figure 1.1).

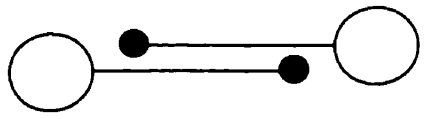

Figure 1.1. A model of the reciprocal inhibition network.

This network was proposed by Brown to explain the generation of walking in mammals. The two-neuron reciprocal inhibition network has also been proposed as the basis for the

up-and-down movements of locust wings during flight (Wilson and Waldron, 1968), the chewing movements in the lobster stomach (Rowat and Selverston, 1993), and the swimming movements of the mollusc *Tritonia* (Getting, 1983) and the lamprey (Grillner, 1993).

Feedback Inhibition. A network formed by two neurons where one neuron excites a second neuron, which then inhibits the first neuron (Figure 1.2).

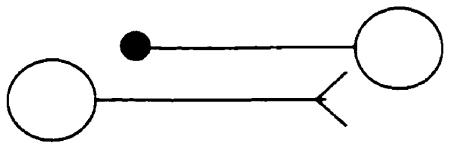

Figure 1.2. A model of the feedback inhibition network.

This network has been proposed to explain the generation of the mammalian respiratory rhythm by groups of neurons in the medulla (Wyman, 1977).

Mutual Excitation. A network formed by two neurons that excite each other (Figure 1.3).

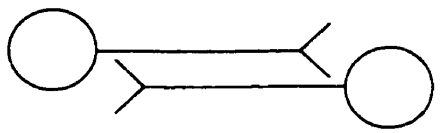

Figure 1.3. A model of the mutual excitation network.

The mutual excitation network has been implicated in the swimming movements of the mollusc *Tritonia* (Getting, 1983) and the lamprey (Grillner, 1993).

Parallel Excitation and Inhibition. In this network configuration, a single postsynaptic cell is both excited and inhibited by separate pathways (Figure 1.4).

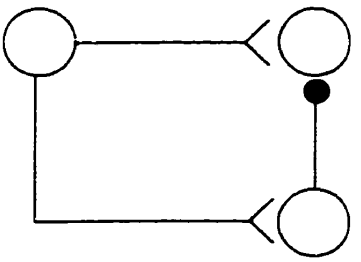

Figure 1.4. A Model of the parallel excitation and inhibition network.

The parallel excitation and inhibition network is thought to be implicated in the production of the swimming movements in the mollusc *Tritonia* (Getting, 1983).

1.2.2 Cellular Properties

There is an extensive list of ionic currents that have been discovered experimentally in neurons of rhythm-generating networks (Berridge and Rapp, 1979; Bargas, 1995). Different combinations of these currents endow the neuronal cells with different sets of neural properties. Some important cellular properties that contribute to rhythm generation are: 1) *Threshold*, which determines the level of excitation needed for a neuron to initiate an action potential (Getting, 1983). 2) *F-I relationship* between firing rate F and input current I determines the gain characteristics of neurons (Hopfield and Tank, 1986). 3) *Spike-frequency adaptation* - the F-I relationship is not fixed but may undergo a variety of modifications depending on the recent firing history of the neuron. This property is manifested as a decrease in action potential frequency during a maintained input. 4)

Postburst hyperpolarization, which is manifested as a transient hyperpolarization and cessation of firing for a period of time following a burst of spikes, ranging from milliseconds to seconds, depending upon the strength and duration of the preceding burst. The underlying neural mechanisms seem to be similar to those responsible for spike frequency adaptation. Both characteristics are usually found together (Hume and Getting, 1982b); 5) *Delayed excitation*, which is manifested as a delay between the onset of a depolarizing stimulus and the first spike. The delay may range from hundreds of milliseconds in mammalian neurons (Dekin and Getting, 1984) to several seconds in molluscan neurons (Getting, 1983). 6) *Postinhibitory Rebound*, which is in the inverse of the postburst hyperpolarization, and is expressed as a transient depolarization (excitation) following hyperpolarization (inhibition). If the depolarization exceeds threshold, the cell may fire a burst of spikes (Satterlie, 1985). 7) *Plateau Potentials*, where neurons have two membrane potential states: a resting state and a depolarized state (Russel and Hartline, 1978). Small or transient depolarization can cause transition from the resting state to the depolarized state, where the potential may remain for considerable lengths of time (tens to hundreds of milliseconds) before it either spontaneously reverts or is converted by a short hyperpolarizing input back to the resting state. This characteristic provides a mechanism for translating a transient input into sustained firing (Russel and Hartline, 1978; Dickinson and Nagy, 1983; Dickinson, 1995; Marder, 1993). 8) *Endogenous and conditional bursting*, which is characterized by the ability to produce recurrent bursts in the absence of any synaptic actions from other neurons (Alving, 1968).

Conditional burster neurons express bursting properties only upon synaptic activation (Miller and Selverston, 1982).

1.2.3 Synaptic Properties

Neurons are interconnected via synapses and thus subjected to a variety of influences from other neurons. The nature and properties of these synaptic interactions play an important role in determining how neurons respond and impact network operation. Synaptic properties that impact directly network performance are: 1) *Nature of synaptic mechanism*, which fall into two broad categories: electrical and chemical. Within each category, however, a wide diversity of processes have been described, including both rectifying and nonrectifying (bi-directional) electrical synapses, as well as conductance-depended chemical synapses. All of these properties influence not only the characteristics of each postsynaptic potential (PSP) but also how the PSPs from different sources interact (Pinsker and Willis, 1980). 2) *Sign, strength, and time course.* Synapses are either excitatory (positive) or inhibitory (negative). Time course plays an important role in network operation. It is particularly important in determining summation properties of a neuron. Also included under temporal properties are characteristics such as facilitation, depression, and potentiation that modulate the strength of connections in a history dependent manner (Hume and Getting, 1982a and 1982b; Getting, 1983; Katz et al., 1994). 3) *Transmitter release*, which has a profound influence upon the nature of the information being conveyed at a particular synaptic connection (Graubard et al., 1983). 4) *Multicomponent synaptic potential* - a synapse may produce multiple effects on a single

postsynaptic neuron, which can lead to numerous interesting integrative properties. The mechanism for producing multiple actions appears to reside in the interaction of a single transmitter substance with multiple postsynaptic receptors with different time constants. This introduces the temporal order of action as well as the relative amplitude and time course of each component to the set of parameters. Such multi-action synapses have so far been identified only in invertebrates (Hume and Getting, 1982a and 1982b; Getting, 1983).

1.3 Research Objectives

The main objective of this research is the development of theoretical and computational models of elementary rhythm-generating or oscillatory networks and the study of the dynamics of these networks at the cellular and synaptic levels. Questions of interest include the following: a) What cellular and synaptic mechanisms are involved in the generation of rhythmic output? b) Does the oscillatory behaviour arise from the oscillatory behaviour of a single cell that drives other cells to fire at different phases relative to this master cell, or does it arise as a network effect from the mutual interaction of multiple cells none of which can individually oscillate, or does it arise from some combination of these two mechanisms? c) Is there just one or are there several mechanisms that may give rise to oscillations of the network? d) What is the minimum set of 'building blocks' required for the generation of oscillatory behaviour? e) How sensitive is model output to changes in model variables?

The specific objectives are:

1. Definition and identification of cellular and synaptic properties of four elementary rhythm-generating networks that are required for the generation of rhythmic output.

2. Development of computer models of the 'building blocks'. The intention is to use these models in conducting simulation experiments and exploration of the dynamics of the elementary rhythm generating networks.

3. Investigation of the processing capabilities of various 'building blocks' and their combinations and assessment of how the building block properties contribute to the generation of rhythmic output in the oscillatory networks.

4. Conducting sensitivity analyses to explore the sensitivity of model output to changes in model parameters.

Given the fact that the present experimental knowledge of complex neuronal networks (especially mammalian) is limited, it is not expected that computer network simulations undertaken in this research could deliver a unique solution. Instead, they should help identify general classes of solutions.

1.4 Thesis Outline

CHAPTER 2 presents the description of the mathematical formalism (i.e., the extended Hodgkin-Huxley equations) and its implementation in the NEURON simulation system used in this research. The extended Hodgkin-Huxley equations have been used to model

active and passive cellular properties, synaptic receptors, and the elementary neuronal networks listed in 2.3.1.

CHAPTER 3 describes the mathematical models of the 'building blocks' at the cellular and synaptic levels and their implementation in NEURON. The list includes the models of sodium, potassium, and calcium channels, and excitatory and inhibitory synapses. It also presents the results of computer simulations of cellular and synaptic properties with the use of these models.

CHAPTER 4 uses the mathematical models of ionic channels and synaptic receptors in the development of the elementary rhythm-generating networks. It examines the results of computer simulations and sensitivity analyses of these networks.

Finally, CHAPTER 5 presents a research summary and concluding remarks, including ideas for future research directions.

2 METHODS

Electrical signals in excitable cells are transmitted in two ways: the passive spread of graded potentials and the propagation of all-or-none action potentials. Graded potentials are carried by ions that diffuse down their electrochemical gradients via time- and voltage-independent conductances and the magnitude of the signals varies with the ionic currents. Action potentials, on the other hand, are carried by voltage- and time-dependent conductances. Studies of the ionic mechanisms underlying the initiation and propagation of action potentials in the squid giant axon conducted by Hodgkin and Huxley led to the development of a quantitative model of the membrane of the squid axon. The basis of the model is a fast sodium current I_{Na} and a delayed potassium current I_K. The Hodgkin-Huxley formalism represents the cornerstone of quantitative models of nerve cell excitability and it is described in Section 2.1. The Hodgkin-Huxley model, however, does not capture a number of important biophysical phenomena in nervous cells, such as adaptation of the firing frequency to long-lasting stimuli or the transmission of electrical signals between neurons. Over the last few decades, dozens membrane conductances have been characterized. They differ in principal carrier, voltage, and time dependence, dependence on the presence of intracellular calcium and on their susceptibility to modulation by synaptic input and second messengers. Also, significant progress has been achieved in the understanding of properties of synaptic receptors and the mechanisms involved in the transmission of signals between neurons. The classical Hodgkin-Huxley

model has been extended to accommodate other ionic channels and synaptic mechanisms. The extended Hodgkin-Huxley model is described in Section 2.2.

2.1 The Hodgkin Huxley Model of Action Potential Generation

Studies of the ionic mechanisms underlying the initiation and propagation of action potentials in the squid giant axon conducted by Hodgkin and Huxley led to the development of a quantitative model of the membrane of the squid axon. According to the model, the electrical properties of a membrane patch can be represented as an equivalent circuit presented in Figure 2.1.

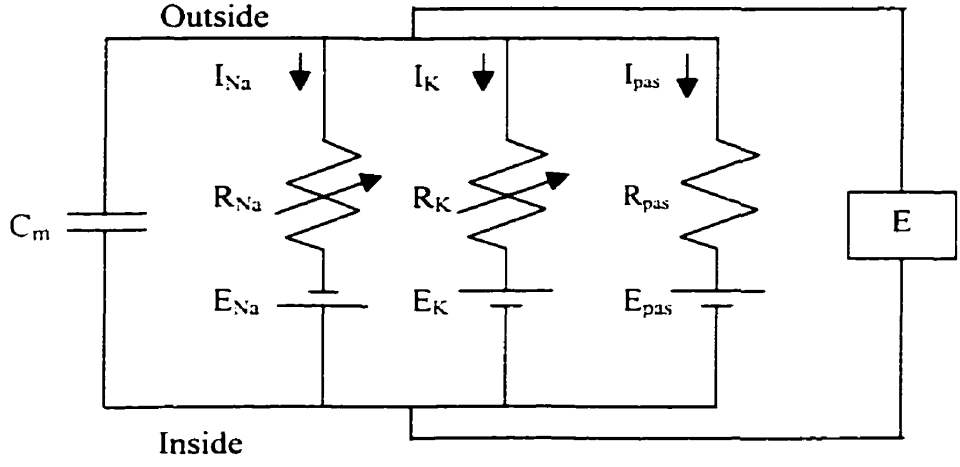

Figure 2.1. Electrical circuit representing membrane of squid giant axon. $R_{Na} = 1/g_{Na}$; $R_K = 1/g_K$; $R_{pas} = 1/g_{pas}$. g_{Na} and g_K are voltage and time dependent, and other components are constant. Note that in the original paper, I_{pas}, R_{pas}, and E_{pas} were referred to as "leakage" variables and the inward ionic current was considered positive. Modern convention reverses this i.e., the outward ionic current is considered positive (adapted from Hodgkin and Huxley, 1952).

In the electrical circuit, current flow across the membrane has two major components, one associated with charging the membrane capacitance, C_m, and one associated with the movement of specific types of ions across the membrane. The ionic current is further subdivided into three distinct components, a sodium current, I_{Na}, a potassium current, I_K, and a small passive current, I_{pas}, made up of chloride and other ions. The behaviour of the electrical circuit is described by the following differential equation (Hodgkin and Huxley, 1952):

$$I_m = C_m \frac{dV}{dt} + I_{ion} \tag{2.1}$$

The total I_m membrane current is composed of the capacity current, $C_m\ dV/dt$, and the ionic current, I_{ion}, where C_m is the membrane capacity per unit area (assumed constant), and V is the displacement of the membrane potential from its resting value (depolarization negative). The ionic current, I_{ion}, is further subdivided into I_{Na}, I_K, and I_{pas} carried out by sodium, potassium, and other ions respectively:

$$I_{ion} = I_{Na} + I_K + I_{pas} \tag{2.2}$$

The individual ionic currents are linearly related to the driving potential via Ohm's law:

$$\begin{aligned} I_{Na} &= g_{Na}(E - E_{Na}) \\ I_K &= g_K(E - E_K) \\ I_{pas} &= g_{pas}(E - E_{pas}) \end{aligned} \tag{2.3}$$

where E is the membrane potential, g_{Na}, g_K, and g_{pas} are the sodium, potassium, and passive conductances, E_{Na} and E_K are the equilibrium potentials for the sodium and potassium ions respectively, and E_{pas} is the equilibrium potential for the passive current

due to chloride and other ions. For the practical applications it is convenient to write the equations in the form:

$$\begin{aligned} I_{Na} &= g_{Na}(V - V_{Na}) \\ I_K &= g_K(V - V_K) \\ I_{pas} &= g_{pas}(V - V_{pas}) \end{aligned} \tag{2.4}$$

where

$$\begin{aligned} V &= E - E_r \\ V_{Na} &= E_{Na} - E_r \\ V_K &= E_K - E_r \\ V_{pas} &= E_{pas} - E_r \end{aligned} \tag{2.5}$$

where E_r is the absolute value of the resting potential. V, V_{Na}, V_K, and V_{pas} can then be measured directly as displacements from the resting potential. Taking into account the above the total I_m membrane current can be expressed:

$$I_m = C_m \frac{dV}{dt} + g_{Na}(V - V_{Na}) + g_K(V - V_K) + g_{pas}(V - V_{pas}) \tag{2.6}$$

The g_{Na} and g_K ionic conductances are voltage and time dependent and are expressed as products of gating variables m, h, and n and maximum conductances $\bar{g}_{Na}$ and $\bar{g}_K$:

$$\begin{aligned} g_{Na}(V,t) &= m^3 h \bar{g}_{Na} \\ g_K(V,t) &= n^4 \bar{g}_K \end{aligned} \tag{2.7}$$

The gating variables m, h, and n are expressed:

$$\frac{dm}{dt} = \alpha_m(1-m) - \beta_m m \qquad m_\infty = \frac{\alpha_m}{\alpha_m + \beta_m} \qquad \tau_m = \frac{1}{\alpha_m + \beta_m} \tag{2.8}$$

$$\frac{dh}{dt} = \alpha_h(1-h) - \beta_h h \qquad h_\infty = \frac{\alpha_h}{\alpha_h + \beta_h} \qquad \tau_h = \frac{1}{\alpha_h + \beta_h} \tag{2.9}$$

$$\frac{dn}{dt} = \alpha_n(1-n) - \beta_n n \qquad n_\infty = \frac{\alpha_n}{\alpha_n + \beta_n} \qquad \tau_n = \frac{1}{\alpha_n + \beta_n} \tag{2.10}$$

Values of α_i and β_i ($i = m, h, n$) are expressed as follows:

$$\alpha_m = \frac{0.1(V+25)}{\exp\frac{V+25}{10} - 1} \qquad \beta_m = 4\exp(\frac{V}{18}) \tag{2.11}$$

$$\alpha_h = 0.07\exp(\frac{V}{20}) \qquad \beta_h = \frac{1}{\exp\frac{V+30}{10} + 1} \tag{2.12}$$

$$\alpha_n = \frac{0.01(V+10)}{\exp\frac{V+10}{10} - 1} \qquad \beta_n = 0.125\exp(\frac{V}{80}) \tag{2.13}$$

where α_i and β_i ($i = m, h, n$) are expressed in $msec^{-1}$ and V is in mV. The variables i_x ($i = m, h, n$) calculated by substituting Equations 2.11-2.13, to Equations 2.8–2.10 are called the steady-state activation/inactivation curves. They give the voltage range and slope of activation for voltage-gated channels.

2.2 The Extended Hodgkin-Huxley Model

The Hodgkin-Huxley (HH) model of the squid giant axon represented by the electrical circuit depicted in Figure 2.1 and described by the equations 2.1 through 2.13 has been extended to accommodate other cellular ionic channels and synaptic mechanisms. The electrical properties of this extended model can be represented as an equivalent circuit presented in Figure 2.2.

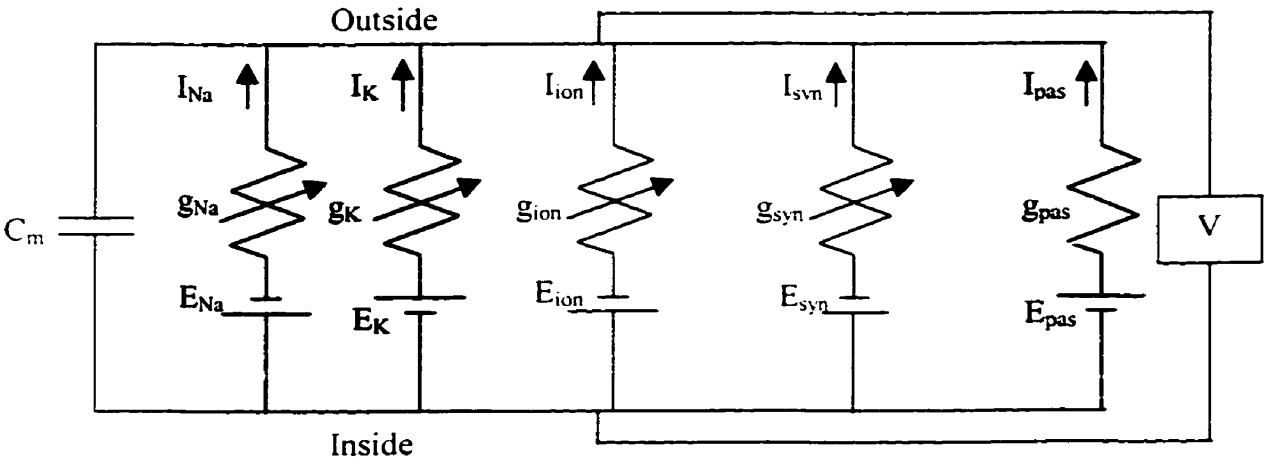

Figure 2.2. Equivalent circuit model of isopotential patch of nerve membrane that consists of several basic classes of transmembrane channels. The currents in the shaded areas represent the classical HH currents (active I_{Na} and I_K, and passive I_{pas}). The time- and voltage-dependent resistor g_{ion} in series with battery E_{ion} represent other active ionic currents I_{ion} ($ion = Ca^{2+}$, Ca^{2+}-dependent K^+, etc.). Synaptic chemically gated channels are represented by the time-varying $g_{syn}(t)$ which is in series with a battery E_{syn}, representing reversal potential of the synaptic process. Note that the outward ionic current is considered positive (adapted from Segev and Burke, 1998).

Passive membrane channels are electrically represented by a constant (time- and voltage-independent) transmembrane conductance g_{pas} in series with a fixed voltage source E_{pas} that designates the reversal potential of the passive (leakage) currents. The ionic current through this branch is assumed to obey Ohm's law and can be represented as

$$I_{pas} = g_{pas}(V - E_{pas}) \tag{2.14}$$

The active ionic currents I_{ion} (including I_{Na} and I_K) are electrically represented by a voltage- and time-dependent conductance g_{ion} in series with a voltage source E_{ion} and expressed by a general equation:

$$I_{ion} = g_{ion}(V - E_{ion}) \tag{2.15}$$

The g_{ion} ionic conductances are expressed as products of gating variables m, h, and n and the maximum conductance $\bar{g}_{ion}$

$$g_{ion} = \bar{g}_{ion} m^p h^q n^r \tag{2.16}$$

where $p, q, r = \{0, 1, 2, 3, 4\}$. The gating variables m and n represent activation state variables while h represents inactivation state variable. They vary between zero and one, and are described by differential equations:

$$\frac{d\eta}{dt} = \alpha_\eta(V)(1 - \eta) - \beta_\eta(V)\ \eta = \frac{\eta_\infty - \eta}{\tau_\eta} \tag{2.17}$$

where $\alpha_\eta(V)$ *and* $\beta_\eta(V)$ are the voltage-dependent opening and closing rates for the gating variables and

$$\eta_\infty = \frac{\alpha_\eta}{\alpha_\eta + \beta_\eta} \qquad \tau_\eta = \frac{1}{\alpha_\eta + \beta_\eta} \qquad \eta = (m, h, n) \tag{2.18}$$

Synaptic channels change their conductance to certain ions when the appropriate chemical stimulus binds to the receptor associated with these channels. Synaptic pathway is modeled as a conductive pathway g_{syn} in series with a constant voltage source E_{syn} which is the reversal potential of the ionic species involved. The synaptic current I_{syn} is expressed:

$$I_{syn} = g_{syn}(V - E_{syn}) \tag{2.19}$$

The conductive pathway g_{syn} is expressed differently for the different synaptic receptors leading to the following equations describing the synaptic currents (Destexhe et al., 1994b):

a) For AMPA and $GABA_A$ receptors

$$I_{AMPA} = \bar{g}_{AMPA}\, r\, (V - E_{AMPA}) \tag{2.20}$$

where $\bar{g}_{AMPA}$ is the maximal conductance of the AMPA receptor channel, V is a postsynaptic voltage, E_{AMPA} is the reversal potential, and r represents the probability that a synaptic receptor channel is in an open, conducting state and is described by the first-order kinetic equation:

$$\frac{dr}{dt} = \alpha\, [T](1 - r) - r\beta \tag{2.21}$$

where α and β are voltage-independent forward and backward rate constants and $[T]$ is the neurotransmitter concentration.

b) For NMDA receptors

$$I_{NMDA} = \bar{g}_{NMDA} M\, r\, (V - E_{NMDA}) \tag{2.22}$$

where $\bar{g}_{NMDA}$ is the maximial conductance, r is the fraction of receptors in the open state and described by Equation 2.21, V is the postsynaptic voltage, E_{NMDA} is the reversal potential, and M represents the voltage-dependent magnesium block expressed as follows:

$$M(V) = \frac{1}{1 + \frac{[Mg^{2+}]_o \exp(-aV)}{b}} \tag{2.23}$$

Here, $[Mg^{2+}]_o$ is the external magnesium concentration and constants a and b are determined experimentally.

c) For $GABA_B$ receptors

$$I_{GABAb} = \bar{g}_{GABAb} \frac{[GP]^n}{[GP]^n + K_D} (V - E_K) \tag{2.24}$$

where $\bar{g}_{GABAb}$ is the maximial conductance of potassium channels activated the G-proteins, $[GP]$ represents the concentration of G-protein, n is the number of binding sites, and K_D is the dissociation constant of the binding of G-protein on the K^+ channels.

The total membrane current through a patch of membrane that has all three types of ionic channels (i.e., passive, active, and synaptic) is the sum of all those currents plus the capacitive current:

$$I_m = C_m \frac{dV}{dt} + g_{pas}(V - E_{pas}) + \sum [g_{act}(V - E_{act})] + \sum [g_{syn}(V - E_{syn})] \tag{2.25}$$

The extended HH model represented by equation 2.25 has been used to model ionic conductances (i.e., passive, active) and synaptic properties.

2.3 Computer Modeling

Conservation of charge requires that the sum of currents flowing into any region from all sources (e.g., adjacent interior regions, transmembrane ionic fluxes, microelectrodes) must equal zero, i.e.,

$$\sum I_a - \int I_m \, dA = 0 \tag{2.26}$$

where the sum is over all the axial currents I_a (expressed in units of charge / time e.g., milliamperes) flowing into the region through cross-section boundaries, I_m is the transmembrane current density (mA/cm^2), and the integral is taken over the membrane area A of the region (Figure 2.3).

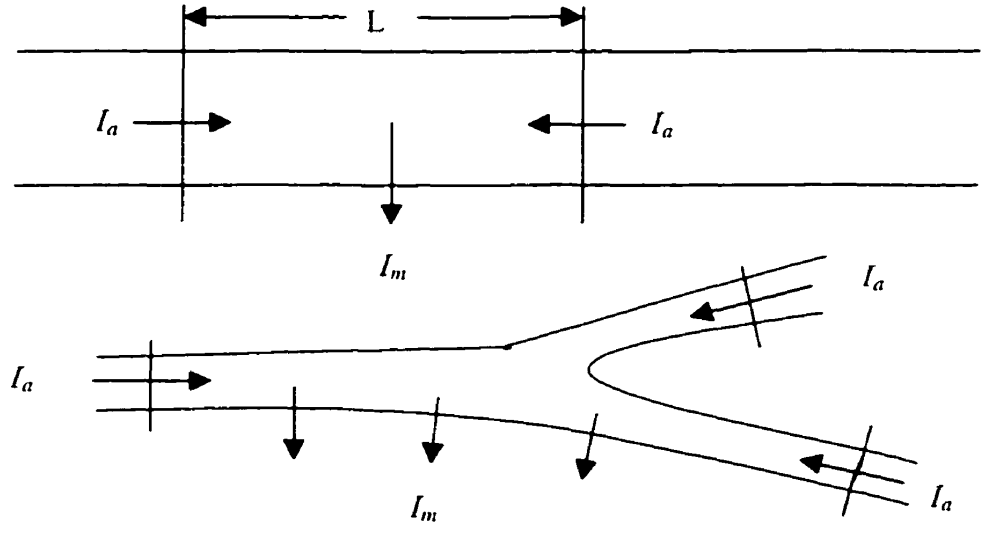

Figure 2.3. The net current entering a region must equal zero.

The convention is that the outward transmembrane current is positive and the axial current flow into a region is positive. The approach used in computer modeling is to divide the neuron into regions or compartments small enough that the spatially varying I_m in any compartment j is well approximated by its value $I_{m,j}$ at the centre of compartment j. Therefore Equation 2.26 becomes

$$\sum I_a = I_{m,j} A_j \tag{2.27}$$

From Ohm's law, the axial current between adjacent compartments j and k is approximated by the voltage drop between the centres of the compartments divided by the resistance of the path between them r_{jk}. This transforms Equation 2.27 into

$$I_{m,j} A_j = \sum_k \frac{V_k - V_j}{r_{jk}} \tag{2.28}$$

The total membrane current $I_{m,j} A_j$ is the sum of the capacitive and ionic components

$$I_{m,j} A_j = c_j \frac{dV_j}{dt} + I_{ion} \tag{2.29}$$

where c_j is the membrane capacitance of the compartment and the voltage and time dependent ionic component I_{ion} includes all currents through ionic channel conductances.

In summary, the spatial discretization of branched cables is equivalent to reducing the spatially distributed neuron to a set of connected compartments and yields a set of ordinary differential equations in the form

$$c_j \frac{dV_j}{dt} + I(V,t) = \sum \frac{V_k - V_j}{r_{jk}} \tag{2.30}$$

Equations 2.30 involve two approximations. First, axial current is specified in terms of the voltage drop between the centres of adjacent compartments. The second approximation is that spatially varying membrane current I_m is represented by its value at the center of each compartment.

Equations 2.30 can be solved numerically with the use of integration algorithms. The list of integration methods most commonly used in neuronal simulations are the backward Euler method and the Crank-Nicholson method. They offer sufficient stability, accuracy and efficiency and have been used extensively in neuronal simulations (Hines and Carnevale, 1997; Bower and Beeman, 1995).

2.4 Software Modules

A set of software tools composed of 'building blocks' or modules was designed to provide a means of constructing biologically realistic simulations of elementary rhythm generating networks. These tools are capable of addressing simulation problems at many levels of detail (e.g., cellular, synaptic, and network) and are user-extensible (i.e., allow the incorporation of new models). These modules perform well-defined functions and have standardized means for communicating with each other. An object-oriented programming approach was adapted to ensure modularity, flexibility, and reusability of the code. The programs designed for this study were arranged in a hierarchy as presented in Figure 2.4.

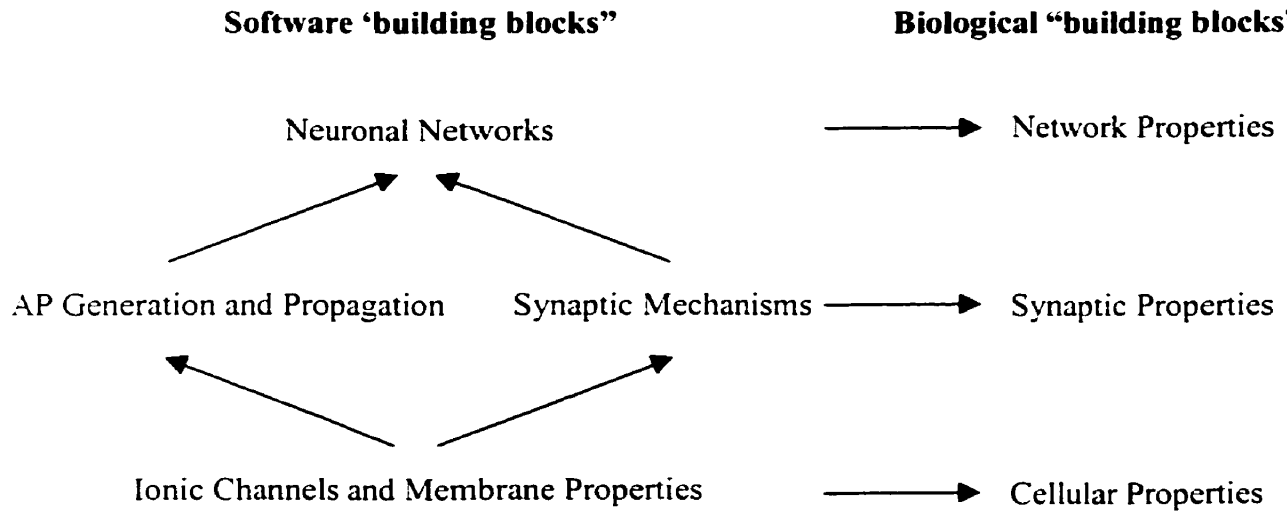

Figure 2.4. Hierarchy of the software modules.

The software modules that define the dynamics of ionic channels and membrane properties form the foundation of the hierarchy. They were used to study the cellular properties (e.g., relationships between firing rate *F* and input current *I*, spike-frequency adaptation) in isolated cells and were embedded in programs at the higher level to simulate synaptic mechanisms and the generation and propagation of APs in neurons. These programs, in turn, were used to study the synaptic properties (e.g., strength and time course, transmitter release) and formed a basis for the development of simulation experiments of neuronal networks and studying various network connectivity schemas and properties (e.g., reciprocal inhibition, feedback inhibition).

The software modules were developed and simulation experiments conducted with the use of NEURON program developed at Yale University. NEURON incorporates *hoc*

programming language with C-like syntax and structure. The object-oriented extensions of *hoc* (excluding polymorphism and inheritance) can be used to implement abstract data types and data encapsulation. The *hoc* interpreter was used to execute *hoc* simulation programs, customize the user interface, optimize parameters, analyze experimental data, and calculate new variables. For more computationally intensive tasks related to integration of differential equations or emulation of biological mechanisms that generate or control chemical and electrical signals, NEURON provides the model description language (NMODL). The NMODL translator then constructs the appropriate C programs, which are compiled, linked and become available for use in NEURON as a shared library (e.g., Dynamic-Link Library, or DLL, in the MS Windows environment). The models of ionic channel and synaptic receptors were developed in NMODL as a set of simultaneous equations (e.g., nonlinear algebraic equations or differential equations) and stored as files with .mod extension.

NEURON offers the user a choice of two stable implicit integration methods: backward Euler and Crank-Nichols (C-N). The backward Euler method can be used with large time steps in order to find the steady-state solution for a linear (passive) system. The C-N method is more accurate for small time steps. These two methods are almost identical in terms of efficiency (Hines and Carnevale, 1997).

3 MODELS OF THE BUILDING BLOCKS

Action potentials in nerve cells are brief changes in the membrane potential, which result from changes in membrane permeability to individual ionic species. In the squid giant axon studied by Hodgkin and Huxley, depolarization of the membrane causes a rapid increase in the number of Na^+ channels that are open, thereby allowing more Na^+ ions to enter the cell, resulting in even more depolarization of the membrane and increased entry of Na^+ ions. Two other processes are involved in the generation of action potentials: the rapid inactivation of I_{Na} and the activation of I_K. The rate of inactivation of I_{Na} is only slightly slower than the rate of activation. The I_K is activated by the membrane depolarization associated with the action potential, allowing K^+ to leave the cell. At some point the hyperpolarizing influence of K^+ leaving overcomes the depolarization influence of Na^+ entering causing termination of action potential and repolarization of the membrane.

In addition to the currents described by Hodgkin and Huxley responsible for the production of action potentials, it appears that two other mechanisms are required to produce rhythmic output:

a) an inward current with a long time constant to produce the sustained depolarization that initiates and maintains the burst, and

b) a current that terminates the burst and provides a long, but finite, period of hyperpolarization between the bursts.

These two mechanisms involve time scales that are much longer than those for the generation of the action potentials.

An extensive literature search was conducted (Table 3.1) with the primary objective to identify relevant studies, summarize their findings and organize the knowledge about generation of rhythmic output, specifically, locomotion-related rhythmic output.

Table 3.1. Studies of generation of patterned output

Behaviour	**Animal**	**Reference**	**Study Type**
Invertebrates			
Feeding	Snail	Yeoman et al, 1995	Experimental & modeling
Respiration	Snail	Bulloch and Syed, 1992	Experimental & modeling
Escape	Crayfish	Wiersma and Ikeda, 1964	Experimental
		Krasne and Wine, 1984	Experimental
Swimming	Leech	Weeks and Kristian, 1978	Experimental
		Brodfuehrer and Friesen, 1986	Modeling
		Calabrese et al, 1995b	Modeling
	Tritonia	Getting, 1981-89	Experimental & modeling
		Katz et al, 1994	Modeling
		Frost and Katz, 1996	Experimental & modeling
	Clione	Satterlie et al, 1985b	Experimental & modeling
		Arshavski et al, 1985 & 1993	Experimental & modeling

	Xenopus	Dale, 1995	Experimental & modeling
		Arshavski et al, 1993	Experimental & modeling
	Aplysia	Alving, 1968	Behavioural & experimental
		Fredman et al., 1983	Experimental
		Baxter and Byrne, 1991	Experimental & modeling
		Canavier et al, 1991 & 1993	Modeling
Jump	Fly	Wyman, 1977	Experimental
Flight	Locust	Pearson, 1993	Experimental
		Robertson, 1995	Experimental & modeling
Vertebrates			
Escape	Fish	Eaton and Hecket, 1984	Behavioural & experimental
	Lamprey	Grillner et al, 1991	Experimental & modeling
		Ekeberg et al, 1991	Modeling
		Hellgren et al, 1992	Modeling
		Wallen et al, 1992	Modeling
		McClellan and Jang, 1993	Modeling
		Traven et al, 1993	Experimental & modeling
		Nishii et al, 1994	Modeling
Walking	Cat	Grillner and Wallen, 1985	Behavioural & experimental

A detailed review of these studies revealed common or similar cellular and synaptic mechanisms that exist in rhythm-generating networks in diverse species. The list of ionic currents found in neuronal cells involved in the production of rhythmic output include Hodgkin-Huxley-type currents, certain potassium currents, calcium activated potassium currents, calcium currents, and cation currents (Table 3.2).

Table 3.2. Ionic channels involved in the production of rhythmic output.

Current	Description	Function
Hodgkin-Huxley-type Currents		
Fast I_{Na}	Rapidly activating and inactivating	Generates action potentials
Fast I_K	Activated by strong depolarization	Repolarizes action potentials
I_{pas}	Contributes to neuronal resting potential	
Potassium Currents		
I_A	Transient, inactivating current	Delays onset of firing Lengthens interspike interval Repolarizes action potentials
I_M	Slowly activating, non-inactivating current Activated by depolarization	Contributes to spike-frequency adaptation Blocks repetitive firing Blocking it enhances cell excitability
I_{AHP}	Slow afterhyperpolarization current	Hyperpolarizes a cell after a spike train

	Activated by increases in $[Ca^{2+}]_i$	Slows down the rate of APs
		Blocking of I_{AHP} enhances cell excitability
I_C	Activated by increases in $[Ca^{2+}]_i$	Repolarizes action potentials
Calcium Currents		
I_L	High-threshold current	Underlies Ca^{2+} spikes in dendrites
	Long lasting and slowly inactivating	Involved in synaptic transmission
		Allows Ca^{2+} entry during action potential
I_T	Low threshold, transient current	Underlies rhythmic burst firing
	Rapidly inactivating	
Ca pump	Intracellular calcium pump	Responsible for removal of calcium from the cytoplasm
Cation Currents		
I_{CAN}	Outward cation current	Accelerates the rising phase of the burst
	Activates by increases in $[Ca^{2+}]_i$	Increases the frequency of burst sequence
I_h	Depolarizing current	Contributes to rhythmic burst firing
	Activated by hyperpolarization	

The release of neurotransmitters at the synapses was found to be the common method by which neurons communicate in rhythm generating networks. The action potentials that propagate down the axon and invade the presynaptic terminal depolarize the membrane and activate voltage-gated Ca^{2+} channels, allowing the entry of Ca^{2+} ions. The entry of Ca^{2+} ions near the release sites triggers a series of events leading to the fusion of neurotransmitters into the synaptic cleft. The released neurotransmitters diffuse across the cleft, make contact with the postsynaptic membrane, and bind to the specialized receptors in the postsynaptic membrane. This, in turn, causes the rapid opening of ion channels. At some synapses the binding of neurotransmitters to receptors triggers either the release of second-messenger molecules into the cytoplasm of the postsynaptic neuron, which then modulate ion channels, or the activation of proteins (e.g., GTP- binding) that couple to ion channels in the membrane and alter their functions.

Using an in vitro preparation of the lamprey spinal cord, Cohen and Wallen (1980) were the first to show that excitatory amino acids, such as glutamate, can activate locomotory movements in vertebrates. Later studies in the lamprey suggested that glutamate activated the CPG through the NMDA and kainate sites producing either slow (0.1 – 3 Hz) or fast (1 – 8 Hz) fictive swimming, respectively (Grillner et al., 1981b). More recent experiments in lamprey have provided evidence for the involvement of the AMPA sites in the generation of swimming (Alford and Grillner, 1990). Experiments in higher vertebrates, including the chick embryo (Barry and O'Donavan, 1987), the neonatal rat (Smith and Feldman, 1987), the adult rabbit (Fenaux et al., 1991), the mouse (Harnadez

et al., 1991), the cat (Douglas et al., 1993), and the monkey (Hultborn et al., 1993), provided wealth of evidence for the involvement of AMPA/kainate and NMDA receptors in the generation of various forms of locomotion. These experiments also suggest that several other receptors-transmitter combinations can be involved in the generation of locomotion. However, these combinations have yet to be determined.

Some experimental evidence from a variety of preparations supports the conclusion that the GABA and glycinergic neurotransmission are the principal mechanisms underlying the reciprocal organization of the locomotor pattern. Both $GABA_A$ and $GABA_B$ receptors cause inactivation of locomotor CPGs in both the lamprey (Tegner et al., 1993) and the neonatal rat (Cowley and Smith, 1995) although experiments in the neonatal rat conducted by Cazalets (1994) showed that bicuculline, the $GABA_A$ receptor blocker, did not prevent the reciprocal inhibition, but rather increased the cycle frequency of the locomotion. This is an indication that other factors may contribute to this phenomenon.

The role of glycine receptors is less certain. Blocking glycine receptors with strychnine during locomotion in the tadpole (Soffe, 1989), the neonatal rat (Kudo et al, 1991), the adult lamprey (Cohen and Harris-Warrick, 1984), and the cat (Noga et al., 1993) disrupts left/right alternation or midcycle inhibition and causes co-activation of flexor and extensor muscles in legged animals. However, when interpreting such data, it is well to recall that strychnine also blocks various ion channels (Dale, 1995) and GABA receptors (Tauck et al., 1988) at concentrations 1-20 μM usually used to block glycine-mediated

reciprocal inhibition. This illustrates the need for further investigation of inhibitory components of spinal networks involved in controlling locomotion.

In summary, synaptic transmission is mediated by excitatory and inhibitory amino acid neurotransmitters, glutamate and GABA, respectively. Glutamate activates AMPA/kainate receptors, responsible for most fast excitatory transmission, and N-methyl-D-aspartate (NMDA) receptors, whose activation is much slower than that of AMPA/kainate receptors. γ-aminobutyric acid (GABA) also activates two classes of receptors, $GABA_A$ receptors, which have relatively fast dynamics, and $GABA_B$ receptors, which are much slower and involve second messenger.

This chapter describes the models of ionic currents, including passive and active presented in Table 3.1, and synapses, including excitatory receptors AMPA and NMDA, and inhibitory receptors $GABA_A$ and $GABA_B$. For each model, the following were included: a) description of biological phenomena; b) mathematical model and default values and state variables; and c) results of computer simulation experiments that were conducted to study the role of ionic currents on the properties of neuronal membrane.

A patch of membrane that was used as a membrane model is considered to represent an isolated soma with ionic channels uniformly distributed. Parameters of the patch of membrane are listed in Table 3.3.

Table 3.3. Parameters of the patch of membrane.

Variable	Description	Units	Value
Ra	The cytoplasmic resistivity	ohm-cm	100
Vinit	The initial membrane voltage	mV	-65
L	The length of the section	μm	100
diam	The diameter	μm	100
cm	The capacitance	$\mu F/cm^2$	1
celsius	Temperature	°deg	36

3.1 Hodgkin-Huxley-Type Currents

The models of the HH-type currents (i.e., fast Na^+ and K^+, and passive current), primarily responsible for the generation of action potentials were developed using Equations 2.14 through 2.18. The electrophysiological parameters were derived from the data of Huguenard and McCormick (1992) obtained from thalamocortical relay neurons in the rodent and cat dorsal lateral geniculate nucleus.

3.1.1 Fast Sodium Current

As per Equations 2.15 and 2.16, the fast Na^+ current, I_{Na}, is described as follows:

$$I_{Na} = \bar{g}_{Na} m^3 h (V - E_{Na}) \tag{3.1}$$

The values for the maximum specific sodium conductance and the equilibrium potential for the sodium channel are:

$$\begin{aligned} \bar{g}_{Na} &= 0.1 \ S/cm^2 \\ E_{Na} &= 50 \ mV \end{aligned} \tag{3.2}$$

The steady-state activation and inactivation variables m, and h are described by a set of differential equations:

$$\frac{dm}{dt} = \alpha_m(1-m) - \beta_m m$$
$$\frac{dh}{dt} = \alpha_h(1-h) - \beta_h h \tag{3.3}$$

Empirically determined expressions for α_m, β_m, α_h, and β_h, are (Huguenard and McCormick, 1992):

$$\alpha_m = \frac{0.091(V+38)}{1-\exp[-(V+38)/5]} \qquad \beta_m = \frac{-0.062(V+38)}{1.0-\exp[(V+38)/5]}$$
$$\alpha_h = 0.016\exp[(-55-V)/15] \qquad \beta_h = \frac{2.07}{1.0+\exp[(17-V)/21]} \tag{3.4}$$

3.1.2 Fast Potassium Current

The fast K+ current, I_K, is expressed as follows:

$$I_K = \bar{g}_K n^4 (V - E_K) \tag{3.5}$$

The values for the maximum specific potassium conductance and the equilibrium potential for the potassium channel are:

$$\bar{g}_K = 0.01\ S/cm^2$$
$$E_K = -77\ mV \tag{3.6}$$

The steady-state activation variable n is described by a differential equation:

$$\frac{dn}{dt} = \alpha_n(1-n) - \beta_n n \tag{3.7}$$

Empirically determined expressions for α_n and β_n are (Huguenard and McCormick, 1992):

$$\alpha_n = \frac{0.01(V+45)}{1-\exp[-(V+45)/5]} \qquad \beta_n = 0.17 * \exp[-(V+50)/40] \tag{3.8}$$

3.1.3 Passive Currents

Passive membrane is electrically represented by a constant (time- and voltage-independent) transmembrane conductance g_{pas} in series with a fixed voltage source E_{pas} that designates the reversal potential of the passive channels. The passive current is

$$I_{pas} = g_{pas}(V - E_{pas}) \tag{3.9}$$

The values of transmembrane conductance g_{pas} and the reversal potential for the passive current E_{pas} are:

$$g_{pas} = 0.001 \ S/cm^2$$
$$E_{pas} = -70 \ mV \tag{3.10}$$

3.1.4 Simulation of Patch of Membrane with HH-type Currents

The patch of membrane defined in Table 3.3 with the HH-type channels defined by Equations 3.1 through 3.10 were used in the simulation experiment. The patch of membrane was subjected to a 100 msec stimulation with a current pulse of 0.02 nA amplitude. The simulation results are depicted in Figure 3.1.

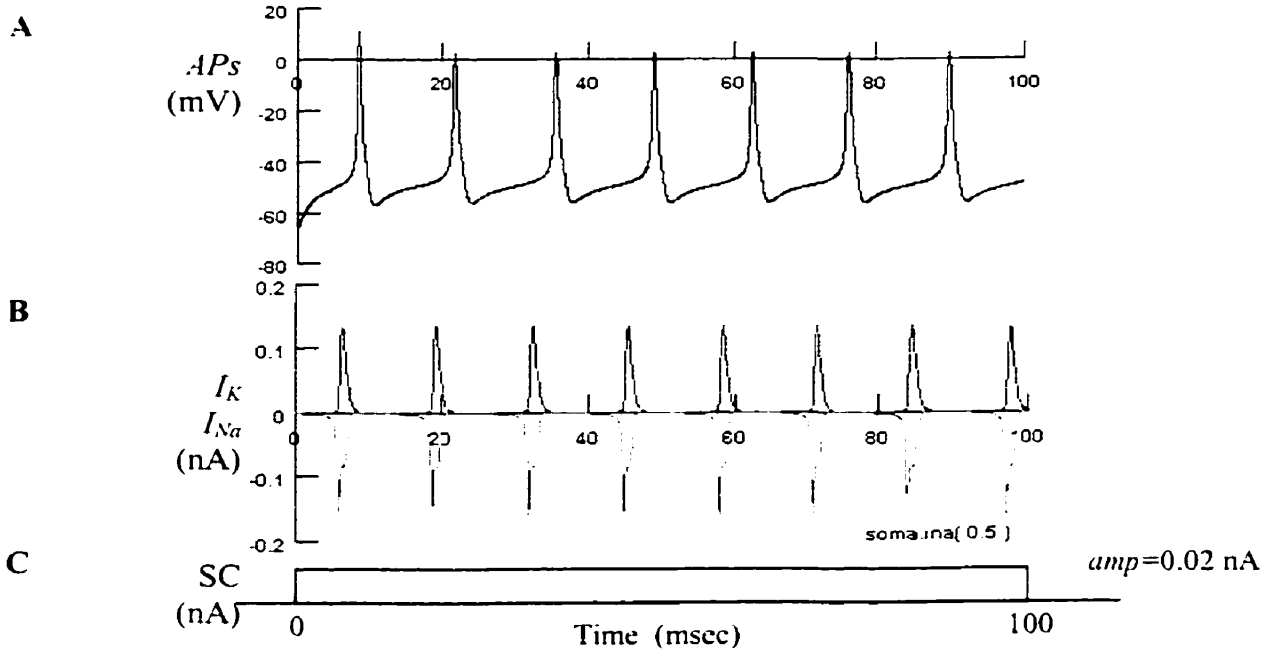

Figure 3.1. Simulation of a patch of membrane with the HH-type channels. A: Action potentials (mV). B: Sodium and potassium currents (nA). C: Stimulation current with amplitude *amp*=0.02 nA and duration *dur*=100 msec.

3.2 Potassium and Calcium Currents

Under normal physiological conditions, potassium channels are activated by depolarization and current flow through these channels is outward. Given the physiological reversal potential of K^+ is in the neighborhood of −100 mV, potassium currents are thought to stabilize the membrane potential, since activating a potassium current repolarizes the membrane i.e., pulls the membrane potential to hyperpolarizing levels. As in the case of I_K, the delayed rectified potassium current in the squid axon, potassium currents serve to keep fast action potential short. In the absence of a potassium current the action potential would be much longer and would follow the time course of inactivation of the sodium channel. They also delay the generation of an action potential following synaptic or current input, lengthen interspike intervals, and reduce the firing frequency in the case of a constant input.

The models of K^+ currents include the A-current - a transient outward current responsible for slowing the rate of spike generation, the M-current – a slowly activating potassium current responsible for blocking repetitive firing, and two calcium-dependent potassium currents: I_{AHP} – a slow current that hyperpolarizes the cell after a spike train, and the C-current – a fairly large current involved in the repolarization of the membrane after an action potential (Table 3.2).

Calcium ions play key roles in triggering synaptic release upon the invasion of an action potential at a presynaptic site and the generation of rhythmic output. They are also the key determinant for axonal growth and muscle contraction, and are involved in the initiation of synaptic plasticity (Koch, 1998). They can be thought of as coupling the membrane potential to cellular output or action such as secretion, growth, and plasticity. The associated Ca^{2+} currents are inward, activated by depolarization, and have some degree of inactivation that occurs on a much slower time scale than does inactivation of the Na^{+} current. Different Ca^{2+} currents differ in their sensitivity to depolarization. Some currents activate in response to a depolarization of a few millivolts, while others require 20 mV or more. Some show rapid and some very slow voltage-dependent inactivation. While Ca^{2+} currents appear to be largely absent in axons, they can be found throughout the dendritic tree, the soma, and the presynaptic terminals.

The models of Ca^{2+} currents include the L-current – a high-threshold, long-lasting and slowly inactivating current, the T-current – a low-threshold, transient and rapidly inactivating current, and the Ca^{2+} pump involved in the removal of Ca^{2+} ions from the cells (Table 3.2).

3.2.1 A-current

The A-current is present in cortical pyramidal cells (Johnston and Wu, 1995), thalamic neurons (Huguenard and McCormick, 1992), and neurons involved in the production of rhythmic control of locomotion in gastropods (Adams et al., 1980) and *Tritonia* (Getting, 1983). The A-current is expressed as follows:

$$I_A = \bar{g}_A m^4 h (V - E_A) \tag{3.11}$$

The values for the maximum specific conductance and the equilibrium potential are:

$$\bar{g}_A = 0.00345 \ S/cm^2 \tag{3.12}$$

$$E_A = -110 \ mV$$

The steady-state activation and inactivation variables m, h are described by a set of differential equations:

$$\frac{dm}{dt} = \frac{m_\infty - m}{\tau_m} \qquad \frac{dh}{dt} = \frac{h_\infty - h}{\tau_h} \tag{3.13}$$

The electrophysiological parameters for the activation and inactivation variables have been derived from the data of Huguenard and McCormick (1992) obtained from acutely dissociated rat thalamic relay neurons. The activation variable m is expressed as follows:

$$m_\infty = \frac{1}{1 + exp[-(V + 60)/8.8]} \tag{3.14}$$

$$\tau_m = \frac{1}{exp[(V + 35.8)/19.7] + exp[(V + 79.7)/-12.7]} + 0.37$$

The inactivation variable h is:

$$h_\infty = \frac{1}{1 + exp[(V + 78)/6]} \tag{3.15}$$

If V_m < -63 mV

$$\tau_h = \frac{1}{exp[(V + 46)/5] + exp[(V + 238)/-37.5]}$$

else

$$\tau_h = 19$$

Simulations of the voltage-clamp experiment depicted in Figure 3.2 revealed that depolarization of the membrane results in a rapid activation and slow inactivation of the A-current and that increasing levels of depolarization result in the current becoming larger. The increased amplitude is a product of both increased activation of the current and an increase in the driving force on the K^+ ions, since the membrane potential is moving away from E_K. Furthermore, a change of the extracellular concentration of K^+ ions, $[K^+]_o$, from 3.1 mM to 25 mM, which changes the equilibrium potential of the membrane from –100 mV to –60 mV, results in a decrease in the amplitude of the A-current. These simulation results are consistent with the experimental data and simulation results published in neuroscience literature (Huguenard and McCormick, 1992, page 1378, Figure 3; Huguenard and McCormick, 1994, pages 35-38, Figure 17).

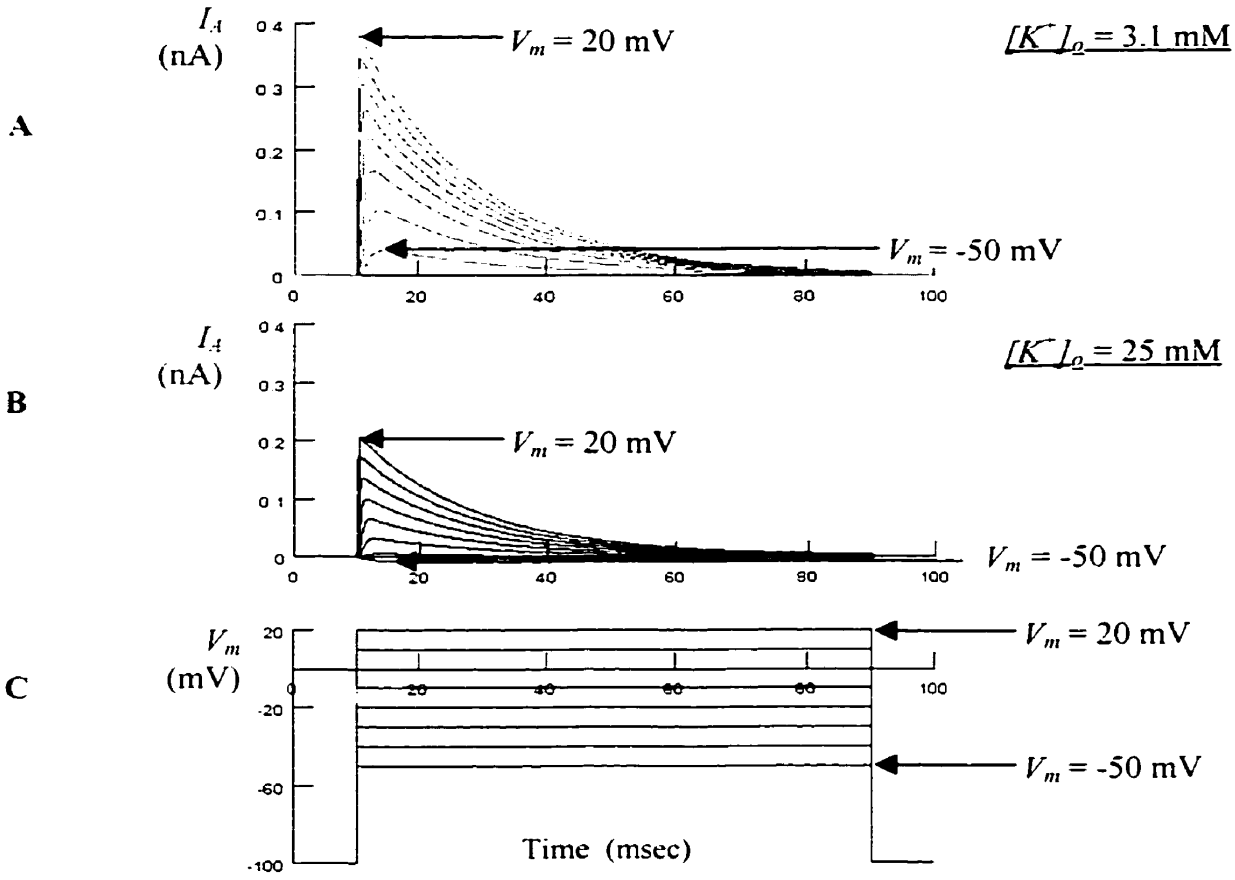

Figure 3.2. Simulation of voltage-clamp experiment of the A-current. Duration of simulation experiment *dur* = 100 msec. A: Depolarization of the membrane results in a rapid activation and slow inactivation of I_A. B: Increase in $[K^+]_o$ results in the decrease of I_A amplitude. C: Membrane potentials in the range of –50 mV to 20 mV.

The patch of membrane defined in Table 3.3 with the HH-type currents (Equations 3.1 – 3.10) and the A-current (Equations 3.11 – 3.15) were used in the simulation experiments.

The conductances were assumed to be uniformly distributed throughout the membrane. The stimulation current was assumed to be identical as in the simulation presented in Figure 3.1. Figure 3.3 shows the effects of the A-current on the time course of the action potentials.

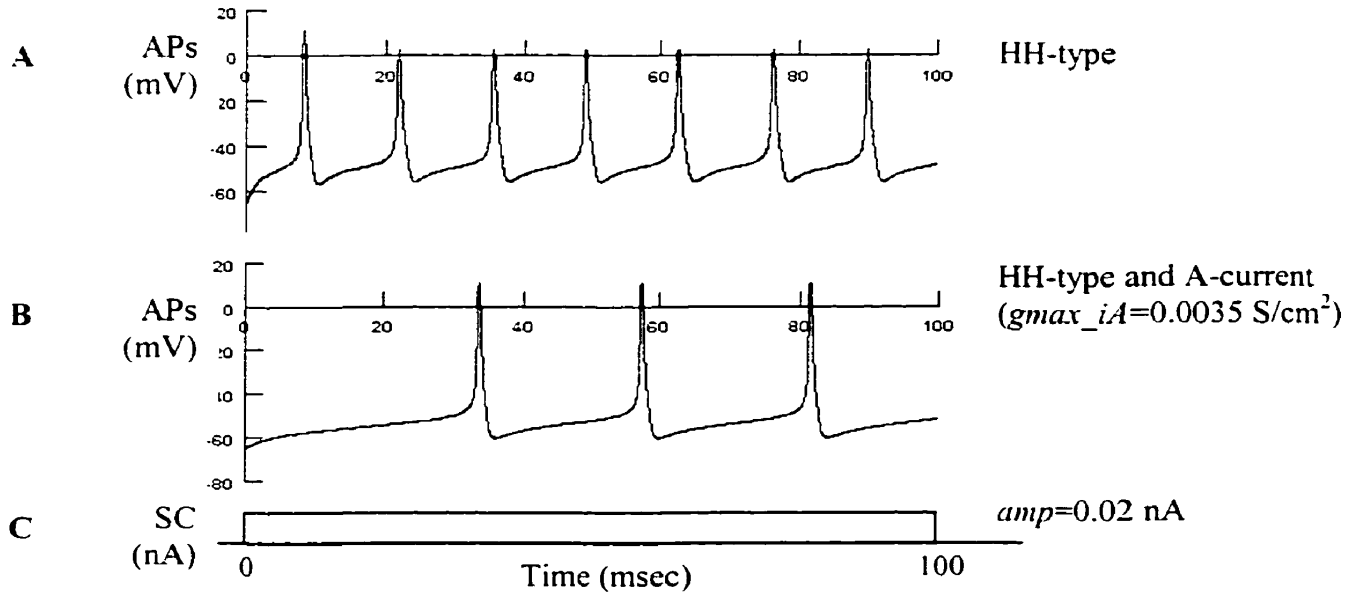

Figure 3.3. Comparison of action potential time courses for different combination of conductances. A: HH-type conductances only; B: HH-type and the A-current with the maximum specific conductance *gmax_iA*=0.0035 S/cm^2. C: Stimulation current with amplitude *amp*=0.02 nA and duration *dur*=100 msec.

The presence of the A-current significantly contributes to an increase in the interval between action potentials, and blocking of the A-channels enhances the response of the neuron by increasing the frequency of action potential discharge. The A-current contributes to the maintenance of the hyperpolarization, slowing the onset of the next

action potential. This gives the cell the ability to perform frequency encoding, transforming the membrane potential level to spike frequency. With increasing input to the cell (and higher membrane potentials), the A-current is less effective in prolonging the hyperpolarization.

3.2.2 M-Current

The M-current was discovered in the sympathetic ganglion cells of the bullfrog (Brown and Adams, 1980). It is a slow outward voltage-dependent current. It is activated by a depolarization of the membrane at approximately –65 mV and does not inactivate with time. It is blocked by stimulation of muscarinic receptors (hence its name, I_M). Because its slow kinetics and modest amplitude, I_M does not affect substantially the waveform of a single action potential, but rather contributes to the slow adaptation of spike frequency seen during maintained depolarization and blocking of repetitive firing. The M-current, I_M, is expressed as follows:

$$I_M = \bar{g}_M m\,(V - E_M) \tag{3.16}$$

The values for the maximum specific conductance and the equilibrium potential for the M channel are:

$$\bar{g}_M = 0.00031\ S/cm^2$$
$$E_M = -105\ mV \tag{3.17}$$

The steady-state activation variable m is described by a differential equation:

$$\frac{dm}{dt} = \frac{m_\infty - m}{\tau_m} \tag{3.18}$$

The electrophysiological parameters for the steady-state activation variable were derived from the data of Yamada et al. (1998) obtained from the bullfrog sympathetic ganglion cells and are:

$$m_\infty = \frac{1}{1 + exp[-(V + 35)/10]}$$
$$\tau_m = \frac{1}{3.3\{exp[(V + 35)/40] + exp[-(V + 35)/20]\}} \quad (3.19)$$

Simulations of the voltage-clamp experiment depicted in Figure 3.4 revealed that increasing the membrane potential results in a slow activation of the M-current, and returning the membrane potential back to its original level turns the M-current off (a process known as deactivation). Furthermore, the increasing level of depolarization results in the current becoming larger.

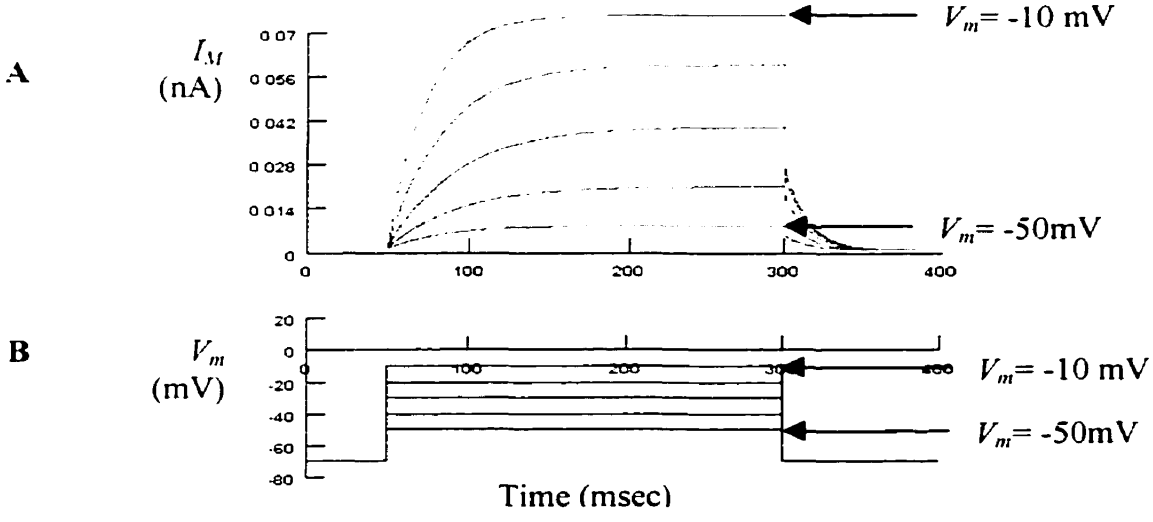

Figure 3.4. Simulation of voltage-clamp demonstration of the M-current. Duration of the simulation experiment *dur*=400 ms. A: Depolarization of the membrane results in a slow activation followed by deactivation of the M-current. B: Membrane potentials in the range of –50 mV to –10 mV.

The patch of membrane defined in Table 3.3 with the HH-type currents (Equations 3.1 – 3.10) and the M-current (Equations 3.16 – 3.19) were used in the simulation experiments. Figure 3.4 shows the effects of the M-current on the time course of the action potentials.

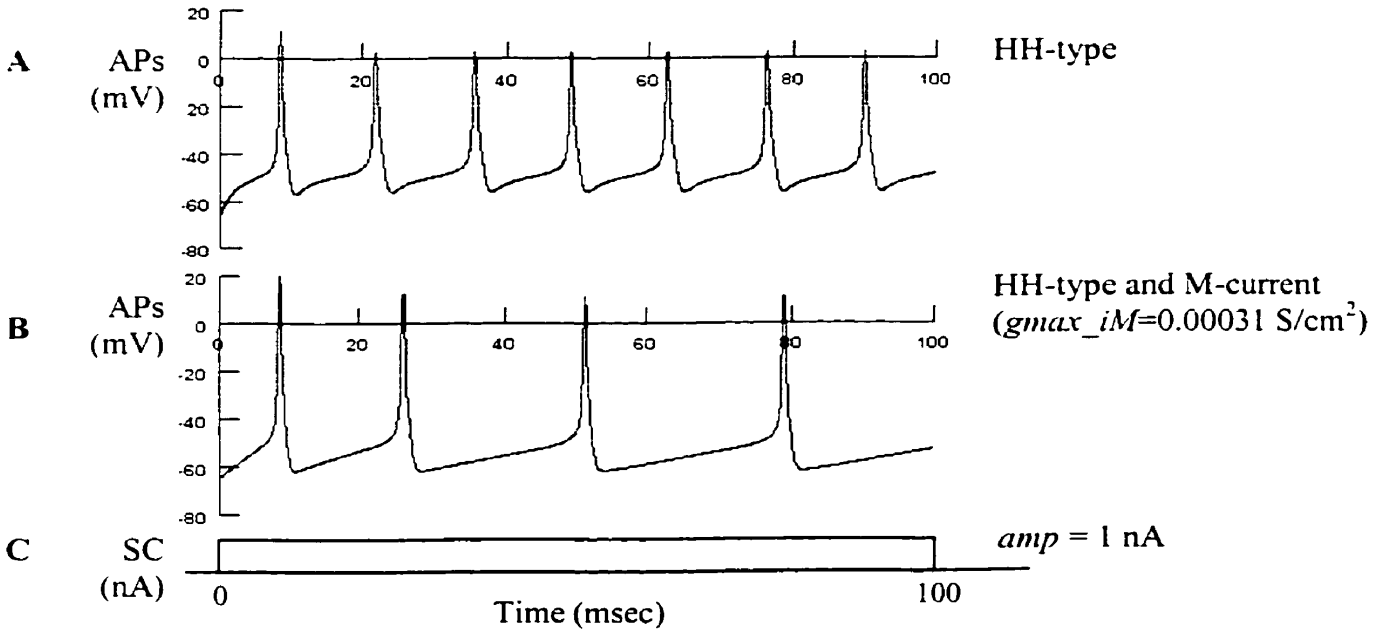

Figure 3.5. Comparison of action potential time courses for different combination of conductances. A: HH-type conductances only; B: HH-type and the M-conductance with the maximum specific conductance *gmax_iM*=0.00031 S/cm^2. C: Stimulation current with amplitude *amp*=1 nA and duration *dur*=100 msec.

The M-current contributes the slow adaptation of spike frequency seen during maintained depolarization and blocking of repetitive firing. Blocking the M-current enhances the cell excitability.

These simulation results are consistent with the data published in neuroscience literature (Huguenard and McCormick, 1994, pages 46-49; Jassar et al., 1994, pages 355-356).

3.2.3 Afterhyperpolarization (AHP) Current

The afterhyperpolarization current, I_{AHP}, is present in many neurons throughout the nervous system including cortical pyramidal cells. It has been found in the bullfrog sympathetic ganglion cell (Yamada et al., 1998), and the oscillatory neurons of the reticular thalamus (Destexhe et al., 1994a). The AHP-current, I_{AHP}, is expressed as follows:

$$I_{AHP}=\bar{g}_{AHP}\, m^2\, (V-E_{AHP}) \tag{3.20}$$

The values for the maximum specific conductance and the equilibrium potential for the AHP current obtained from the bullfrog sympathetic ganglion cells are:

$$\bar{g}_{AHP}=0.00108 \ \ S/cm^2 \tag{3.21}$$

$$E_{AHP} = -95 \ \ mV$$

The steady-state activation variable m is described by a differential equation:

$$\frac{dm}{dt}=\frac{m_\infty - m}{\tau_m} \tag{3.22}$$

The electrophysiological parameters for the steady-state activation variable m have been derived from the data of Yamada et al. (1998) obtained from the bullfrog sympathetic ganglion cells and are:

$$m_\infty = \frac{f(Ca)}{f(Ca)+b}$$

$$\tau_m = \frac{1000}{f(Ca)+b} \tag{3.23}$$

where $[Ca^{2+}]_i$ is in mM and $f(Ca)$ and b are expressed as follows:

$$f(Ca) = 1.25 * 10^8 * [Ca^{2+}]_i^2 \qquad (3.24)$$

$$b = 2.5$$

I_{AHP} is a small and slow, calcium-activated, voltage independent current. As each action potential occurs, Ca^{2+} enters the cell through high-threshold Ca^{2+} channels. The increases in $[Ca^{2+}]_i$ give rise to the activation of I_{AHP}. Furthermore, the increasing level of the intracellular concentration of Ca^{2+} results in the current becoming larger (Figure 3.6).

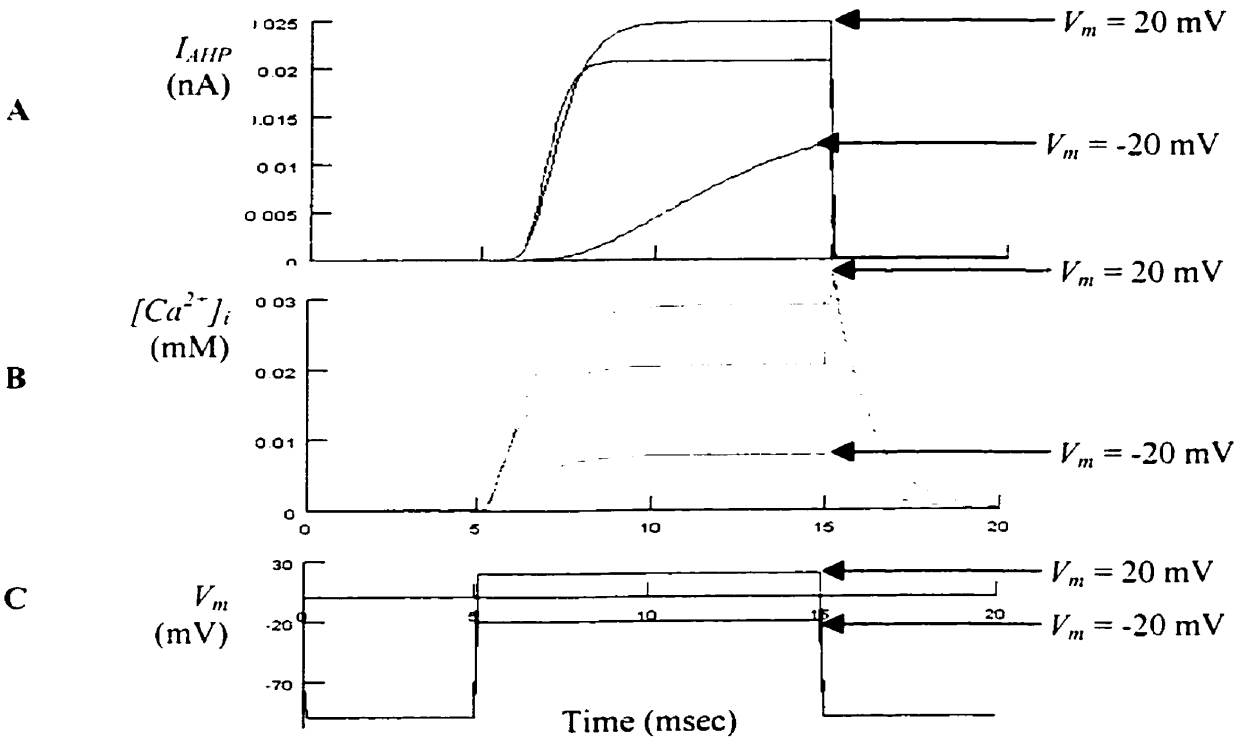

Figure 3.6. Simulation of voltage-clamp demonstration of the AHP current. Duration of simulation experiment *dur*=20 msec. A: The AHP current activated by the intracellular Ca^{2+} concentration presented in diagram B. C: Membrane potentials in the range of —20 mV to 20 mV.

The patch of membrane defined in Table 3.3 with the HH-type currents and I_{AHP} (Equations 3.20 – 3.24) were used in the simulation experiments (Figure 3.7).

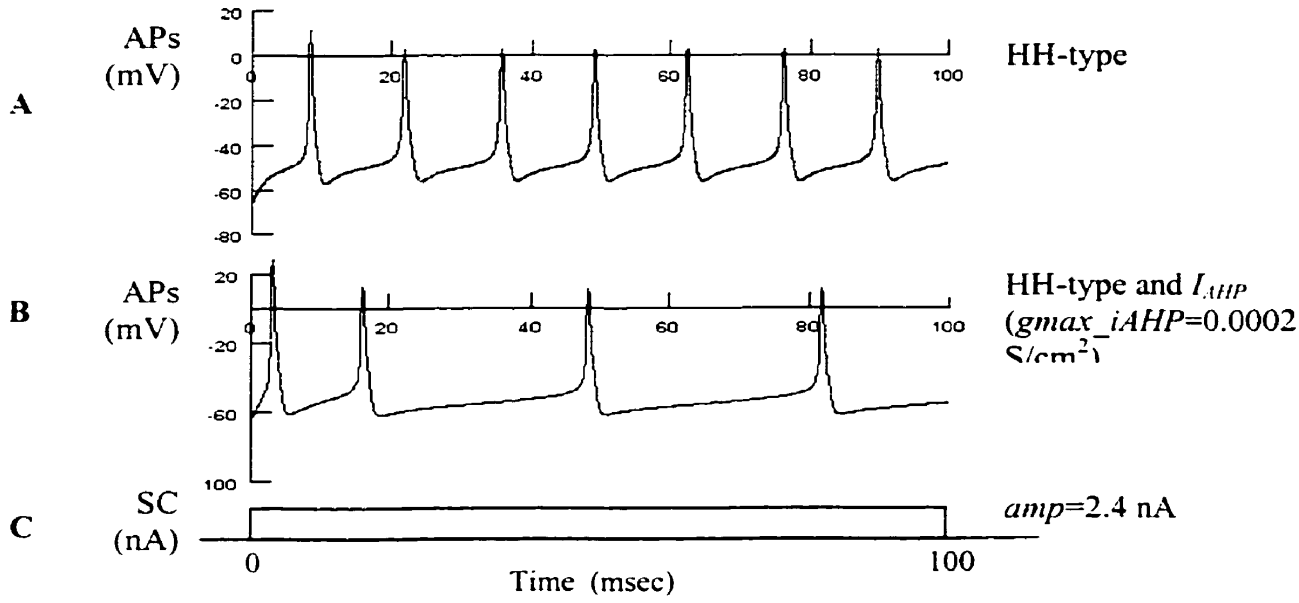

Figure 3.7. Comparison of action potential time courses for different combination of conductances. A: HH-type conductances; B: HH-type conductances and I_{AHP} with the maximum specific conductance *gmax_iAHP*=0.0002 S/cm^2. C: Stimulation current with amplitude *amp*=2.4 nA and duration *dur*=100 msec.

The slow AHP-current profoundly affects the firing pattern of a cell. When a steady stimulation current induces a train of action potentials, the accumulating I_{AHP} gradually slows the rate of firing (a process referred to as spike-frequency adaptation) and eventually is strong enough to prevent the cell from reaching its firing threshold. These findings are consistent the simulation results published by Huguenard and McCormick (1994, pages 41-43).

3.2.4 C- and L-Currents

The C-current is large, calcium- and voltage-dependent potassium current. The C-current, I_C, is expressed as follows:

$$I_C = \bar{g}_C \; m \; (V - E_C) \tag{3.25}$$

The values for the maximum specific conductance and the equilibrium potential for the C current obtained from the bullfrog sympathetic ganglion cells are:

$$\bar{g}_C = 0.00345 \;\; S/cm^2 \tag{3.26}$$

$$E_C = -105 \;\; mV$$

The steady-state activation variable m is described by a differential equation:

$$\frac{dm}{dt} = \frac{m_\infty - m}{\tau_m} \tag{3.27}$$

The electrophysiological parameters for the steady-state activation variable m were derived from the data of Yamada et al. (1998) obtained from the bullfrog sympathetic ganglion cells and are:

$$m_\infty = \frac{f(V, Ca)}{f(V, Ca) + b(V)} \tag{3.28}$$

$$\tau_m = \frac{1}{f(V, Ca) + b(V)}$$

$[Ca^{2+}]_i$ is in mM and $f(V, Ca)$ and $b(V)$ are:

$$f(V, Ca) = 250 \, [Ca^{2+}]_i \;\; exp(V / 24)$$

$$b(V) = 0.1 \, exp(-V / 24) \tag{3.29}$$

The L-current is a high-threshold calcium current activated by depolarization. It shows inactivation that is $[Ca^{2+}]_i$ dependent and voltage independent. The L-current is expressed as follows:

$$I_L = \bar{g}_L \, m^2 \, F(V, [Ca^{2+}]_i, [Ca^{2+}]_o, z) \tag{3.30}$$

The steady-state activation variable m is described by a differential equation:

$$\frac{dm}{dt} = \frac{m_\infty - m}{\tau_m} \tag{3.31}$$

The electrophysiological parameters have been derived from the data of McCormick and Huguenard (1992) obtained from pyramidal cells in thalamic relay neurons of the rodent:

$$m_\infty = \frac{A}{A+B} \qquad \tau_m = \frac{1}{A+B} \tag{3.32}$$

and variables A and B are:

$$A = \frac{1.6}{1 + exp[-0.072(V - 5.0)]} \qquad B = \frac{0.02(V - 1.31)}{exp\{[(V - 1.31)/5.36] - 1\}} \tag{3.33}$$

The function $F(V, [Ca^{2+}]_i, [Ca^{2+}]_o, z)$ in Equation 3.30 is expressed as follows:

$$F = z^2 \frac{EF^2}{RT} * \frac{\{[Ca^{2+}]_i - [Ca^{2+}]_o\} exp(\frac{-zFE}{RT})}{1 - exp(\frac{-zFE}{RT})} \tag{3.34}$$

The C-current is activated by a combination of cell depolarization and Ca^{2+} entering into the cell during the action potential. As the cell is depolarized, Ca^{2+} ions enter via the L-

conductance, gradually activating the C-current. As the voltage increases, the inflow of Ca^{2+} decreases, causing reduction in the activation of the C-current. Figure 3.8 depicts the effects of the C- and L-currents on the time course of the action potential. As the cell is depolarized, Ca^{2+} ions enter via the L-conductance, gradually activating the C-current. As the voltage increases, the inflow of Ca^{2+} decreases, causing reduction in the activation of the C-current.

These simulation results are comparable with the data published by Huguenard and McCormick (1994, pages 38-41) and McCormick and Huguenard (1992).

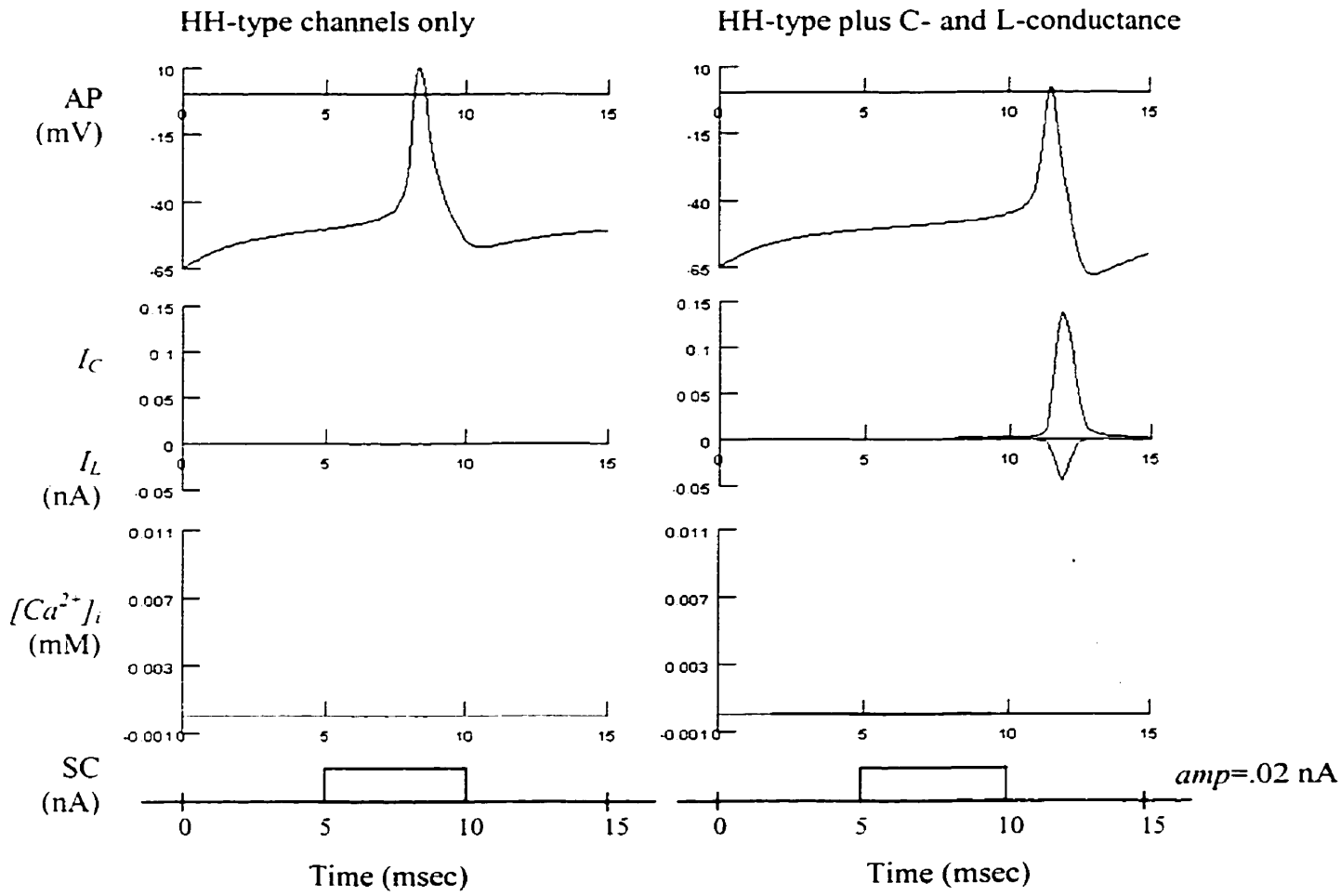

Figure 3.8. Addition of I_C and I_K (right-hand side diagrams) results in the increase of repolarization of the membrane following the action potential, and decrease in the duration of action potential.

3.2.5 T-Current

The T-current has been identified in mammalian spinal motorneurons and thalamic relay neurons. It is a low-threshold and transient Ca^{2+} current that is activated at hyperpolarized membrane potentials (-75 mV and below). It is inactivated by maintained depolarization. The T-current, I_T, is expressed as follows:

$$I_T = \bar{g}_T \, m^2 \, h F(V, [Ca^{2+}]_i, [Ca^{2+}]_o, z) \tag{3.35}$$

The values for the maximum specific conductance and the equilibrium potential for the T current obtained from the ferret reticular thalamic neurons (Destexhe et al., 1994) are:

$$\bar{g}_T = 0.002 \quad S/cm^2 \tag{3.36}$$

$$E_T = 50 \quad mV$$

The steady-state activation and inactivation variables m and h respectively are described by differential equations:

$$\frac{dm}{dt} = \frac{m_\infty - m}{\tau_m}$$

$$\frac{dh}{dt} = \frac{h_\infty - h}{\tau_h} \tag{3.37}$$

The electrophysiological parameters were derived from the data of Destexhe et al., (1994) obtained from the ferret reticular thalamic neurons and are:

$$m_\infty = \frac{1}{1 + exp[-(V + 52)/7.4]}$$

$$\tau_m = 0.44 + \frac{0.15}{exp[(V + 27)/10] + exp[-(V + 102)/15]} \tag{3.38}$$

$$h_\infty = \frac{1}{1 + exp[(V + 80)/5]}$$

$$\tau_h = 22.7 + \frac{0.27}{exp[(V + 48)/4] + exp[-(V + 407)/50]}$$

The T-current appears to be important for the generation of bursts. As illustrated in Figure 3.9, a thalamic relay neuron exhibits two different modes of firing depending upon membrane potential. Intracellular stimulation of the cell at the initial membrane potential of –85 mV results in a burst of action potentials. Depolarization of the cell to –65 mV inactivates the T-current resulting in the generation of Na^+/K^+ action potentials.

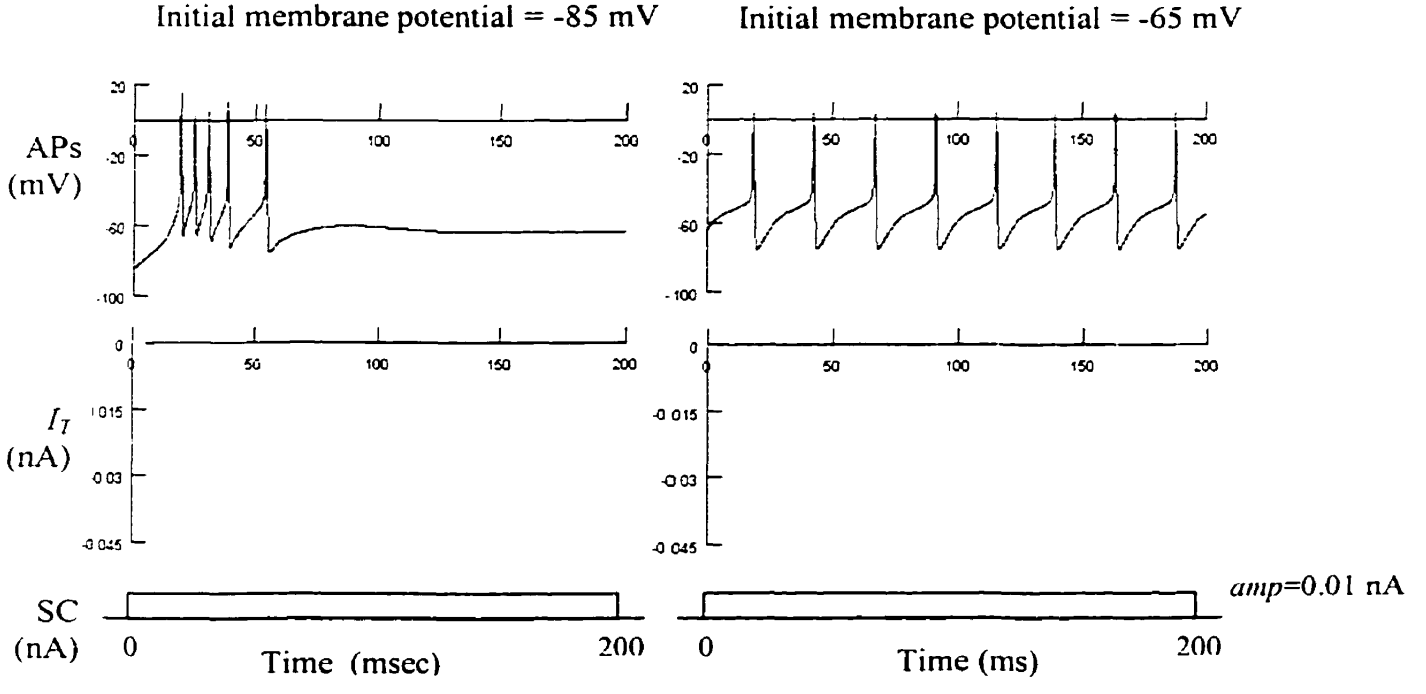

Figure 3.9. Action potentials generated by the model of a thalamic relay cell with the T-current. At the membrane potential = -85 mV, the cell generates bursts due to the activation of the T-current. Depolarization of the cell to –65 mV results in the inactivation of the T-current and the production of HH-type action potentials.

3.2.6 Calcium Pump

The dynamics of intracellular Ca^{2+} was modeled taking into account a fast removal process due to an active pump, and Ca^{2+} entry due to the Ca^{2+} currents. The influx of Ca^{2+} into a thin shell beneath the membrane is

$$\frac{d[Ca]_i}{dt} = -\frac{k\, I_T}{2Fd} \tag{3.39}$$

where F = 96489 C · mol^{-1} is the Faraday constant, d = 1 μm is the depth of the shell beneath the membrane, and k = 10000 is the unit conversion constant for the Ca^{2+} currents (mA) and $[Ca]_i$ (millimolar). The contribution of the Ca^{2+} pump is

$$\frac{d[Ca]_i}{dt} = -\frac{K_T[Ca]_i}{[Ca]_i + K_D} \tag{3.40}$$

where K_T = 10^{-4} mM/ms^{-1} and K_D = 10^{-4} mM are the parameters obtained from a Michaelis-Menten equation (Destexhe et al., 1994). The Ca^{2+} reversal potential strongly depends on the intracellular Ca^{2+} concentration and was calculated using the Nernst equation

$$E_{Ca} = k' \cdot \frac{RT}{2F} log \frac{[Ca]_o}{[Ca]_i} \tag{3.41}$$

where R = 8.31441 J · mol^{-1} °K^{-1}, T = 309.15 °K, and k' = 1000 is the unit conversion factor for E_{Ca} (mV). For $[Ca]_i$ = 2.4e10^{-4} mM and $[Ca]_o$ = 2 mM, which are typical values as rest, E_{Ca} = 120 mV.

3.2.7 Ca-dependent Nonspecific Cation Current I_{CAN}

Pharmacological studies of thalamic cells involved in the generation of rhythmic output have revealed a nonspecific, voltage independent outward cation current activated by $[Ca^{2+}]_i$, I_{CAN}. It is assumed to have the same activation scheme as the AHP current but with slower kinetics and is expressed as follows (Destexhe et al., 1994):

$$I_{CAN}=\bar{g}_{CAN}\, m^2\, (V-E_{CAN}) \tag{3.42}$$

where

$$\bar{g}_{CAN} = 0.00025 \ \ S/cm^2$$
$$E_{CAN} = -20 \ \ mV \tag{3.43}$$

The steady-state activation variable m is described by a differential equation:

$$\frac{dm}{dt}=\frac{m_\infty - m}{\tau_m} \tag{3.44}$$

where

$$m_\infty = \frac{20 * [Ca^{2+}]_i^2}{20 * [Ca^{2+}]_i^2 + 0.002}$$
$$\tau_m = \frac{1}{20 * [Ca^{2+}]_i^2 + 0.002} \tag{3.45}$$

3.2.8 Hyperpolarization-activated Cation Current I_h

An inward, mixed K^+/Na^+, hyperpolarization activated current I_h has been identified in rhythm-generating circuits including networks of motoneurons in the turtle spinal cord (Kiehn et al., 1997; Hounsgaard et al., 1988), and tharmocortical relay neurons (McCormick et al., 1990). Mathematical description of the h-current has been derived

from data obtained with voltage-clamp recordings of guinea pig dorsal lateral geniculate relay neurons maintained in vitro as a thalamocortical slice (McCormick et al., 1990; Huguenard et al., 1992). The h-current is expressed as follows:

$$I_h = \bar{g}_h \; m \; (V - E_h) \tag{3.46}$$

where

$$\bar{g}_h = 2e\text{-}5 \;\; S/cm^2$$
$$E_h = -40 \;\; mV \tag{3.47}$$

The steady-state activation variable m is described by a differential equation:

$$\frac{dm}{dt} = \frac{m_\infty - m}{\tau_m} \tag{3.48}$$

where

$$m_\infty = \frac{1}{1 + exp[-(V + 75)/5.5]}$$
$$\tau_m = \frac{1}{exp(-0.086V - 14.59) + exp(0.0701V - 1.87)} \tag{3.49}$$

3.3 Synaptic Receptors

Synaptic channels change their conductance to certain ions when the appropriate chemical stimulus binds to the receptor associated with these channels. The synaptic current I_{syn} is

$$I_{syn} = g_{syn}(V - E_{syn}) \tag{3.50}$$

A convenient expression for time-varying conductance waveform g_{syn} is based on the alpha function derived from the cable theory by Rall (1967):

$$g_{syn} = \bar{g}_{syn}\, \alpha\, t^{\alpha}\, exp(-\alpha t / \tau) \tag{3.51}$$

where τ is the time-to-peak of the conductance transient and α is constant. This function increases rapidly to a maximum of $\alpha\ \tau^{\alpha}/e^{\alpha}$ at $t = \tau$. Following its peak, $g_{syn}(t)$ decreases more slowly. A powerful synapse, which opens many channels and produces a significant conductance change, is modeled by a relatively small τ and a large g_{syn}. A slow synapse is modeled by a relatively large τ and a small g_{syn}. The alpha function has a few drawbacks: (1) the relationships to actual synaptic conductances is based only on an appropriate correspondence of the time-course of the waveform to physiological recordings of the post-synaptic response, rather than plausible biophysical mechanisms; (2) summation of multiple waveforms can be cumbersome, and (3) there is no natural provision for saturation of the conductance.

An alternative approach to modeling synaptic connections is based on a kinetic model. This approach allows a more realistic biophysical representation and is consistent with

the HH formalism. Furthermore, complex three-state and higher schemes of the kinetic model can be simplified to make them more efficient while retaining the most important properties. A two-state kinetic scheme developed by Destexhe et al. (1998 and 1994) was used to simulate the synaptic receptors in this study.

3.3.1 AMPA/Kainate Receptor

The simple model that approximates the kinetics of the fast AMPA/Kainate receptor is represented by the two-state diagram (Destexhe et al., 1998):

$$C + T \underset{\beta}{\overset{\alpha}{\rightleftarrows}} O \tag{3.52}$$

where α and β are voltage independent forward and backward rate constants for transmitter binding. The postsynaptic current I_{AMPA} is given by:

$$I_{AMPA} = \bar{g}_{AMPA} r (V - E_{AMPA}) \tag{3.53}$$

where r represents the fraction of the receptors in the open state and is expressed:

$$\frac{dr}{dt} = \alpha [T](1-r) - r\beta \tag{3.54}$$

Because T is assumed to occur as a pulse in the synaptic cleft, such as $[T] = T_{max}$ for $t_0 < t < t_1$, the above equation can be solved as follows:

When the pulse is on ($t_0 < t < t_1$) and the transmitter is being released ($[T] > 0$)

$$r(t - t_0) = r_\infty + (r(t_0) - r_\infty) exp(-(t - t_0)/\tau_r) \tag{3.55}$$

When the pulse is off ($t > t_1$) and $[T] = 0$

$$r(t-t_1) = r(t_1)\ exp(-\beta(t-t_1)) \tag{3.56}$$

where

$$r_\infty = \frac{\alpha T}{\alpha T+\beta} \qquad \tau_r = \frac{1}{\alpha T+\beta} \tag{3.57}$$

and $r(t_0)$ and $r(t_1)$ represent open channels at the start and end of release, respectively.

The best fit of this kinetic scheme to whole-cell recorded I_{AMPA} obtained from rat hippocampal slices yields the following (Destexhe et al., 1998):

Table 3.4. AMPA receptor parameters.

Variable	Units	Value
Forward (binding) rate α	$msec^{-1}\ mM^{-1}$	1.1
Backward (unbinding) rate β	$msec^{-1}$	0.19
Reversal potential E_{AMPA}	mV	0
Maximum transmitter concentration C_{max}	mM	1
Transmitter duration (raising phase) T_{dur}	msec	1

The simulation results of the AMPA receptor are presented in Figure 3.10. The PSP amplitude is proportional to the number of presynaptic spikes.

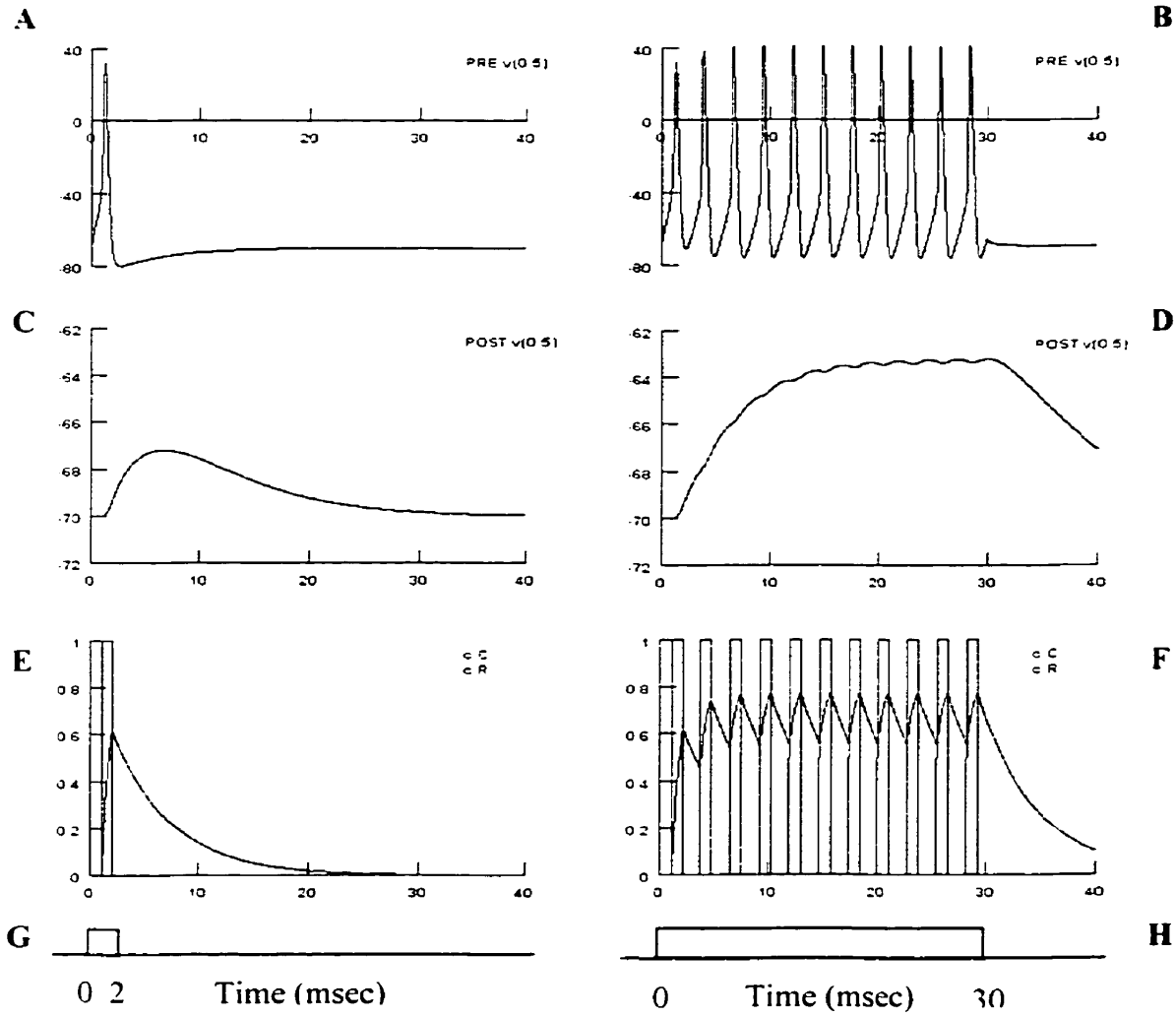

Figure 3.10. Simulation of summation of postsynaptic potentials in the model of AMPA synapse. A-B: Presynaptic voltage (mV). C-D: Postsynaptic voltage (mV). E-F: Transmitter release (mM) and fraction of open channels, for a single and multiple APs respectively. G-H: Stimulation current applied at the soma of the presynaptic cell.

3.3.2 NMDA Receptor

The NMDA receptor is represented by a two-state model (Equation 3.52). The postsynaptic current I_{NMDA} is

$$I_{NMDA} = \bar{g}_{NMDA} r \; M(V - E_{NMDA}) \tag{3.58}$$

where r represents the fraction of the receptors in the open state (Equations 3.54-3.57) and M represents the voltage-dependent magnesium block:

$$M(V) = \frac{1}{1 + \frac{[Mg^{2+}]_o \, exp(-0.062V)}{3.57}} \tag{3.59}$$

The unique and important property of the NMDA receptor channel is its sensitivity to block by a physiological concentration of Mg^{2+}. The block is voltage-dependent, allowing NMDA receptor channels to conduct ions only when depolarized.

Experimental data for the NMDA receptor obtained from the whole-cell recording from rat hippocampal slices are given in Table 3.5 (Destexhe et al., 1998):

Table 3.5. NMDA receptor parameters.

Variable	Units	Values
Forward (binding) rate α	$msec^{-1}\ mM^{-1}$	0.072
Backward (unbinding) rate β	$msec^{-1}$	0.0066
Reversal potential E_{NMDA}	mV	0
Maximum transmitter concentration C_{max}	mM	1
Transmitter duration (raising phase) T_{dur}	msec	1
External Mg^{2+} concentration $[Mg^{2+}]_o$	mM	1

NMDA receptor mediates synaptic currents that are substantially slower than AMPA/kainate currents. The simulation results of the AMPA receptor are presented in Figure 3.11.

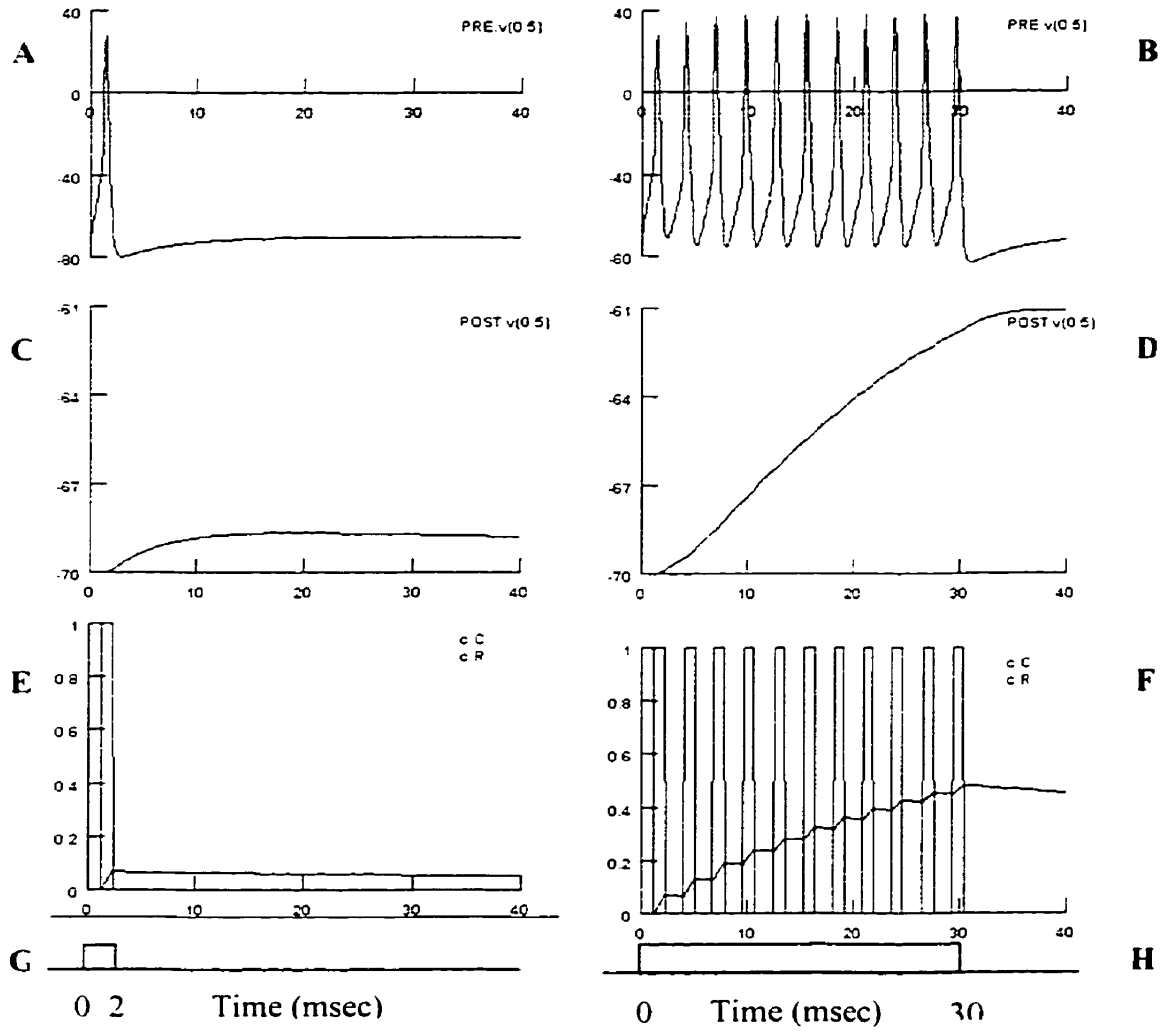

Figure 3.11. Simulation of summation of postsynaptic potentials in the model of NMDA synapse. A-B: Presynaptic voltage (mV). C-D: Postsynaptic voltage (mV). E-F: Transmitter release (mM) and fraction of open channels, for a single and multiple APs respectively. G-H: Stimulation current applied at the soma of the presynaptic cell.

3.3.3 $GABA_A$ Receptor

The $GABA_A$ receptor is also represented by a two-state model (Equation 3.52). The postsynaptic current I_{GABAa} is

$$I_{GABAa} = \bar{g}_{GABAa} r\ (V - E_{GABAa}) \tag{3.60}$$

where r represents the fraction of the receptors in the open state (Equations 3.54-3.57)

Experimental data for the $GABA_A$ receptor obtained from the whole-cell recording from rat hippocampal slices are given in Table 3.6 (Destexhe et al., 1998):

Table 3.6. $GABA_A$ receptor parameters

Variable	Units	Value
Forward (binding) rate α	$msec^{-1}\ mM^{-1}$	0.53
Backward (unbinding) rate β	$msec^{-1}$	0.18
Reversal potential E_{GABAa}	mV	-80
Maximum transmitter concentration T_{max}	mM	1
Transmitter duration C_{dur}	msec	1

The simulation results of the $GABA_A$ receptor are presented in Figure 3.12.

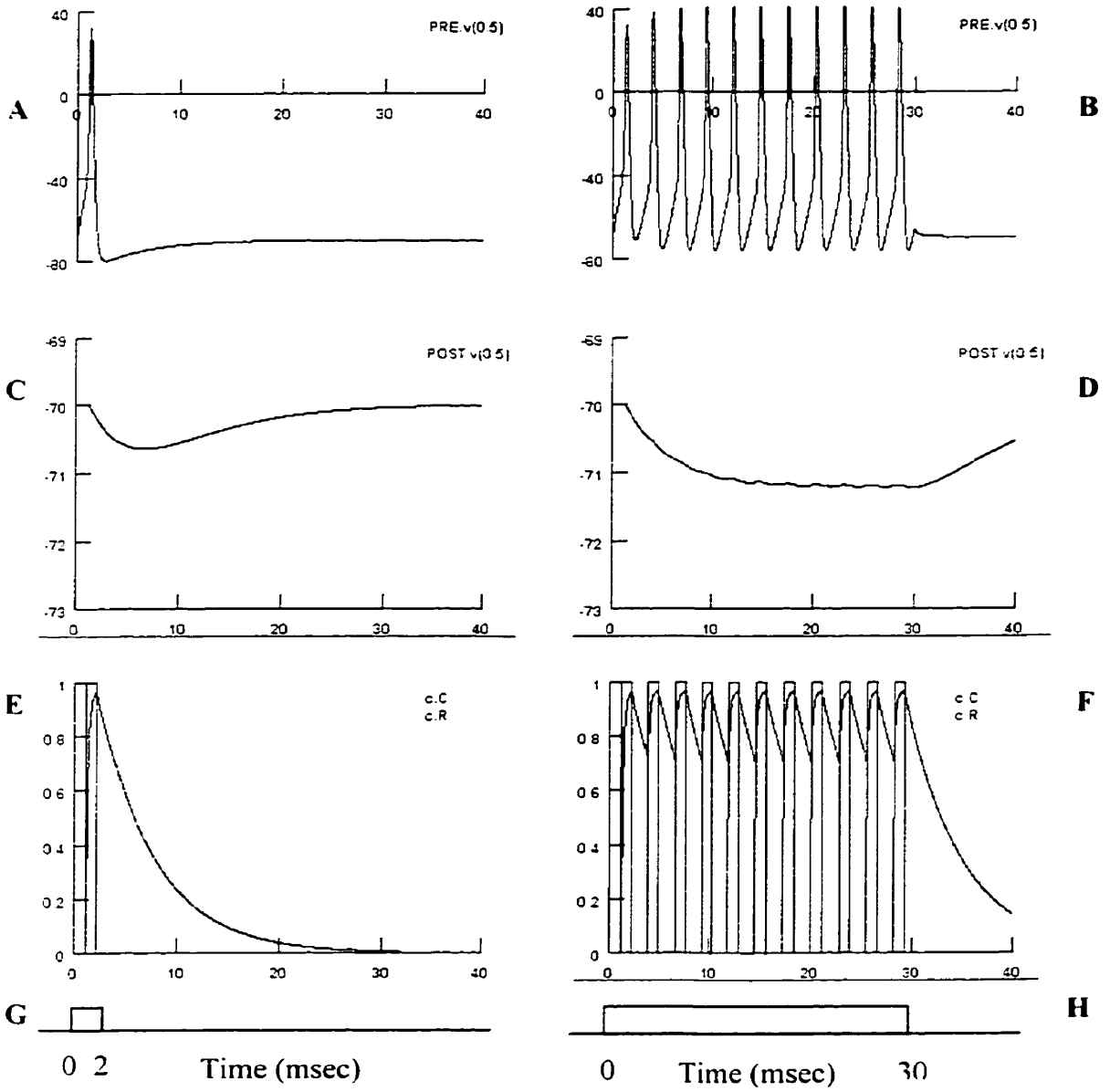

Figure 3.12. Simulation of summation of postsynaptic potentials in the model of $GABA_A$ synapse. A-B: Presynaptic voltage (mV). C-D: Postsynaptic voltage (mV). E-F: Transmitter release (mM) and fraction of open channels, for a single and multiple APs respectively. G-H: Stimulation current applied at the soma of the presynaptic cell.

3.3.4 $GABA_B$ Receptor

In contrast to the AMPA, NMDA, and $GABA_A$ receptors, where the receptor and ion channels are both part of the same protein complex, the electrical response to stimulation of the $GABA_B$ receptor is mediated by K^+ channels that are not directly coupled to the receptor and are activated when neurotransmitter binds to G-proteins. To produce responses, $GABA_B$ receptors require a high level of presynaptic activity. Here the transmitter T binds to the receptor R_O, leading to its activation to form R. The G-protein is transformed from its inactive (GDP-bound) form G_O to an activated form G. Finally, G binds to open the K^+ channel. This leads to the following kinetic scheme:

$$\frac{dr}{dt} = K_1[T]*(1-r) - K_2 r$$

$$\frac{dGP}{dt} = K_3 r - K_4[GP] \tag{3.61}$$

$$GP = \frac{[GP]^n}{[GP]^n + K_D}$$

where r represents fraction of activated receptors, GP represents the G-protein – K^+ interaction, n is the Hill coefficient, which, in the simplest case, represents the number of binding sites, K_D is the dissociation constant of the binding of G-protein on the K^+ channels, T is a transmitter, and K_1, K_2, K_3, and K_4 are kinetic rate constants. The postsynaptic current I_{GABAb} is:

$$I_{GABAb} = \bar{g}_{GABAb} \frac{[GP]^n}{[GP]^n + K_D} (V - E_K) \tag{3.62}$$

The best fit of this kinetic scheme to whole-cell recorded $GABA_B$ currents yields the parameters listed in Table 3.7 (Destexhe et al., 1998):

Table 3.7. $GABA_B$ receptor parameters.

Variable	Units	Values
Dissociation constant of G-protein binding on the K^+ channels K_D	μM	100
Number of binding sites n		4
Forward (binding) rate to receptor K_1	$msec^{-1}\ mM^{-1}$	0.09
Backward (unbinding) rate of receptor K_2	$msec^{-1}$	0.0012
Rate of G-protein production K_3	$msec^{-1}$	0.180
Rate of G-protein decay K_4	$msec^{-1}$	0.034
Potassium reversal potential E_K	mV	-90
Maximum transmitter concentration T_{max}	mM	1
Transmitter duration T_{dur}	msec	0.3

The simulation results of the $GABA_B$ receptor are depicted in Figure 3.13. In contrast to the transmitter-gated receptor types (i.e., AMPA, NMDA, and $GABA_A$), a single postsynaptic potential cannot activate enough G-protein to evoke detectable currents. $GABA_B$-mediated currents are evoked when a burst of presynaptic spikes occurs.

The simulation results presented in Figures 3.10 – 3.13 are comparable with the simulation results published in the literature by Destexhe et. al., (1998, pages 1-25, Figure 1.4).

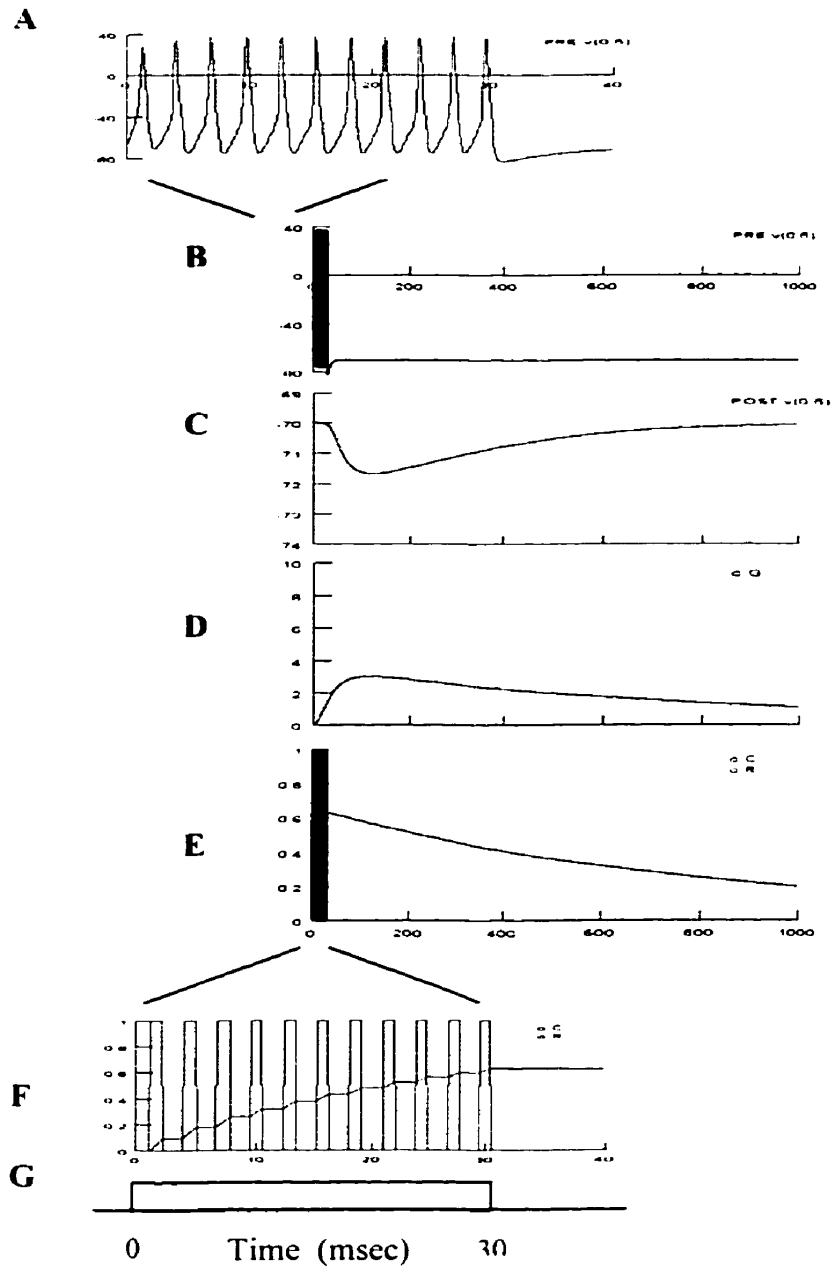

Figure 3.13. Simulation of summation of postsynaptic potentials in the model of $GABA_B$ synapse. A-B: Presynaptic voltage (mV). C: postsynaptic voltage (mV). D: Concentration of G-protein; and E-F: transmitter release (mM) and fraction of open channels for multiple APs.

3.4 Model of the Neuron

The model of the neuron has several anatomical features (sections) whose existence and spatial relationships include the soma, the dendrites and the axon. While the cytoplasmic resistivity is assumed to be uniform throughout the cell, the geometry and electrical properties of each section may be different. The soma is modeled as a sphere, the dendrites and the axon as a cylinder. The axon and the dendrites arise from opposite sides of the soma. The electrical and chemical signals distributed over the membrane of the cell are modeled as density mechanisms and point processes. The density mechanisms are described in terms of current per unit area and conductance per unit area and include ionic channels that define the biophysical mechanisms in each section. The point processes include synapses and electrodes. The model emulates the use of an electrode to inject a stimulating current into the section by placing a current pulse stimulus in the middle of the section. The stimulus is defined by its amplitude, duration, and delay. The model of the neuronal network is created by linking the models of the neurons with the synapses.

For a given model of the neuron, the geometry, membrane properties, and ionic channels were set based the data published in the literature. The characteristics of the stimulation current, however, were set based on the results of simulation experiments with the main objective to obtain the same or similar results as published in the literature.

4 RESULTS - MODELS OF ELEMENTARY NETWORKS

The models of conductances and synapses described in Chapter 3 were used in the computer simulation experiments of elementary rhythm-generating networks. In all simulations, the integration time step was set to 0.025msec. These simulation experiments primarily focused on:

1. Identification of a minimal set of the cellular, synaptic, and network properties that are essential for the initiation and generation of rhythmic output.
2. Exploration of the relationships between parameters of ionic currents and characteristics of rhythmic output in response to external stimuli in the elementary rhythm-generating circuits.
3. Conducting sensitivity analyses of the model output to changes in model variables. The rhythmic output generated by the models has been described by three variables: number of action potentials per burst (AP/B), burst firing rate (BFR), and burst frequency (BF).

The models of the elementary networks include the reciprocal inhibition network, the feedback inhibition network, the reciprocal excitation network, and the parallel excitation and inhibition network. To facilitate the process of building these elementary networks, a model of a neuron composed of the soma, the axon, and a single dendrite was designed. The properties of the model were based on the properties of the rat thalamic reticular neurons (Destexhe et al., 1994). In this model the soma and axon contain HH-type sodium, potassium, and passive channels, while the dendrite has passive channels (Table

4.1). This model neuron was then augmented by inserting additional ionic channels and other properties as required for a specific simulation experiment.

Table 4.1. Anatomical and biophysical properties of the model neuron.

Variable	Description	Units	Value
Global variables			
Ra	The cytoplasmic resistivity	ohm-cm	100
Vinit	The initial membrane voltage	mV	-70
cm	The capacitance	$\mu F/cm^2$	1
celsius	The temperature	°C	36
Soma			
L	The length of the section	μm	100
diam	The diameter	μm	100
nseg	The number of segments		1
Axon	The initial membrane voltage		-70
L	The length of the section	μm	1000
diam	The diameter	μm	10
nseg	The number of segments		10
Dendrite			
L	The length of the section	μm	200
diam	The diameter	μm	10
nseg	The number of segments		5
HH-type current			
gmax_iNa	The maximum specific Na^+ conductance	S/cm^2	0.1
gmax_iK	The maximum specific K^+ conductance	S/cm^2	0.01
gmax_p	The maximum specific passive conductance	S/cm^2	0.0005
ena	The reversal potential for Na^+ channel	mV	50
ek	The reversal potential for K^+ channel	mV	-95
ep	The reversal potential for passive channel	mV	-78

4.1 Reciprocal Inhibition Network

Reciprocal inhibition between populations of neurons was proposed by Brown (1914) as a pattern-generating mechanisms in walking cats. Reciprocal inhibition is a common feature of rhythm-generating circuits in many species and is regarded as the mechanism producing stable alternating bursts of activity (Friesen and Stent, 1978; Arbas and Calabrese, 1987; Getting, 1989; Satterlie, 1985; Marder et al., 1997).

4.1.1 Model of the Reciprocal Inhibition Network

The model of the reciprocal inhibition network is composed of two neurons reciprocally connected with inhibitory synapses as depicted in Figure 4.1.

Figure 4.1. Model of the reciprocal inhibition network.

The model neurons defined in Table 4.1 were augmented by adding the T-current, and the Ca^{2+}-pump. The neurons were connected with the $GABA_A$ synapses. The geometry and electrophysiological properties of both cells were assumed to be identical. The stimulation currents applied to the somas had different amplitudes and were offset by 10 msec (Table 4.2).

Table 4.2. Properties of the reciprocal inhibition network.

Variable	Description	Units	Cell 0&1
	Properties listed in Table 4.1		Yes
T-current			
gmax_iT	The maximum specific Ca^{2+} conductance	S/cm^2	0.002
eca	The reversal potential for Ca^{2+} channel	mV	120
Ca-pump			
eca	The reversal potential for Ca^{2+} channel	mV	120
GABAa			
Cmax	Maximum transmitter concentration	mM	1
Cdur	Transmitter duration (raising phase)	msec	1
Alpha	Forward binding rate	/msec mM	0.53
Beta	Backward unbinding rate	/msec	0.18
Erev	Reversal potential	mV	-80
Deadtime	Maximum time between release events	msec	1
Prethresh	Voltage level for release	mV	0
gmax_gabaa	Maximum synaptic conductance	nS	1
Stimulation			Cells 0/1
amp	Stimulation amplitude	nA	0.2/0.3
dur	Stimulation duration	msec	100
del	Stimulation delay	msec	0/10

An example of oscillatory behaviour of two cells interconnected with $GABA_A$ synapses is presented in Figure 4.2.

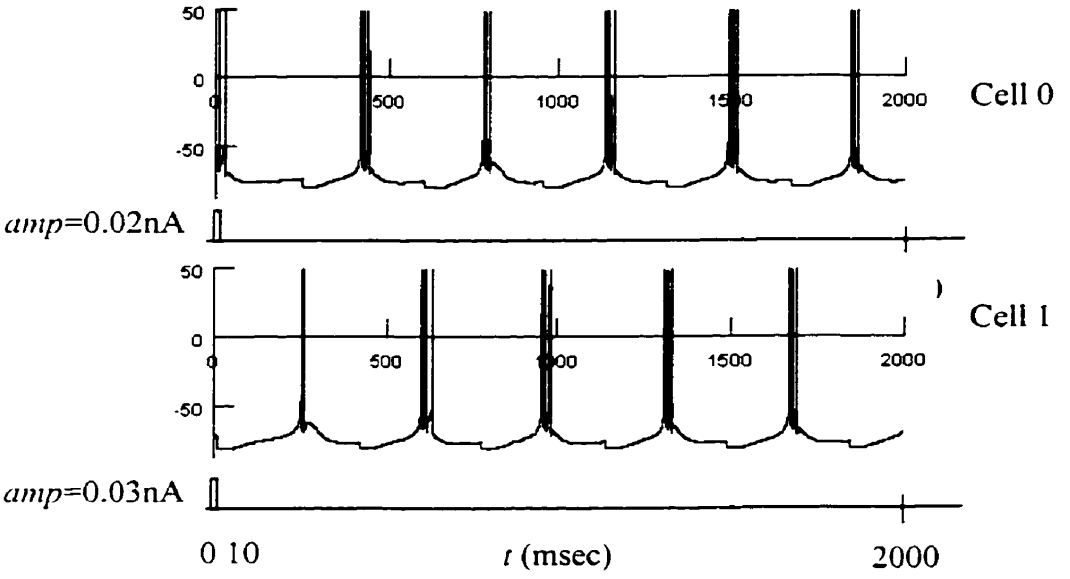

Figure 4.2. Oscillatory output generated by the reciprocal inhibition network. Both cells (Cell 0 and Cell 1) have identical conductances (HH-type, T-current, and Ca^{2+} pump) and are connected via $GABA_A$ synapses with identical properties and synaptic strength. Different stimulation currents have been applied at the somas to create asymmetry between cells (Cell 0: *amp* = 0.2 nA, *dur* = 10 msec and *delay* = 0 msec; Cell 1: *amp* = 0.3 nA, *dur* = 10 msec, *delay* = 10 msec).

The ionic currents and synaptic properties involved in the generation of bursts presented in Figure 4.2 are depicted in Figure 4.3.

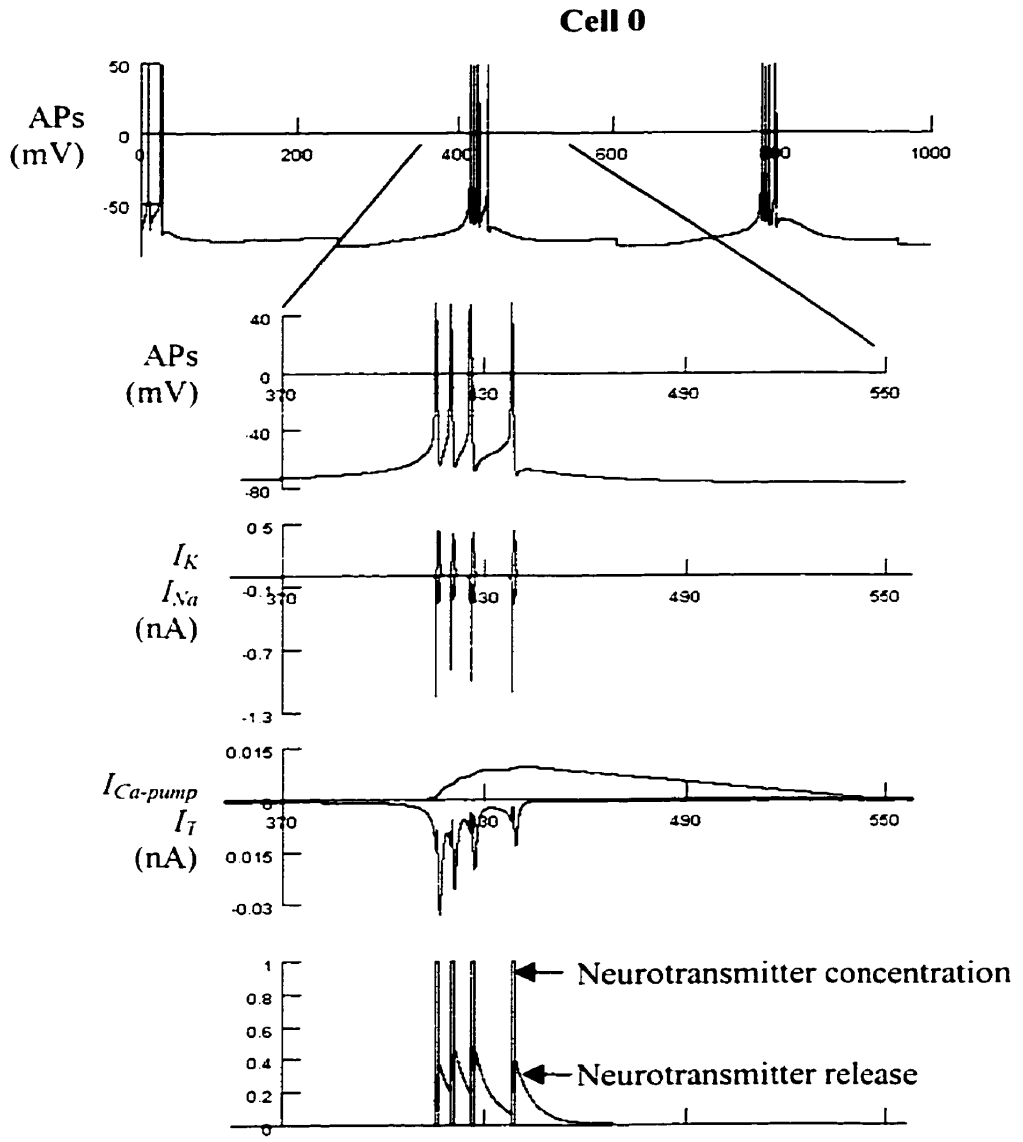

Figure 4.3. Action potentials, ionic currents, and synaptic properties exhibited by Cell 0 in the reciprocal inhibition network.

The inward T-current with fast kinetics and the outward Ca^{2+} pump with slow kinetics play key roles in the generation of alternating bursts. While the T-current (in conjunction with the fast K^+ and Na^+ currents) activate Cell 0 resulting in a production of bursts, the

Ca^{2+} pump inactivates the cell at a much slower pace causing a decrease of its membrane potential necessary for the production of bursts and for graded synaptic transmission. This inactivation subsequently shuts Cell 0 down leading to releasing Cell 1 from inhibition. This results in the generation of bursts in Cell 1 and inhibition of Cell 0. The same sequence of events is repeated in Cell 1. Two reciprocally inhibitory cells can produce stable oscillations even in the absence of tonic excitatory input. In case tonic excitatory input is supplied, the period and burst duration increases with increasing excitatory input.

In the absence of either the T-current or the Ca^{2+} pump the pattern of activation and inactivation of the cells is altered and the reciprocal inhibition network does not produce alternating bursts. In the absence of the Ca^{2+} pump, the model lacks the mechanism of termination the bursts through hyperpolarization. In the case when the T-current is absent, the model lacks the mechanism that produces the sustained depolarization and initiates and maintains the bursts. Figure 4.4 depicts the output produced by the model of the reciprocal inhibition network with the HH-type channels and the Ca^{2+} pump only. The original stimulation of the model defined in Table 4.1 with the currents of 0.2 nA (Cell 0) and 0.3 nA (Cell 1) was not sufficient to produce APs (Figure 4.4A). When the level of stimulation increased to 0.4 nA (Cell 0) and 0.6 nA (Cell 1), Cell 1 generated single APs, which inhibited Cell 0 preventing its firing (Figure 4.4B). Increasing the level of stimulation to 0.6 nA for both cells resulted in the production of single APs in both cells (Figure 4.4C). The model, however, was not capable of producing bursts.

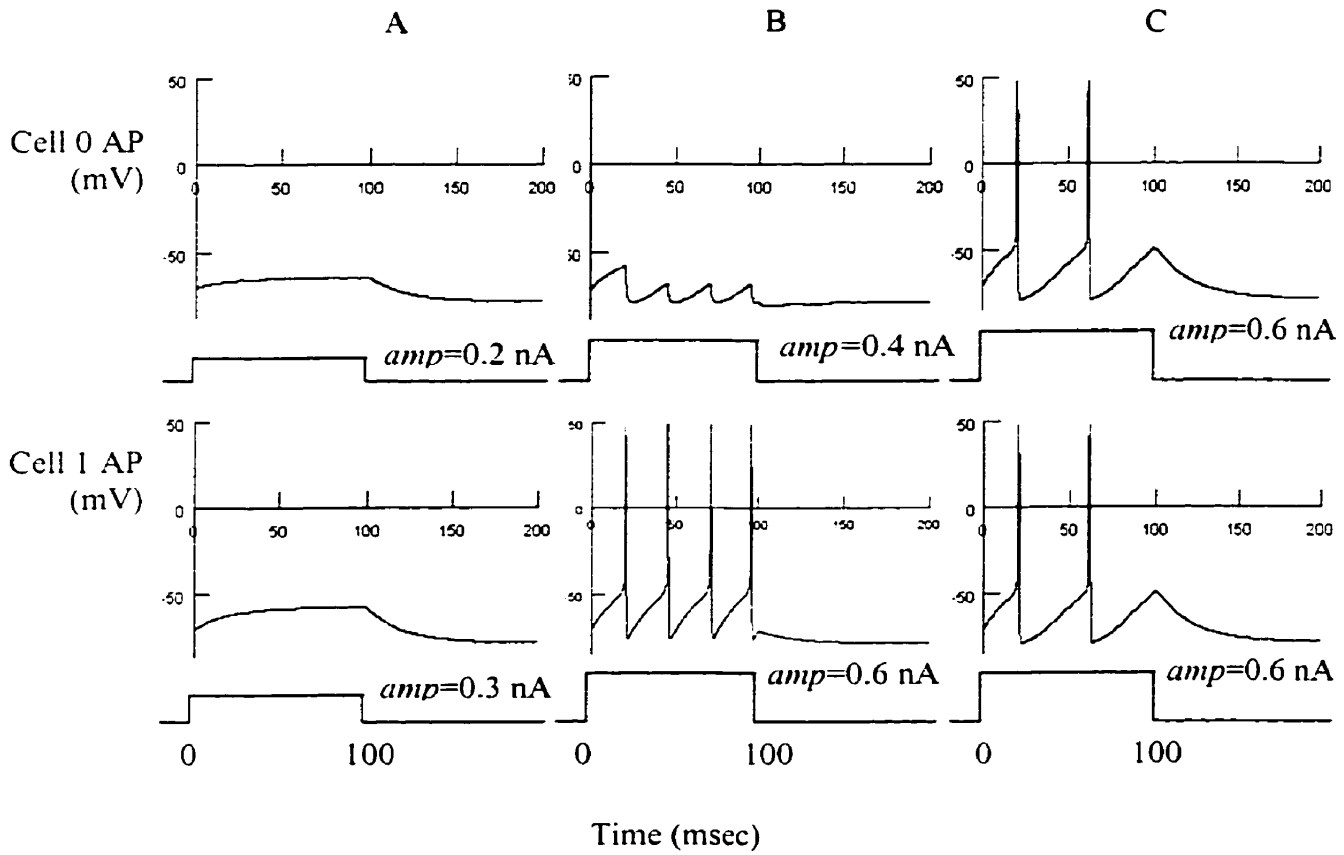

Figure 4.4. The output generated by the model of the reciprocal inhibition network in the absence of the T-current. A: The model output when the model is stimulated with the current of 0.2 nA (Cell 0) and 0.3 nA (Cell 1). B: The model output for an increased level of stimulation to 0.4 nA and 0.6 nA at Cell 0 and Cell 1, respectively. C: Further increase in the level of stimulation to 0.6 nA at both cells results in the production of synchronous APs.

Addition of the afterhyperpolarization (AHP) current defined in Table 4.3 to the model of the reciprocal inhibition network with properties defined in Table 4.2 changed the characteristics of the bursts (Figure 4.4).

Table 4.3. Properties of the AHP current.

Variable	Description	Units	Cell 0&1
gmax_iAHP	The max. specific K^+ (Ca^{2+}) conductance	S/cm^2	0.01
eca	The reversal potential for K^+ (Ca^{2+}) channel	mV	-95

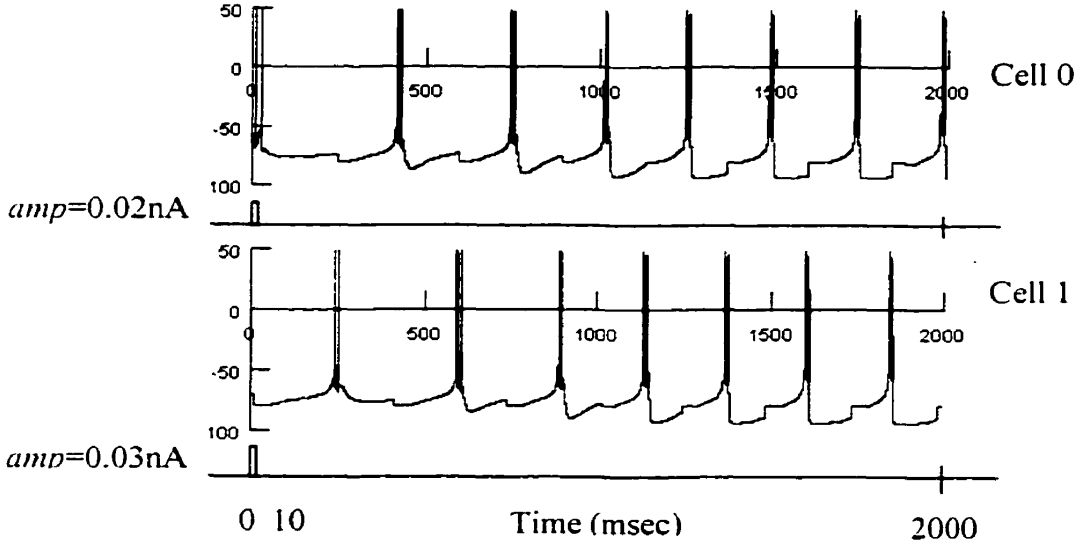

Figure 4.5. Oscillatory output generated by the reciprocal inhibition network. Both cells (Cell 0 and Cell 1) have identical conductances (HH-type, T-current, AHP current, and Ca^{2+} pump) and are connected via $GABA_A$ synapses with identical properties and synaptic strength. Different stimulation currents have been applied at the somas to create asymmetry between cells (Cell 0: *amp* = 0.2 nA, *dur* = 10 msec and *delay* = 0 msec; Cell 1: *amp* = 0.3 nA, *dur* = 10 msec, *delay* = 10 msec).

As each action potential occurs, Ca^{2+} enters the cell through high-threshold channels giving rise to the activation of the AHP current, which hyperpolarizes the cell, resulting in a decrease of number of spikes produced in a single burst and a much more pronounced hyperpolarization after the bursts occur.

For the reciprocal inhibition network to produce bursts, a minimum set of ionic conductances is required, namely: HH-type currents (i.e., the fast Na^+, and K^+ currents, and the passive current), along with the T-current (a low-threshold Ca^{2+} current) and the Ca^{2+} pump. The AHP current also plays an important role in the generation of rhythmic output. If an asymmetric stimulation or an asymmetry in neuronal properties are present, the model generates alternating bursts. If neither of the two conditions are met, the generated output is synchronous.

4.1.2 Sensitivity Analysis of the Reciprocal Inhibition Network

Sensitivity analyses performed for three ionic conductances (fast Na^+, fast K^+, and the T-current) and the maximum synaptic conductance for the $GABA_A$ synapse revealed significant changes in the model behavior. The changes in the characteristics of rhythmic output for a range of values of the maximum specific channel conductance for the fast Na^+ current, *gmax_iNa*, where $0.01 < gmax\_iNa < 0.4$ S/cm^2 are presented in Figure 4.6.

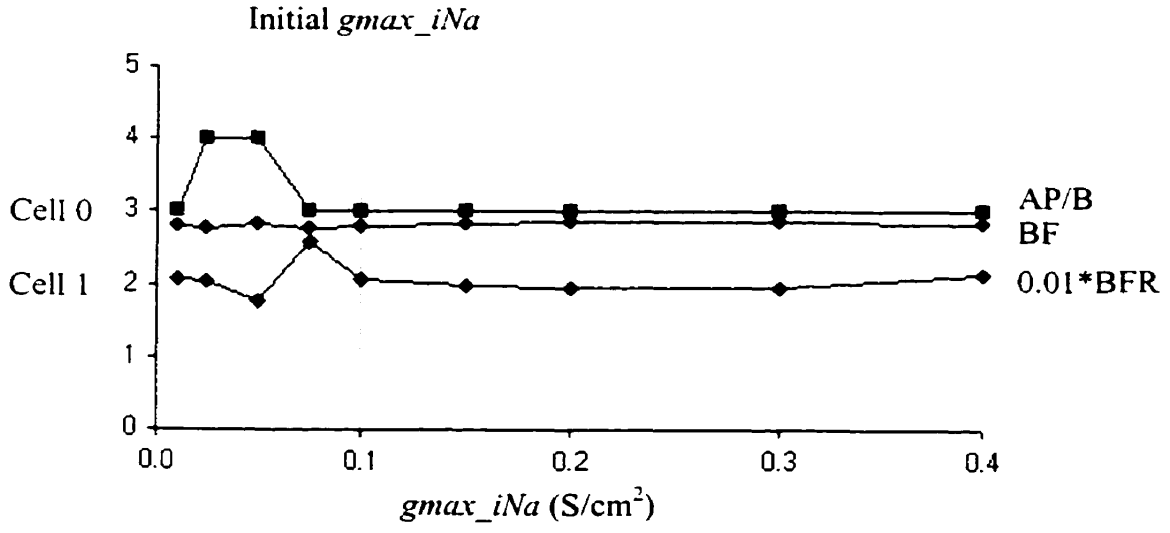

Figure 4.6. Steady-state measures of burst features change with the maximum specific channel conductance for the fast Na^+ current (HH-type), *gmax_iNa*, in the model of the reciprocal inhibition network. The initial value of *gmax_iNa* is set to 0.1 S/cm^2 (Equation 3.2).

Setting *gmax_iNa* below 0.01 S/cm^2 shut down the network. Increasing *gmax_iNa* from 0.01 to 0.05 S/cm^2 resulted in an increase of number of APs per burst and a decrease in burst firing rate. Increasing *gmax_iNa* to the value of 0.1 S/cm^2 (Equation 3.2) resulted in a decrease of number of APs per burst and a transition (an increase followed by a decrease) in burst firing rate. Further increase of *gmax_iNa* to 0.4 S/cm^2 resulted in a small change in burst firing rate and no change in the number of APs per burst. No significant changes in burst frequency occurred for $0.01 < gmax\_iNa < 0.4$ S/cm^2.

The changes in the characteristics of rhythmic output for a range of values of the maximum specific channel conductance for the fast K^+ current, *gmax_iK*, where 0.0042 < *gmax_iK* < 0.05 S/cm^2 are presented in Figure 4.7.

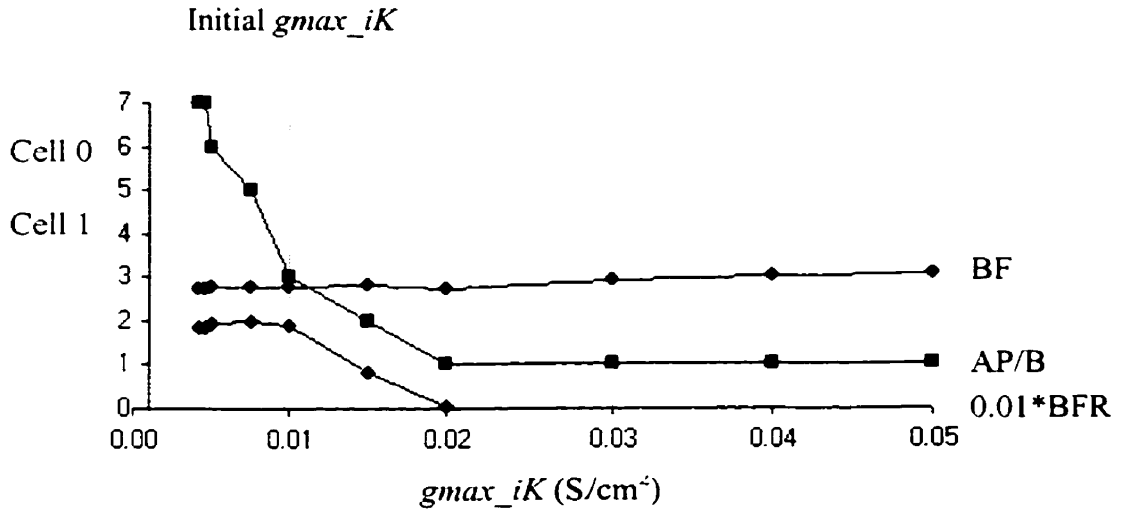

Figure 4.7. Steady-state measures of burst features change with the maximum specific channel conductance for the fast K^+ current (HH-type), *gmax_iK*, in the model of the reciprocal inhibition network. The initial value of *gmax_iK* is set to 0.01 S/cm^2 (Equation 3.6).

Setting *gmax_iK* below 0.0042 S/cm^2 shut down the network. Increasing *gmax_iK* to the value of 0.01 S/cm^2 (Equation 3.6) resulted in a change (an increase followed by a decrease) in burst firing rate and a decrease in the number of action potential per burst. Further increase of *gmax_iK* to 0.02 S/cm^2 resulted in a sharp decrease in burst firing rate and further decrease in the number of APs per burst. No significant changes in bursting features occurred for 0.02 < *gmax_iK* < *0.05* S/cm^2.

The changes in the characteristics of rhythmic output for a range of values of the maximum specific channel conductance for the T-current, *gmax_iT*, where 0.0017 < *gmax_iT* < 0.01 S/cm^2 are presented in Figure 4.8. Setting *gmax_iT* below 0.0017 S/cm^2 shut down the network. Increasing *gmax_iT* to the value of 0.002 S/cm^2 (Equation 3.36) resulted in a rapid increase in burst firing rate and the number of APs per burst, and a small increase in burst frequency. Further increase in *gmax_iT* to the value of 0.01 S/cm^2 resulted in a monotonic increase in the number of APs per burst and small changes in burst firing rate and burst frequency.

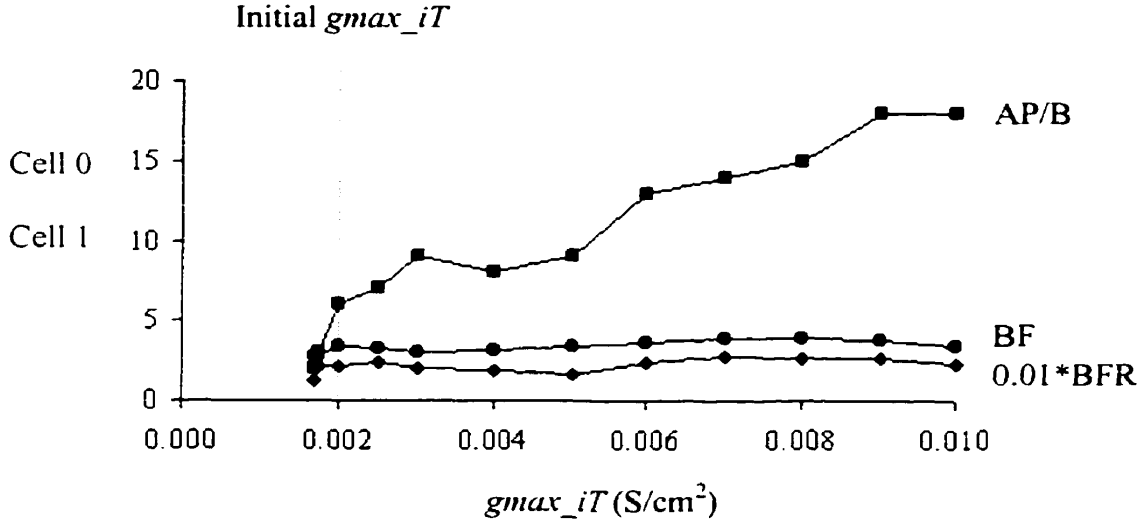

Figure 4.8. Steady-state measures of burst features change with the maximum specific channel conductance for the T-current, *gmax_iT*, in the model of the reciprocal inhibition network. The initial value of *gmax_iT* is set to 0.002 S/cm^2 (Equation 3.36).

Figure 4.9 presents the changes in the characteristics of rhythmic output for a range of values of the maximum synaptic conductance for the GABAa synapse, *gmax_gabaa*, where 0.5 < *gmax_gabaa* < 1.1 nS. Setting *gmax_gabaa* below 0.5 nS shut down the network. Increasing *gmax_gabaa* to the value of 1.0 nS resulted in small changes (decreases followed by increases) in burst firing rate and a small increase in the number of APs per burst. Further increase of *gmax_gabaa* to 1.1 nS resulted in an increase in burst frequency rate and a decrease in the number of APs per burst. In general, the characteristics of the rhythmic output vary smoothly with changes in *gmax_gabaa* for the GABAa synapse.

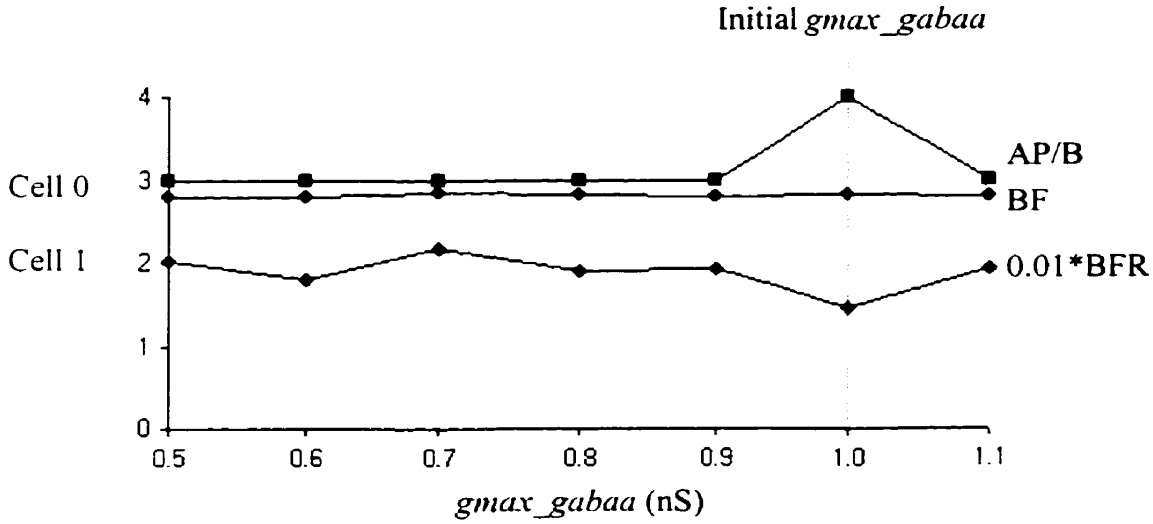

Figure 4.9. Steady-state measures of burst features change with the maximum synaptic conductance for the $GABA_A$ synapse, *gmax_gabaa*, in the model of the reciprocal inhibition network. The initial value of *gmax_gabaa* is set to 1.0 nS.

4.2 Feedback Inhibition Network

A feedback inhibition network formed by two neurons where one neuron excites a second neuron, which then inhibits the first neuron has been studied extensively to explain the generation of the mammalian respiratory rhythm generation (Wyman, 1977). The feedback inhibition network has been found in rhythm-generating circuits the lamprey (Grillner et al., 1992), the medulla (Wyman, 1977), and the mollusc *Tritonia* (Getting, 1989).

4.2.1 Model of the Feedback Inhibition Network

The model of the feedback inhibition network is composed of two neurons where one neuron (Cell 0) excites the second neuron (Cell 1), which then inhibits the first neuron (Figure 4.10)

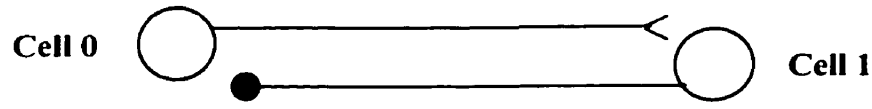

Figure 4.10. The model of the feedback inhibition network.

Two model neurons defined in Table 4.1 were used to build the model of the feedback inhibition network. The neurons were connected with the AMPA and $GABA_A$ synapses. The stimulation current was applied at the soma of Cell 0. Table 4.4 lists the properties of the model of the network.

Table 4.4. Properties of the feedback inhibition network.

Variable	Description	Units	Cell 0	Cell 1
	Properties listed in Table 4.1		Yes	Yes
GABAa				
Cmax	Maximum transmitter concentration	mM		1
Cdur	Transmitter duration (rising phase)	msec		1
Alpha	Forward binding rate	/msec mM		0.53
Beta	Backward unbinding rate	/msec		0.18
Erev	Reversal potential	mV		-80
Deadtime	Maximum time between release events	msec		1
Prethresh	Voltage level for release	mV		0
gmax_gabaa	Maximum synaptic conductance	nS		1
AMPA				
Cmax	Maximum transmitter concentration	mM	1	
Cdur	Transmitter duration (rising phase)	ms	1	
Alpha	Forward binding rate	/msec mM	1.1	
Beta	Backward unbinding rate	/msec	0.19	
Erev	Reversal potential	mV	0	
Deadtime	Maximum time between release events	msec	1	
Prethresh	Voltage level for release	mV	0	
gmax_ampa	Maximum synaptic conductance	nS	1	
Stimulation				
amp	Stimulation amplitude	nA	0.2	
dur	Stimulation duration	msec	2000	
del	Stimulation delay	msec	0	

An example of oscillatory behaviour of the feedback inhibition networks is depicted in Figure 4.11.

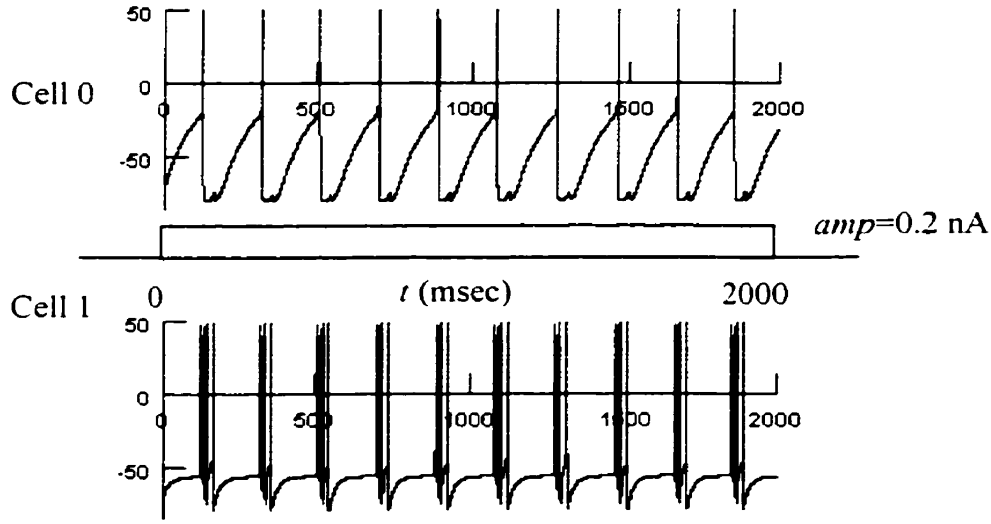

Figure 4.11. Oscillatory output generated by the feedback inhibition network. Both cells Cell 0 and Cell 1 have identical conductances in soma, axon and dendrite (HH-type, and Ca^{2+} pump) and are connected via $GABA_A$ and AMPA synapses. Identical stimulation currents have been applied at the somas of Cell 0 and Cell 1: *amp* = 0.2 nA, *dur* = 2000 msec and *delay* = 0.

The action potentials generated by Cell 0 due to the stimulation applied at the soma generates an excitatory postsynaptic potential and produces bursts in Cell 1. These bursts generate inhibitory postsynaptic potentials in Cell 0 resulting in shutting down its activity. The stimulation current applied to the soma of Cell 0 assists in depolarization of the cell resulting in the production of the action potential and the repetition of the events.

For the feedback inhibition network to produce bursts, the HH-type conductances (i.e., the passive current, the fast Na^+, and K^+ currents) are required as a minimum along with the continuous stimulation at the soma of Cell 0. This stimulation is required to recover from the inhibition generated by Cell 1.

4.2.2 Sensitivity Analysis of the Feedback Inhibition Network

The changes in the characteristics of rhythmic output for a range of values of the maximum specific channel conductance for the fast Na^+ current, *gmax_iNa*, where $0.0125 < gmax\_iNa < 0.4$ S/cm^2 are presented in Figure 4.12. Setting *gmax_iNa* below 0.0125 S/cm^2 shut down the network. Increasing *gmax_iNa* from 0.0125 to 0.4 S/cm^2 resulted in a slow increase of burst frequency in both cells, an increase of number of APs per bursts in Cell 1 and no changes in number of APs per burst in Cell 0. While burst firing rate in Cell 1 varies smoothly with changes in *gmax_iNa*, burst firing rate in Cell 0 remains constant for $0.0125 < gmax\_iNa < 0.4$ S/cm^2.

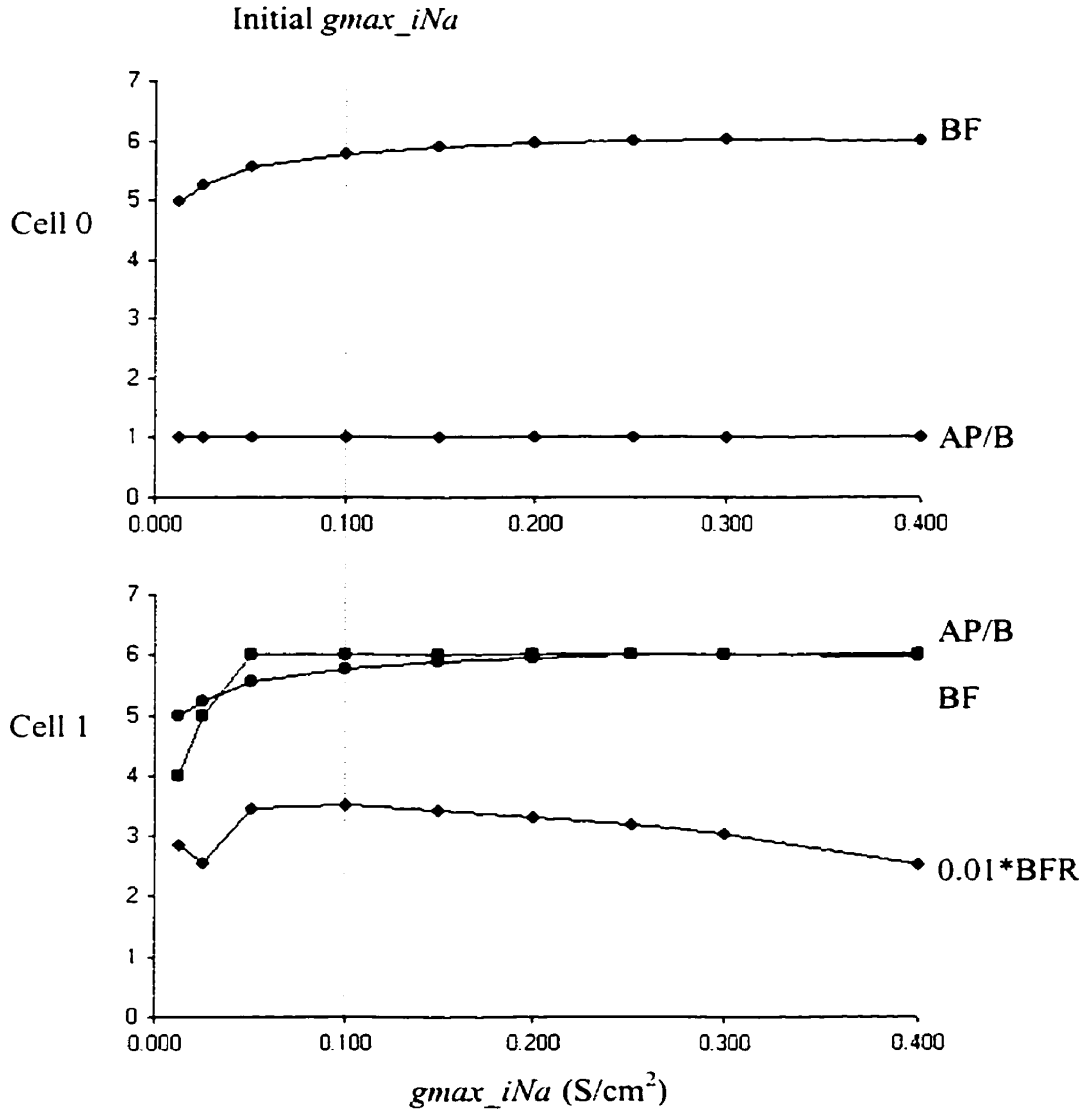

Figure 4.12. Steady-state measures of burst features change with the maximum specific channel conductance for the HH-type Na^+ current, *gmax_iNa*, in the model of the feedback inhibition network. The initial value of *gmax_iNa* is set to 0.1 S/cm^2 (Equation 3.2).

Figure 4.13 presents the changes in the characteristics of rhythmic output for a range of values of the maximum specific channel conductance for the HH-type K^+ current, *gmax_iK*. In this model *gmax_iK* changes between 0.006 and 0.1 S/cm^2.

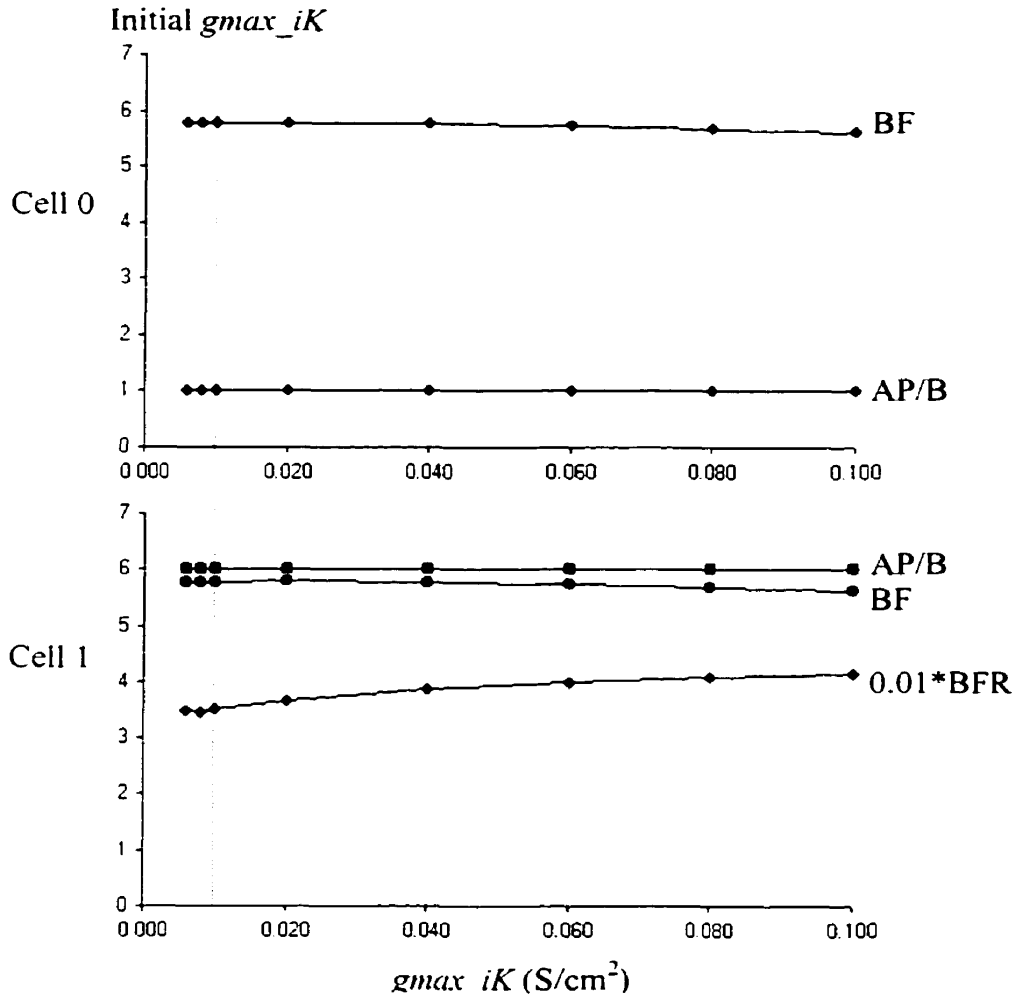

Figure 4.13. Steady-state measures of burst features change with the maximum specific channel conductance for the fast K^+ current (HH-type), *gmax_iK*, in the model of the feedback inhibition network. The initial value of *gmax_iK* is set to 0.01 S/cm^2 (Equation 3.6).

For the fast K^+ current (HH-type), setting *gmax_iK* below 0.006S/cm^2 shut down the network. Increasing *gmax_iK* from 0.006 to 0.1 S/cm^2 resulted in a slow decrease of burst frequency in both cells while the numbers of APs per bursts in Cell 0 and Cell 1 remained constant (1 and 6 respectively). Within this range, burst firing rate in Cell 1 increased, while burst firing rate in Cell 0 remained constant.

Figure 4.14 presents the changes in the characteristics of rhythmic output for a range of values of the maximum synaptic conductance for the AMPA synapse, *gmax_ampa*, where $0.05 < gmax\_ampa < 1.5$ nS. Setting *gmax_ampa* below 0.05 nS shut down the network. While Cell 0 generated single action potentials, the number of APs per burst in Cell 1 increased from one for to seven for $0.05 < gmax\_ampa < 1.5$ nS. This increase was accompanied by very characteristic changes in burst firing rate – an initial decrease followed by an increase in burst firing rate. Every consecutive increase in the number of APs per burst required a greater increase in *gmax_ampa*. Since the burst frequency for the network was set by Cell 0, it remained constant for Cell 1. In general, the characteristics of the rhythmic output varied smoothly with changes in *gmax_ampa* for the feedback inhibition network.

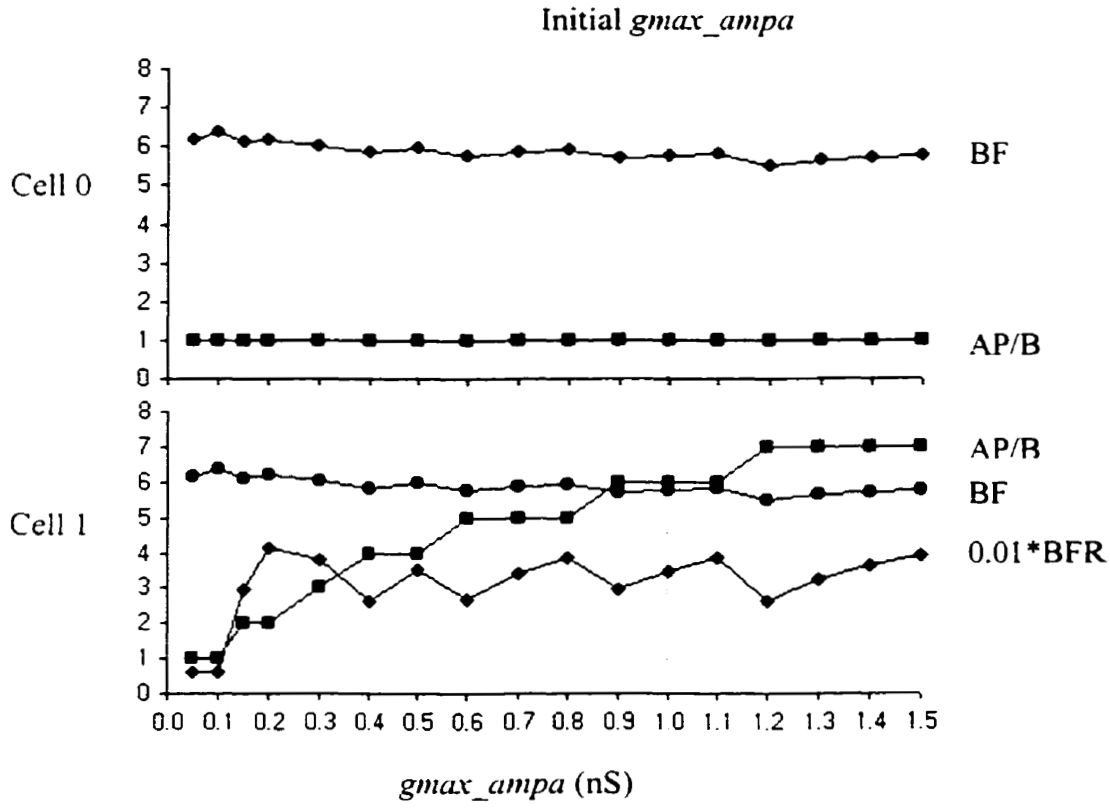

Figure 4.14. Steady-state measures of burst features change with the maximum synaptic conductance for the AMPA synapse, *gmax_ampa*, in the model of the feedback inhibition network. The initial value of *gmax_ampa* is set to 1.0 nS.

The changes in the characteristics of rhythmic output for a range of values of the maximum synaptic conductance for the $GABA_A$ synapse, *gmax_gabaa*, where $0.0 < gmax\_gabaa < 1.5$ S/cm^2 are presented in Figure 4.15.

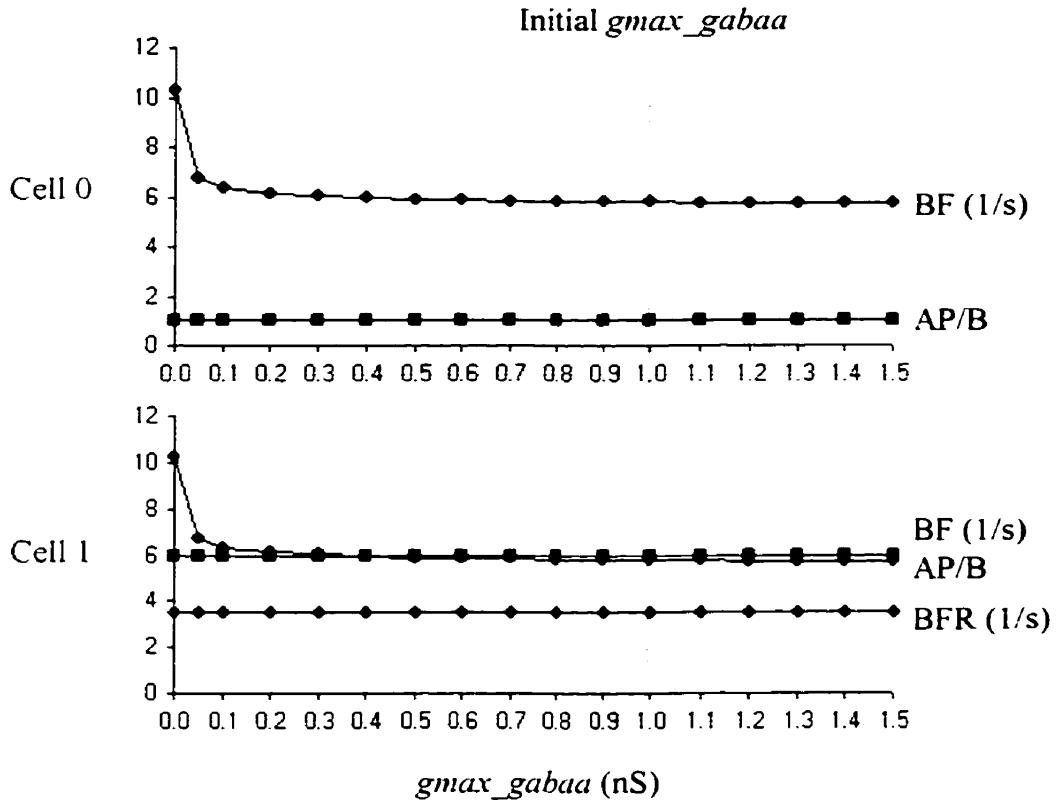

Figure 4.15. Steady-state measures of burst features change with the maximum synaptic conductance for the $GABA_A$ synapse, *gmax_gabaa*, in the model of the feedback inhibition network. The initial value of *gmax_gabaa* is set to 1.0 nS.

With the increase of *gmax_gabaa* from 0.0 to 0.3 nS, inhibition of Cell 0 increased and this resulted in a rapid decrease in burst frequency in Cell 0. This resulted in a decrease in burst frequency in Cell 1. No significant changes in burst characteristics were observed for 0.3 < gmax_gabaa < 1.5 nS.

4.3 Reciprocal Excitation Network

Reciprocal excitation occurs in many neuronal circuits involved in the generation of rhythmic patterns (Friesen and Stent, 1978; Getting, 1989; Wang and Rinzel, 1992). Such networks consist of two or more neurons linked mutually by excitatory synapses whose net gain is positive, which causes the cells to drive each other to produce bursts. To oscillate, reciprocal excitation networks must incorporate some restorative feature that terminates spike production and repolarizes the network as soon as a critical spike characteristics (e.g., frequency) has been attained. Thus the oscillatory cycle of the cells consists of an active phase of gradually increasing membrane depolarization and impulse frequency, and an inactive phase during which the transient impulse termination process repolarizes the membrane.

4.3.1 Model of the Reciprocal Excitation Network

The model of the reciprocal excitation network is composed of two neurons, Cell 0 and Cell 1 defined in Table 4.1, linked by reciprocally excitatory connections. Cell 2, which has identical geometry as Cell 0 and Cell 1, provides both cells with inhibitory input and is provided with excitatory input from both cells (Figure 4.16). In addition to the HH-currents, Cell 2 contains the T-current. Cell 2 has a high threshold for impulse initiation, which is reached only when it receives a high level of excitatory input due to bursting activity in Cell 0 and Cell 1. This was achieved by setting the maximum synaptic conductances between Cell 0 and Cell 2, as well as Cell 1 and Cell2 for the AMPA and $GABA_A$ synapses to 0.2 nS and 0.3 nS respectively.

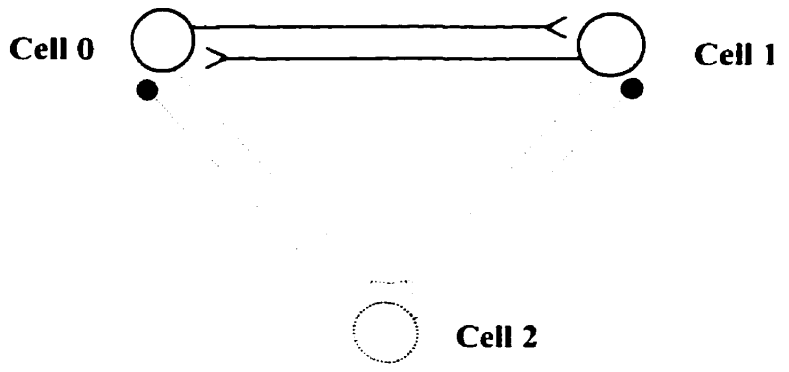

Figure 4.16. The model of the reciprocal excitation network.

The properties of the model of the reciprocal excitation network are listed in Table 4.5. Cell 0 and Cell 1 were used to stimulate the network, as proposed by Friesen and Stent (1978).

Table 4.5. Properties of the model neurons in the reciprocal excitation network.

Variable	Description	Units	Cell 0&1	Cell 2
L	Properties defined in Table 4.1			
T-current				
gmax_iT	The maximum specific Ca^{2+} channel conductance	S/cm^2		.002
eca	The reversal potential for Ca^{2+} channel	mV		120
Stimulation				
amp	Stimulation amplitude	nA	0.5	
dur	Stimulation duration	msec	1000	
del	Stimulation delay	msec	0	

This model circuit generates a rhythm of concurrent bursts in Cell 0 and Cell 1, provided that the gain of the feedback loop between Cell 0 and Cell 1 is positive, the activation of Cell 2 causes substantial repolarization of Cell 0 and Cell 1, and that Cell 0 and Cell 1 have a source of tonic excitation to ensure that after repolarization they drive each other again to higher membrane potential. An example of oscillatory behaviour of the reciprocal excitation network is presented in Figure 4.17.

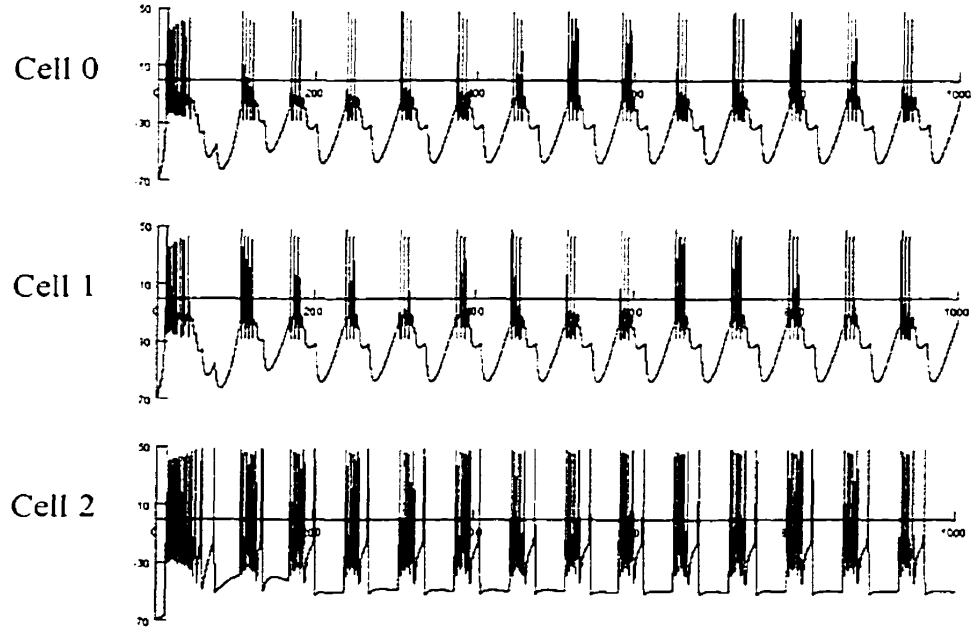

Figure 4.17. Oscillatory output generated by the reciprocal excitation network. Both cells Cell 0 and Cell 1 have identical conductances (HH-type) and are connected via AMPA synapses. Identical stimulation currents have been applied at the somas of Cell 0 and Cell 1: *amp* = 0.5 nA, *dur* = 1000 msec and *delay* = 0 msec.

4.3.2 Sensitivity Analysis of the Reciprocal Excitation Network

Sensitivity analyses were performed for two ionic conductances (fast Na^+ and K^+) and the maximum synaptic conductance for the AMPA synapse. The changes in the characteristics of rhythmic output for a range of the maximum specific channel conductance for the fast Na^+ current, *gmax_iNa*, where $0.01 < gmax\_iNa < 0.4$ S/cm^2 are presented in Figure 4.18.

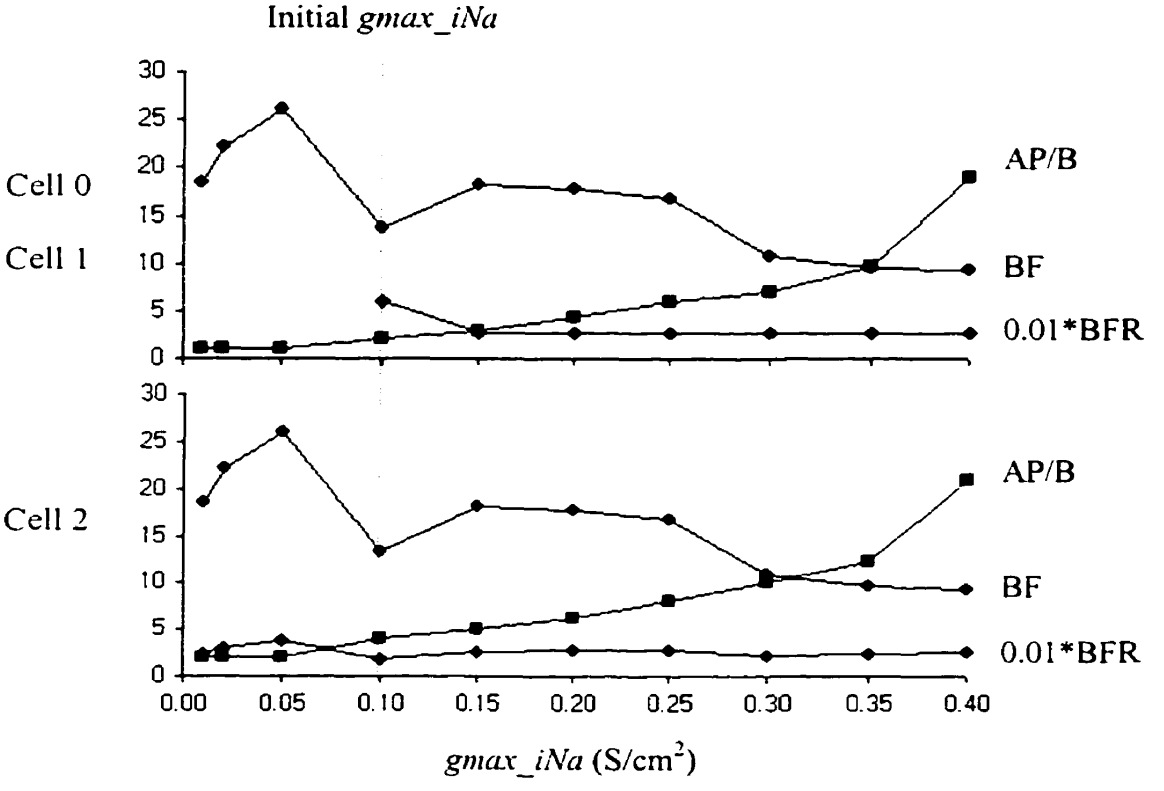

Figure 4.18. Steady-state measures of burst features change with the maximum specific channel conductance for the HH-type Na^+ current, *gmax_iNa*, in the model of the reciprocal excitation network. The initial value of *gmax_iNa* was set to 0.1 S/cm^2 (Equation 3.2).

Setting *gmax_iNa* below 0.01 S/cm^2 shut down the network. While a sharp transition (an increase followed by a decrease) in burst frequency in all cells was observed for 0.01 < *gmax_iNa* < 0.1 S/cm^2, further increase in *gmax_iNa* resulted in a smaller transition. The number of APs per burst in all three cells increased with the increase of *gmax_iNa*. This increase was monotonic for 0.01 < *gmax_iNa* < 0.35 S/cm^2, and quite rapid for 0.35 < *gmax_iNa* < 0.4 S/cm^2. Burst firing rate changed quite rapidly for 0.01 < *gmax_iNa* < 0.1 S/cm^2 and more gradually for 0.1 < *gmax_iNa* < 0.4 S/cm^2.

Figure 4.19 presents the changes in the characteristics of rhythmic output for a range of values of the maximum specific channel conductance for the HH-type K^- current, *gmax_iK*, where 0.002 < *gmax_iK* < 0.1 S/cm^2. Setting *gmax_iNa* below 0.01 S/cm^2 or above 0.1 S/cm^2 shut down the network. The most pronounced changes in output characteristics were observed below the value of 0.01 S/cm^2.

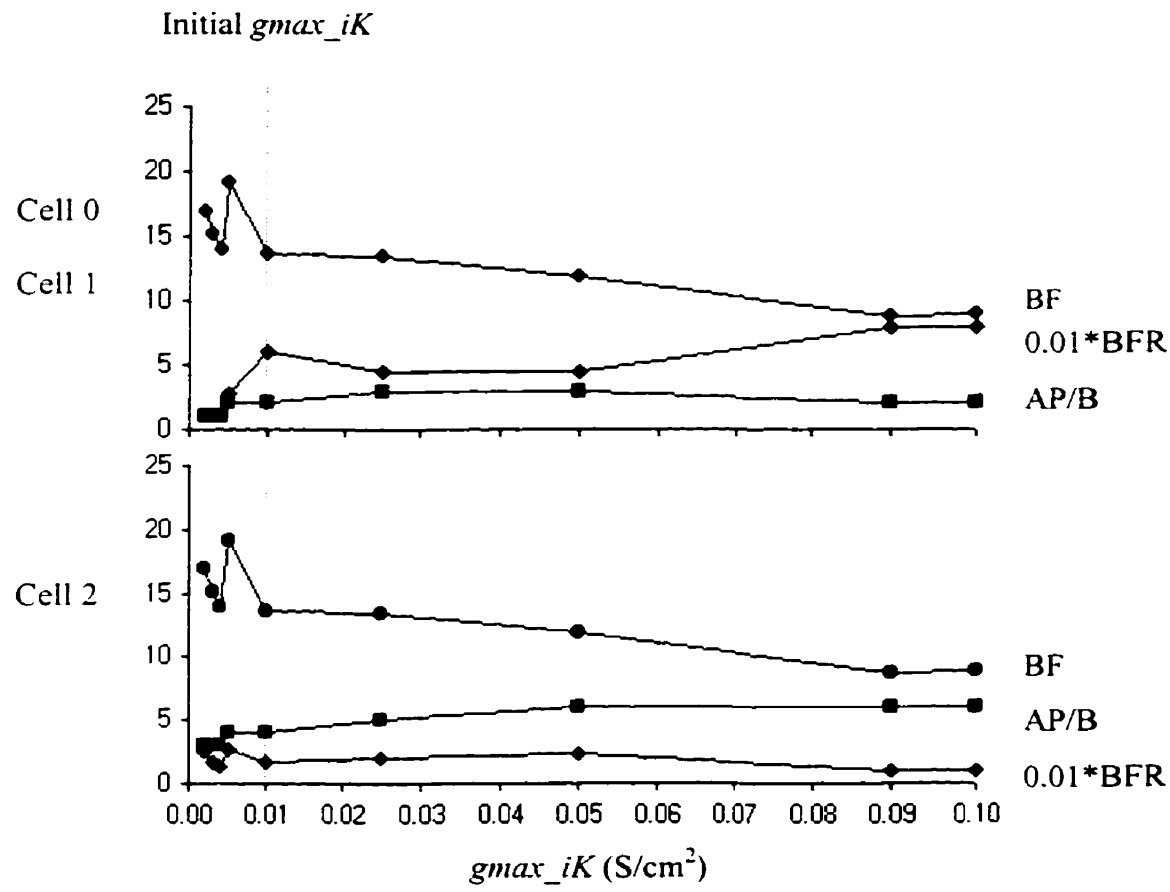

Figure 4.19. Steady-state measures of burst features change with the maximum specific channel conductance for the HH-type K^+ current, *gmax_iK*, in the model of the reciprocal excitation network. The initial value of *gmax_iK* was set to 0.01 S/cm^2 (Equation 3.6).

Figure 4.20 presents the changes in the characteristics of rhythmic output for a range of values in the maximum synaptic conductance for the AMPA synapse, *gmax_ampa*, where $0.1 < gmax\_ampa < 1.5$ nS.

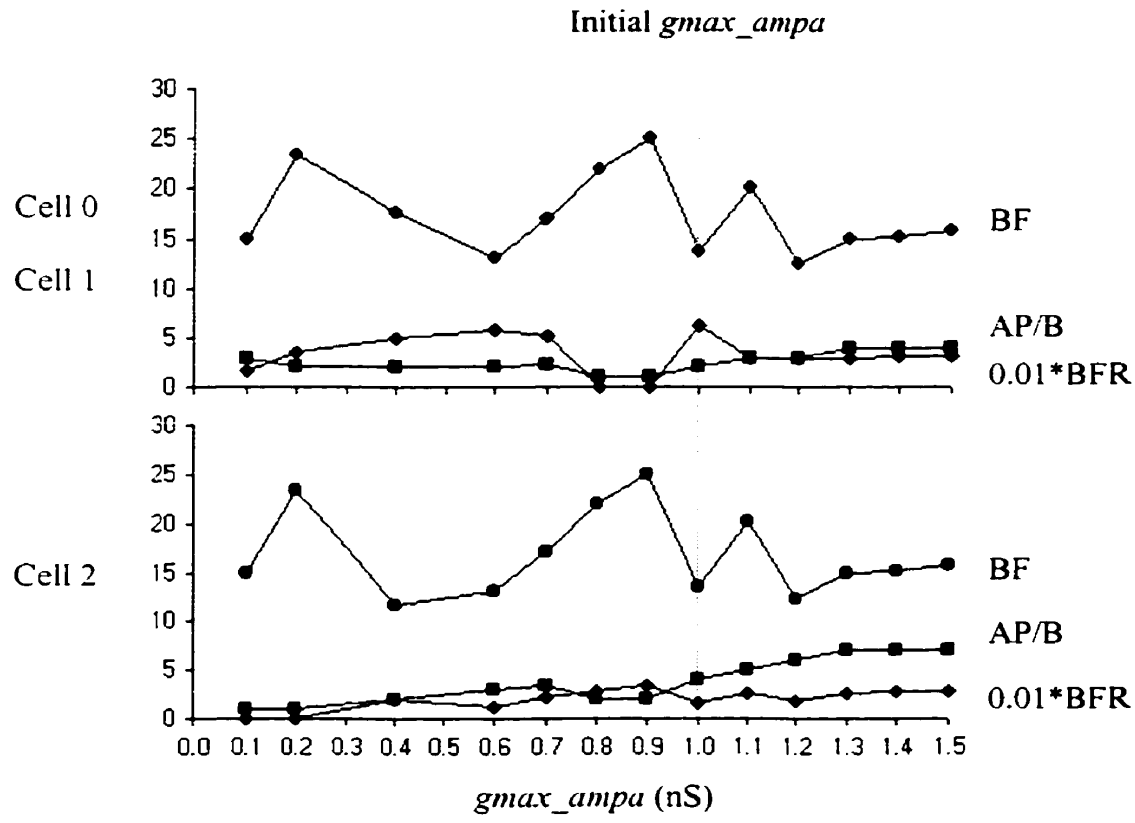

Figure 4.20. Steady-state measures of burst features change with the maximum synaptic conductance for the AMPA synapse, *gmax_ampa*, in the model of the reciprocal excitation. The initial value of *gmax_ampa* was set to 1.0 nS.

Setting *gmax_ampa* below 0.1 nS shut down the network. Increasing *gmax_ampa* from 0.01 nS to 1.5 nS resulted in sharp transitions (increases followed by decreases) in burst frequency in all cells. Changes in the number of APs per burst and burst firing rate were gradual with the increase in *gmax_ampa*.

4.4 Parallel Excitation and Inhibition Network

In this network configuration, a single postsynaptic cell is both excited and inhibited. This network is thought to be implicated in the production of the swimming movements in *Tritonia* (Getting, 1983).

4.4.1 Model of the Parallel Excitation and Inhibition Network

In this network configuration, a single postsynaptic cell, Cell 2, is both excited by Cell 0 and inhibited by Cell 1, which in turn is excited by Cell 0. These two opposite actions (i.e., excitation and inhibition) are mediated by separate pathways (Figure 4.21).

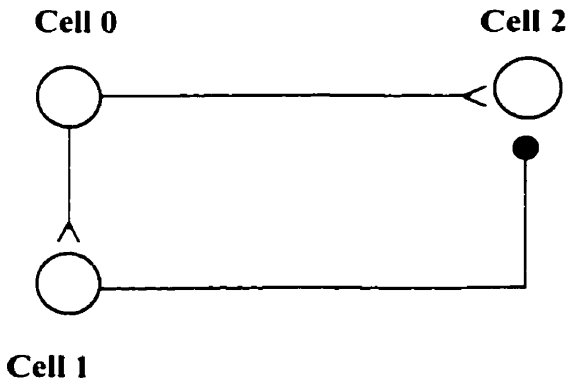

Figure 4.21. The model of the parallel excitation and inhibition network.

Three model neurons defined in Table 4.1 were used to implement the model of the parallel excitation and inhibition network. In this configuration Cell 0 was stimulated. Table 4.6 lists the properties of the network.

Table 4.6. Properties of the parallel excitation and inhibition network.

Variable	Description	Units	Cell 0&2	Cell 1
	Properties included in Table 4.1		Yes	Yes
AMPA				
Cmax	Maximum transmitter concentration	mM	1	
Cdur	Transmitter duration (raising phase)	msec	1	
Alpha	Forward binding rate	/ms mM	1.1	
Beta	Backward unbinding rate	/msec	0.19	
Erev	Reversal potential	mV	0	
Deadtime	Maximum time between release events	msec	1	
Prethresh	Voltage level for release	mV	0	
gmax_ampa	Maximum synaptic conductance	nS	1	
GABAa				
Cmax	Maximum transmitter concentration	mM		1
Cdur	Transmitter duration (raising phase)	msec		1
Alpha	Forward binding rate	/msec mM		0.53
Beta	Backward unbinding rate	/msec		0.18
Erev	Reversal potential	mV		-80
Deadtime	Maximum time between release events	msec		1
Prethresh	Voltage level for release	mV		0
gmax_gabaa	Maximum conductance	nS		1
Stimulation			Cell 0	
amp	Stimulation amplitude	nA	0.1	
dur	Stimulation duration	msec	1000	
del	Stimulation delay	msec	0	

An example of oscillatory output of the parallel excitation and inhibition network is presented in Figure 4.22.

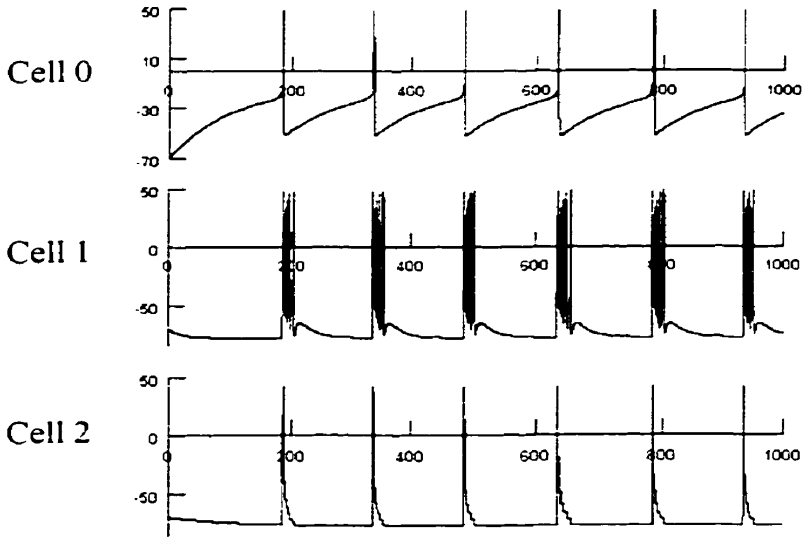

Figure 4.22. Rhythmic output generated by the parallel excitation and inhibition network. All cells have identical conductances (HH-type), and all synapses have identical maximum synaptic conductance The stimulation current (*amp* = 0.1nA, *dur* = 1000 ms and *delay* = 0 ms) has been applied at the soma of Cell 0.

The action potentials produced by Cell 0 induce a sequence of excitatory postsynaptic potentials in Cell 1 and Cell 2 resulting in the production of action potentials. However, the excitatory postsynaptic potentials in Cell 2 are affected by the inhibitory postsynaptic potentials induced by Cell 1 resulting in the production of single spikes. For the parallel excitation and inhibition network to produce bursts, the HH-type conductances (i.e., the

passive current, the fast Na^+ current and the fast K^+ current) are required as a minimum along with the stimulation at the soma of Cell 0.

4.4.2 Sensitivity Analysis of the Parallel Excitation and Inhibition Network

Figure 4.23 presents the results of sensitivity analysis for a range of values of the maximum specific channel conductance for the fast Na^+ current, *gmax_iNa*, where $0.012 < gmax\_iNa < 03$ S/cm^2. Setting *gmax_iNa* below 0.012 S/cm^2 shuts down the network. For $0.012 < gmax\_iNa < 0.05$ S/cm^2, burst frequency in all three cells increases quite rapidly with the increase of *gmax_iNa* while the number of APs per burst increases in Cell 1 and remains constant in Cell 0 and Cell 2. Also, a sharp transition (a decrease followed by an increase) in burst firing rate is observed in Cell 1 for that range of *gmax_iNa*. An increase of gmax_*iNa* from 0.05 to 0.3 S/cm^2 results in a slow increase of burst frequency and no changes in number of action potential per burst in all three cells, while burst firing rate in Cell 2 decreases very gradually with the increase of *gmax_iNa*.

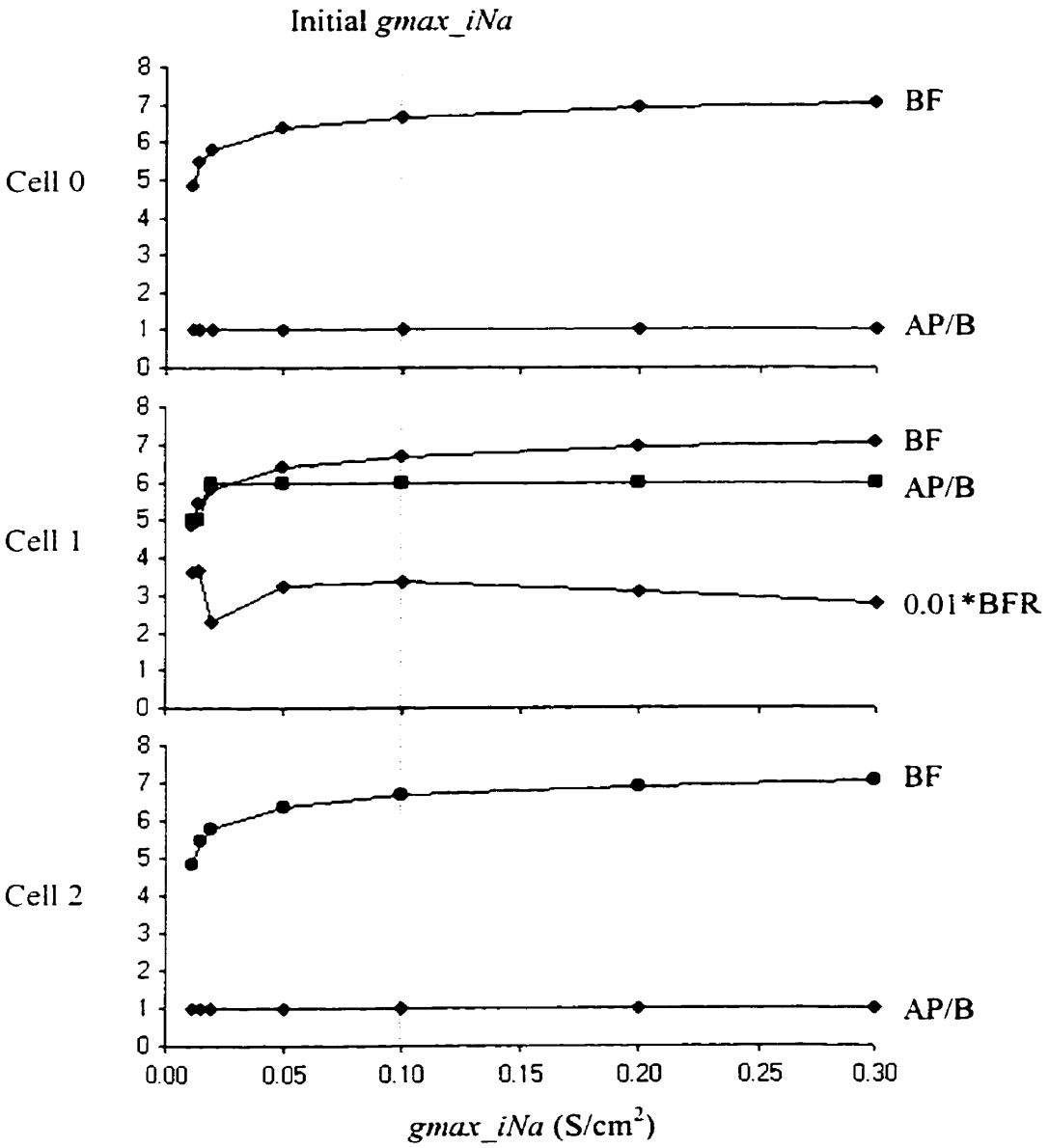

Figure 4.23. Steady-state measures of burst features change with the maximum specific channel conductance for the HH-type Na^+ current, *gmax_iNa*, in the model of the parallel excitation and inhibition network. The initial value of *gmax_iNa* was set to 0.1 S/cm^2 (Equation 3.2).

The characteristics of the rhythmic output generated by the parallel excitation and inhibition network vary smoothly with changes in *gmax_iNa*.

Figure 4.24 presents the changes in the characteristics of rhythmic output for a range of values of the maximum specific channel conductance for the fast K^+ current, *gmax_iK*. where $0.004 < gmax\_iK < 0.1$ S/cm^2. Setting *gmax_iK* below 0.004 S/cm^2 shuts down the network. Burst frequencies in all three cells are almost identical and decrease monotonically with the increase of *gmax_iK*. While Cell 0 and Cell 2 generate single action potentials, the number of APs per burst in Cell 1 changes from 9 for $gmax\_iK = 0.004$ S/cm^2, to 6 for $0.004 < gmax\_iK < 0.1$ S/cm^2. A sharp transition (an increase followed by a decrease) in burst firing rate for $0.004 < gmax\_iK < 0.01$ S/cm^2 observed in Cell 1 was followed by a monotonic increase in burst firing rate for $0.01 < gmax\_iK < 0.1$ S/cm^2. In general, the characteristics of the rhythmic output vary smoothly with changes in *gmax_iK* for the fast K^+ current.

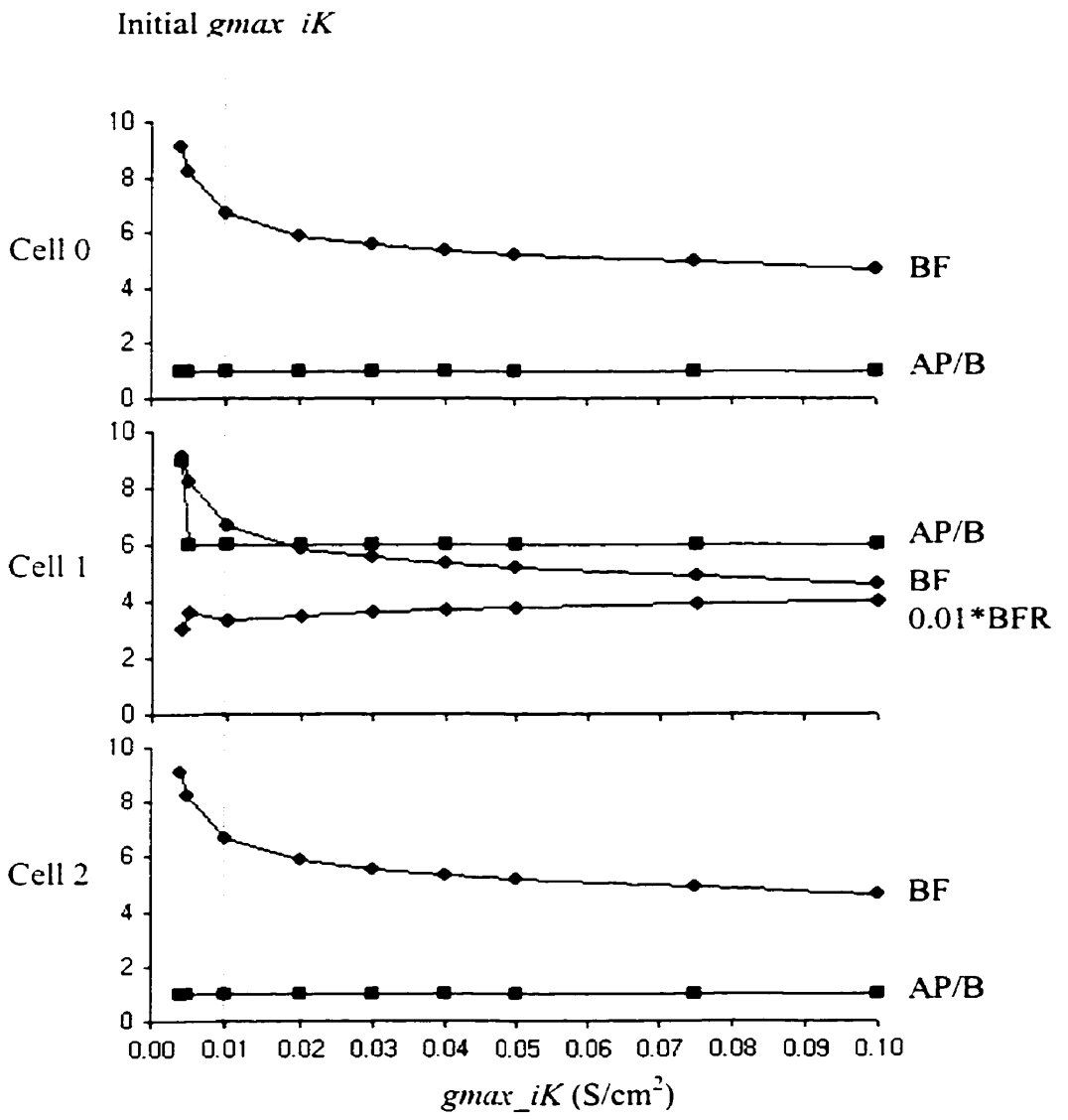

Figure 4.24. Steady-state measures of burst features change with the maximum specific channel conductance for the HH-type K^+ current, *gmax_iK*, in the model of the parallel excitation and inhibition network. The initial value of *gmax_iK* is set to 0.01 S/cm^2 (Equation 3.6).

Figure 4.25 presents the changes in the characteristics of rhythmic output for a range of values of the maximum synaptic conductance for the AMPA synapses, *gmax_ampa*, where 0.1 < *gmax_ampa* < 1.8 nS. Setting *gmax_ampa* below 0.1 nS shuts down the network. While Cell 0 and Cell 2 generate single action potentials, the number of APs per burst in Cell 1 increases from 1 for *gmax_ampa* = 0.1 nS to 8 for *gmax_ampa* = 1.8 nS. This increase in the number of APs per burst in Cell 1 is accompanied by very characteristic changes in burst firing rate – an initial decrease followed by an increase in burst firing rate. Also, every consecutive increase in the number of APs per burst requires a greater increase in *gmax_ampa*. Since the burst frequency for the network is set by Cell 0, it remains constant for the remaining cells for 0.1 < *gmax_ampa* < 1.8 nS. In general, the characteristics of the rhythmic output vary smoothly with changes in *gmax_ampa* for the parallel excitation and inhibition network.

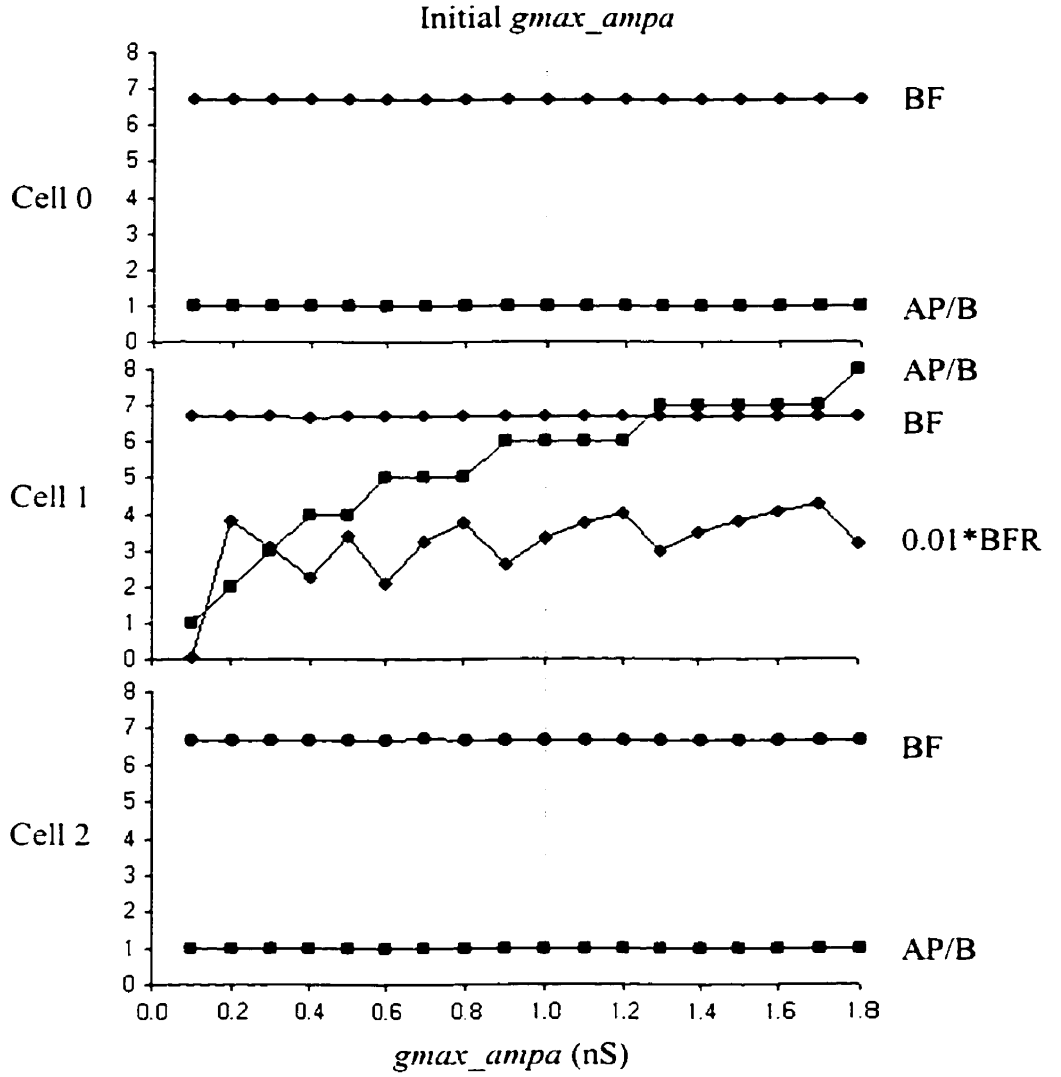

Figure 4.25. Steady-state measures of burst features change with the maximum synaptic conductance for AMPA synapse, *gmax_ampa*, in the model of the parallel excitation and inhibition network. The initial value of the maximum synaptic conductance was set to 1.0 nS.

Figure 4.26 presents the changes in the characteristics of rhythmic output for a range of values of the maximum synaptic conductance for the GABAa synapse, *gmax_gabaa*, where $0.0 < gmax\_gabaa < 1.8$ nS.

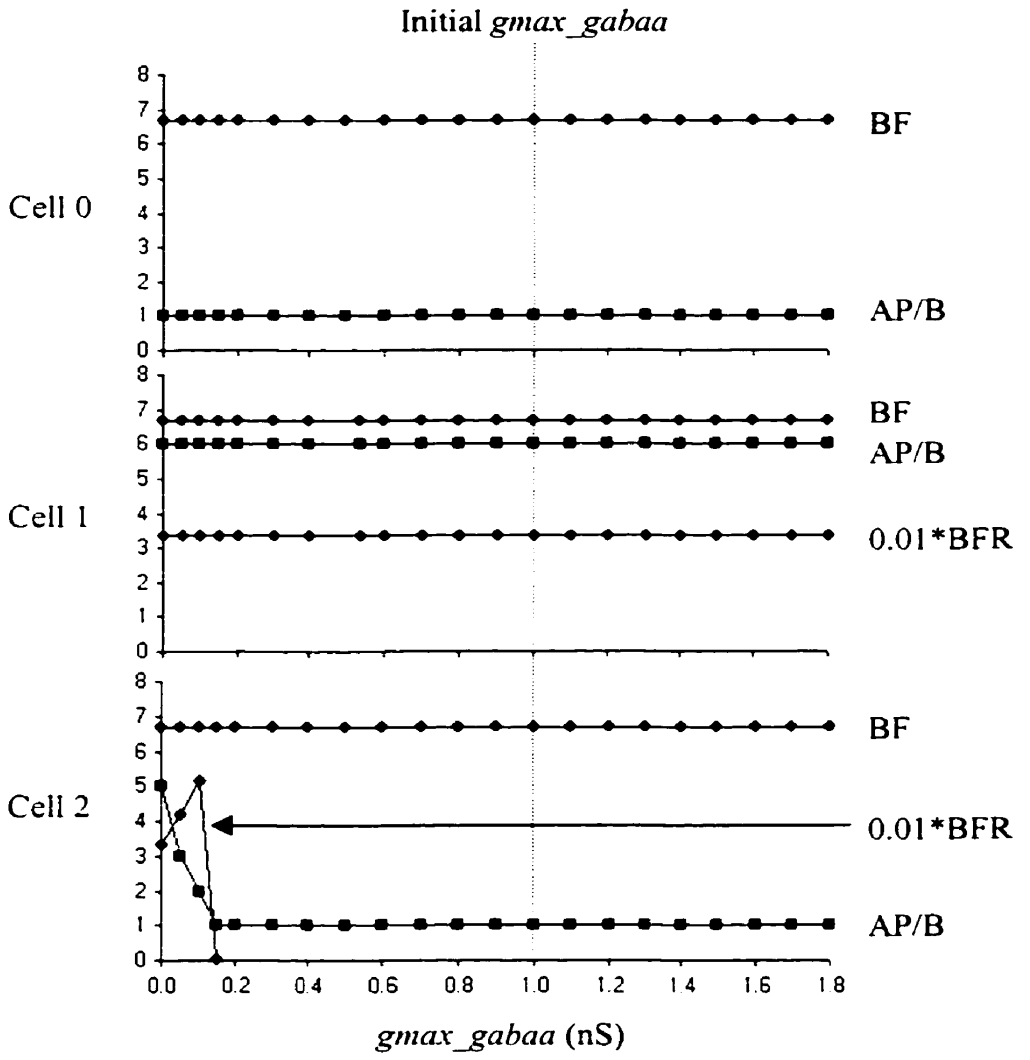

Figure 4.26. Steady-state measures of burst features change with the maximum synaptic conductance for the $GABA_A$ synapse, *gmax_gabaa*. The initial value of *gmax_gabaa* is set to 1.0 nS.

The GABAa synapse affects Cell 2 only, therefore the characteristics of the output generated by Cell 0 and Cell 1 remain constant as *gmax_gabaa* changes. Burst frequency in Cell 2 is driven by burst frequency in Cell 0, therefore it remains constant. An increase of *gmax_gabaa* from 0 to 0.15 nS causes a sharp decrease in the number of APs per burst and a rapid change (an initial increase followed by a decrease) in burst firing rate. Further increase of *gmax_gabaa* from 0.15 to 1.8 nS causes no changes in the number of APs per burst in Cell 2.

5 RESEARCH SUMMARY

5.1 Main Findings

Computer models based on the Hudgkin-Huxley formalism and experimental data obtained from various species were used to simulate the oscillatory behaviour of the elementary rhythm-generating networks. Furthermore, simple sets of cellular and synaptic 'building block' candidates sufficient for the production of rhythmic output were identified. The simulation experiments carried out for this study revealed that even simple networks, modeled at a detailed level, can generate complex behaviour patterns. These simple networks are susceptible to external (e.g., descending) control mediated by variations of voltage- or transmitter-activated conductances.

For the model of the reciprocal inhibition network to produce bursts, the HH-type currents along with the T-current, and the Ca^{2+} pump are required. When the network was stimulated asymmetrically and/or the properties of the component neurons are asymmetric, the model produced alternating bursts. If neither of the conditions were met, the generated output was synchronous. In addition to the minimal set of currents, two other currents are particularly important: a slow, calcium-activated afterhyperpolarization K^+ current, I_{AHP}, and cation current activated by hyperpolarization, I_h.

For the model of the feedback inhibition network to produce bursts, the HH-type currents along with the stimulation of the cell that produces excitatory postsynaptic potentials in

the other cell are required. Computer simulation of this network revealed asymmetrical properties of the bursts.

The model of the reciprocal excitation network composed of three cells of which two were linked with reciprocally excitatory synapses and the third one formed the feedback inhibition-type connections with the first two cells was used to study the oscillatory behaviour of the network. This model was capable of generating bursts, provided that all cells contained the HH-type currents, the first two cells were provided with a suitable excitation and the third cell had a high threshold for impulse initiation, and when activated, it caused substantial repolarization of the first two cells. Computer simulations of this network revealed synchronous properties of the bursts. Numerous attempts to produce alternating bursts were not successful despite the use of different combinations of cellular and synaptic properties and extensive tuning.

For the model of the parallel excitation and inhibition network to produce bursts, the HH-type currents along with the stimulation of the cell that produces excitatory postsynaptic potentials in the other cells are required. Computer simulation of this network revealed asymmetrical properties of the bursts.

The sensitivity analyses conducted for this study assisted in exploring the changes in the network behaviour for a range of values of the maximum specific channel conductance, of selected ionic channels and the maximum synaptic conductance of selected synaptic

receptors. The results of the sensitivity analyses expressed in qualitative terms are summarized in Table 5.1 for changes in the maximum specific channel conductance.

Table 5.1. Sensitivity of model output to changes in the maximum voltage-dependent conductance.

	Na^-	K^-	T^-
Reciprocal inhibition network	AP/B – Medium BF – Very low BFR – Medium	AP/B – High BF – Very low BFR - High	AP/B – High BF – Very low BFR - Low
Feedback inhibition network	AP/B – Medium BF – Medium BFR – Medium	AP/B – Very low BF – Very low BFR – Low-medium	
Reciprocal excitation network	AP/B – Medium-high BF – High BFR – Low	AP/B – Low BF – Medium BFR – Medium	
Parallel excitation and inhibition network	AP/B – Low BF – Low-medium BFR – Medium	AP/B – Low BF – Low-medium BFR – Low	

The results of sensitivity analyses expressed in qualitative terms for changes in the maximum synaptic conductances are summarized in Table 5.2.

Table 5.2. Sensitivity of model output to changes in the maximum synaptic conductance.

	AMPA	$GABA_A$
Reciprocal inhibition network		AP/B – Low BF – Very low BFR – Medium
Feedback inhibition network	AP/B – Medium BF – Very low BFR - High	AP/B – Very low BF – Low-medium BFR – Very low
Reciprocal excitation network	AP/B – Low BF – High BFR – Low-medium	
Parallel excitation & inhibition network	AP/B – Low-medium BF – Very low BFR – High (Cell 1)	AP/B – Low-medium BF – Very low BFR – High (Cell 2)

Intuitively, the number of APs/burst (AP/B), burst frequency (BF), and burst frequency rate (BFR) curves reflect the level of excitability of the models of the networks. Changes of these curves, when combined, provide a qualitative measure of changes in the excitability of the models (Table 5.3).

Table 5.3. Summary of changes in excitability of the models of the elementary networks.

	Reciprocal inhibition network	Feedback inhibition network	Reciprocal excitation network	Parallel excitation & inhibition network
gmax_iNa	Slow increase	Slow increase	Rapid transitions	Slow increase
gmax_iK	Fast decrease	Very slow decrease	Slow decrease	Moderate decrease
gmax_iT	Moderate increase			
gmax_AMPA		Moderate increase	Rapid transitions	Moderate increase (Cell 1)
gmax_$GABA_A$	Monotonic change	Rapid decrease followed by very slow decrease		Rapid decrease followed by no change

The component cells in some models of the elementary rhythm-generating networks display a common behaviour: an increase in a model parameter (e.g., the maximum

specific channel conductance) causes (a) an increase in the number of APs per burst accompanied by a decrease in burst frequency rate at a minimal change in burst frequency, or (b) an increase in burst frequency rate and a decrease in number of APs per burst at a minimal change in burst frequency. This is evident in the behaviour of the reciprocal inhibition network for changes in the maximum specific channel conductance for the fast Na^+ current, *gmax_iNa*, (Figure 4.6, page 84) and the maximum synaptic conductance for the $GABA_A$ synapse, *gmax_gabaa*, (Figure 4.9, page 87) as well as the parallel excitatory and inhibitory network for changes in the maximum synaptic conductance for the $GABA_A$ synapse, *gmax_gabaa*, (Figure 4.26, page 113).

Quite different patterns of behaviour are displayed by other models of the networks: an increase in a model parameter causes an increase in the number of APs per burst accompanied by sharp transition (a decrease followed by an increase) in burst firing rate at a minimal change in burst frequency. This behaviour is displayed by the feedback inhibition network for changes in the maximum specific channel conductance for the fast Na^+ current, *gmax_iNa*, (Figure 4.12, page 92) and the maximum synaptic conductance, *gmax_ampa*, (Figure 4.14, page 95) in Cell 1 as well as by the parallel excitation and inhibition network for changes in the maximum specific channel conductance for the fast Na^+ channel, *gmax_iNa*, (Figure 4.23, page 108) and the maximum synaptic conductance for the AMPA synapse in Cell 1 (Figure 4.25, page 112). In this case, the increase in the number of APs per burst does not occur at the expense of burst firing rate since the member cells are interconnected via the excitatory synapse.

5.2 Critical Discussion of Methods

At the heart of the classical Hodgkin-Huxley formalism is the depiction of the time- and voltage-dependent sodium and potassium conductances it terms of a number of gating variables. The dynamics of these variables are governed by first-order differential equations with voltage dependent terms, the steady-state activation (or inactivation), and the time. The key feature of activating variables is that their amplitude increases with increasing depolarization, while the converse is true for inactivating variables. For rapid input to a patch of squid axonal membrane, spike initiation is achieved whenever a particular voltage threshold is exceeded. The Hodgkin-Huxley equations have been extended to accommodate other cellular ionic channels and synaptic properties in neuronal circuits. The extended Hodgkin-Huxley equations have proven to be a valuable tool and have been used extensively in computer simulation studies of neuronal circuits.

The compartmental model used in this research represents the spatially distributed neuron as a set of connected compartments. Nonuniformity in physical properties (e.g., diameter, current) occurs between compartments rather than within them. For the membrane currents this approach involves two approximations: first, the axial current is specified in terms of the voltage drop between the centres of adjacent compartments, and second, the spatially varying membrane current is represented by its value at the centre of each compartment. One of known problems with the compartmental models based on the extended Hodgkin-Huxley formalism is their sensitivity and, in some cases, instability

and 'unnaturalness' of behaviour (Mainen and Sejnowski, 1996). This means that the behaviour of the model can change dramatically when relative small modifications are made in its parameter values. For example, small changes in the parameters that control voltage dependence or temporal dynamics of any conductance in a model may dramatically alter the model's pattern of activity. Likewise, the addition or removal of a conductance can change the model's dynamics. This problem is more pronounced in large neuronal models with complex morphology, distribution of the channels, and connectivity between the neurons.

The model of the neuron used in this research is simple. It is composed of the soma represented as a single-compartment sphere, the axon and the dendrite composed of multiple cylindrical compartments. This approach was used in this study for three main reasons: (1) lack of detailed data describing the geometry, morphology, and electrophysiological properties of the biological phenomena, (2) reduction of risks associated with the accumulation of numerical errors and instability of the solution, and (3) reduction of computation time. The last argument was quite important for conducting sensitivity analyses that required thousands of simulation runs, each of them taking 10-20 minutes of time.

The simulation experiments were carried out using the NEURON simulation program on a Pentium-based PC running Windows NT. This program was designed specifically to simulate the equations that describe nerve cells and handle problems in which membrane

properties are spatially inhomogenous and where membrane currents are complex. NEURON is computationally most efficient for problems that range from parts of single cells to small numbers of cells in which biophysical properties play a crucial role. However, NEURON has been applied to very large network models: 10^4 cells with six compartments each, for a total of 10^6 synapses in the network (Hines, 1997). It is particularly capable of investigation new kinds of membrane channels and synaptic receptors and allows the expression of models in terms of kinetic schemes or sets of simultaneous differential and algebraic equations. Simulation speed is excellent since membrane voltage is computed by the implicit integration method optimized for branched structures. The performance of NEURON degrades slowly with increased complexity of morphology and membrane mechanisms. The accuracy of the computations was limited to the accuracy offered by the computing environment used to carry out the simulation experiments i.e., a Pentium III-based computer running 32-bit Windows NT operating system. Both the NEURON software and the computing environment affected the stability of computational solutions. No formal analysis of the stability of solutions was performed.

5.3 Critical Discussion of Simulation Results

The objectives of this research included the assessment of the contribution of the properties of 'building blocks' in the models of the oscillatory networks to the characteristics of rhythmic output and the sensitivity of model output to changes in model variables. The results obtained in the simulation experiments were compared with the

results published in the literature, and the models were tuned when required. However, given the fact that the models used in this study had detailed kinetics of membrane and synaptic properties and relatively simple geometry, some errors were introduced. Therefore, the simulation results should be taken as approximations of the biological phenomena.

The basic problem of incomplete knowledge resulting in oversimplification of complex biological phenomena is amplified by instability and 'unnatural' model behaviour when the characteristics of the model output change dramatically when a small change is made in the model parameters. This behaviour can be attributed to: (1) the limitation of the compartmental method and the underlying mathematical formalism (i.e., partial differential equations), (2) simplicity of the models (i.e., only two or three neurons with similar cellular characteristics interconnected and interacting with each other) so a change in the model parameters (e.g., the maximum specific channel conductance) affects a large portion of the system (e.g., channel conductance of a given ion species in all neurons). It is likely that a similar change in the population of neurons would result is less dramatic change in the output.

One of the findings of this study is that for the elementary rhythm-generating networks to produce alternating bursts, an asymmetry in neuronal properties or stimulation is required. This issue begs the question whether or not the biological networks involved in the production of alternating bursts are asymmetrical or are stimulated asymmetrically. It

is unlikely that two neurons are identical or that two paths in the neuronal networks are mediated symmetrically. Therefore it is likely that neuronal populations composed of different neurons have different properties. No quantitative analysis of the asymmetry phenomenon in the rhythm-generating networks was performed in this study.

Computer simulations of the reciprocal excitation network revealed synchronous properties of the bursts. Numerous attempts to produce alternating bursts were not successful despite the use of varies combinations of currents with different temporal characteristics, different kinetics, different threshold levels, and different stimulation currents (e.g., different amplitudes, delays, and duration). Also the changes in the model parameters had dramatic effect on the characteristics of the rhythmic output.

The sensitivity analyses were performed for a number of values of the maximum specific channel conductance for the selected ionic channels or the maximum synaptic conductance for the selected synaptic receptors. For a given value of a model variable, three characteristics of the model output (i.e., the number of APs per burst, burst frequency, and burst frequency rate) were computed. While these characteristics are sufficient for the analysis of output with well-defined rhythmic patterns, they are not entirely satisfactory for the analysis of complex signals with less pronounced rhythmic patterns.

The results of the sensitivity analyses are helpful is the understanding of burst-frequency control by descending (higher order) motor systems. These results can be used as qualitative measures of changes in the behaviour of the four elementary rhythm-generating networks to changes in the maximum synaptic channel conductances for the selected ionic channels and the maximum synaptic conductance for the selected synaptic receptors. In particular, specific characteristics of the rhythmic output and a more precise range for the parameters that have the most dramatic effect on these characteristics can be identified. For example, of the three characteristics of the rhythmic output (i.e., the number of APs per burst, burst frequency, and burst firing rate) only two (i.e., the number of APs per burst and burst frequency rate) are affected by the changes of the maximum specific channels conductance for the fast K^+ current (HH-type) within a specific range of values (e.g., $0.0042\ S/cm^2 < gmax\_iK < 0.02\ S/cm^2$) in the model of the reciprocal inhibition network (Figure 4.7, page 85).

Furthermore, the sensitivity analysis results are helpful in the identification the primary catalyst of changes in the model output for a given pattern of characteristics of the rhythmic output. For example, the results presented in Figure 4.8 (page 86) show that: (1) an increase in the maximum specific channel conductance for the T-current in the model of the reciprocal inhibition network results in an increase in the number of action potentials per burst with a minimal effect on the two remaining characteristics of the rhythmic output (i.e., burst frequency and burst frequency rate), and (2) the value of burst frequency is relatively low ($2.7 < BF < 3.9$ (1/s)). This is an indication that currents with

a long time constant control burst frequency and burst firing rate. In this case, it is very likely that the Ca^{2+} pump in conjunction with the T-current control these two characteristics of the rhythmic output.

The simulation experiments carried out for this study revealed that the elementary rhythm-generating networks, modeled at a detailed level, can produce dramatically different activity patterns and, conversely, similar activity patterns can be produced by neuronal networks of different architecture. Therefore, knowledge of connectivity alone does not explain the operation and function of the neuronal networks.

5.4 Future Considerations and Implications for Science

This research provided the opportunity to develop a set of computational 'building blocks' and explore the dynamics of the elementary rhythm-generating networks. It also provided the opportunities to identify the shortcomings of the methods, the tools, and the results and plan for the development of more comprehensive models.

One of the major hopes of research in computational neuroscience is that we will be able to develop better tools to learn from a wealth of experimental data about the nervous system, ranging from description of the structure of single molecules and ionic channels to imaging brain performing complex, cognitive tasks. The models of the 'building blocks' developed for the purpose of this study can also be used as a form of information storage and a basis for communication. Like a database, models contain detailed

information about a particular phenomenon (e.g., the features necessary to generate a particular neuronal response pattern). Unlike a traditional database, however, models also contain precise information about the relationships between the known phenomena. In addition, by running a simulation, a model can, in fact, internally check the consistency of the information previously stored. Finally, computer simulations can predict the behaviour of the modeled phenomena and actually direct the acquisition of additional information necessary to expand the model. By providing a means of storing and representing information about the nervous system, the increased use of models has the potential to change the way research in neuroscience in conducted.

While the exploration of the dynamics of the models of the elementary rhythm-generating networks and conducting sensitivity analyses are important in understanding the relationships between organization and function of these networks, these models do not necessarily represent the activities of neuronal populations. The models of the membrane and synaptic conductances and the elementary networks developed for this study can form the basis for the models of neuronal populations.

5.5 Conclusion

In this study, a set of models of the 'building blocks' were developed and series of computer simulations of elementary rhythm-generating networks were carried out. Also sensitivity analyses of model output to changes in model variables were conducted. The computer simulations revealed that these simple networks generate complex behaviour

patterns and may be part of the wider neural circuitry controlling rhythmic movement or performing sensory processing functions.

REFERENCES

Abbot, L. and Marder, E. (1998). Modeling Small Networks. *Methods in Neuronal Modeling. From Ions to Networks*. Edited by Koch, C. and Segev, I. The Bradford Book, The MIT Press. ISBN 0-262-11231-0.

Adams, D. J., Smith, S. J. and Thompson, S. H. (1980). Ionic currents in Molluscan soma. *Annual Review of Neuroscience*. 3:141-167.

Aidley, D. J. (1989). *The Physiology of Excitable Cells*. Third Edition. Cambridge University Press. ISBN 0-521-30301 X.

Alford, S. and Grillner, S. (1990). CNOX and DNOX block non-NMDA synaptic transmission but not NMDA-evoked locomotion in lamprey spinal cord. *Brain Research*. 506:297-302.

Alving, B. O. (1968). Spontaneous activity in isolated soma of *Aplysia* pacemaker neurons. *Journal of Gen. Physiology*. 51:29-45.

Arbas, E.A., Calabrese, R.L. (1987). Slow oscillations of membrane potential in interneurons that control heart-beat in the medicinal leech. *Journal of Neuroscience*. 7:3953-3960.

Arshavsky, Y. I., Beloozerova, I. N., Orlovsky, G. N., Panchin, Y. V., and Pavlova, G. A. (1985). Control of locomotion in the marine mollusc *Clione* limarcina. Role of type 12 neurons. *Experimental Brain Research*. 58:285-293.

Arshavsky, Y. I., Orlovsky, G. N., Panchin, Y. V., Roberts, A. and Soffe, S. R. (1993). Neural control of swimming locomotion: analysis of the pteropod mollusc *Clione* and embryos of the amphibian *Xenopus*. *Trends in Neuroscience*. 16:227-233.

Bargas, J. and Galarraga, E. (1995). Ion Channels: Key to Neuronal Specialization. *The Handbook of Brain Theory and Neural Networks*. Edited by Arbib, M. A. The Bradford Book, The MIT Press. ISBN 0-262-01148-4.

Barry, M. and O'Donovan, M.J. (1987). The effects of excitatory amino acids and their antagonists on the generation of motor activity in the isolated chick cord. *Dev. Brain Research*. 36:271-276.

Baxter, D. A. and Byrne, J. H. (1991). Ionic conductance mechanisms contributing to the electrophysiological properties of neurons. *Current Opinion in Neurobiology*. 1:105-112.

Beer, R. D. and Chiel, H. J. (1995). Locomotion, Invertebrate. *The Handbook of Brain Theory and Neural Networks*. Edited by Arbib, M. A. The Bradford Book. The MIT Press. ISBN 0-262-01148-4.

Beer, R. D., Ritzmann, R. E. and McKenna, T. (Editors) (1993). *Biological Neural Networks in Invertebrate Neuroethology and Robotics*. Academic Press, Inc. ISBN 0-12-084728-0.

Bekey, G. A. Walking. *The Handbook of Brain Theory and Neural Networks*. Edited by Arbib, M. A. The Bradford Book, The MIT Press. ISBN 0-262-01148-4.

Berridge, M. J. and Rapp, P. E. (1979). A comparative survey of the function, mechanisms and control of cellular oscillators. *Journal of Experimental Biology*. 81:217-279.

Bower, J. M. and Beeman, D. (1995). *The Book of Genesis. Exploring Realistic Neural Models with the General Neural Simulation System*. Springler-Verlag. Telos, the Eletronic Library of Science. ISBN 0-387094019-7 or 3-540-94019-7.

Brown, D.A. and Adams, P.R. (1980). Muscarininc suppression of a novel voltage-sensitive K+ current in a vertebrate neurone. *Nature*. 283:673-676.

Brown, T.G. (1914). On the nature of the fundamental activity of the nervous centres; together with an analysis of the conditioning of rhythmic activity in progression, and a theory of the evolution of function in the nervous system. *Journal of Physiology. London*. 48:18-46.

Brodfuehrer, P. D., Debski, E. A. O'Gara, B. A. and Friesen, W. O. (1995). Neuronal control of leech swimming. *Journal of Neurobiology*. 27:403-418.

Brodfuehrer, P. D. and Friesen, W. O. (1986). From stimulation to undulation: a neural pathway for the control of swimming in the leech. Science. 234:1002-1005.

Bulloch, A. G. M. and Syed, N. I. (1992). Reconstruction of neural networks in culture. *Trends in Neuroscience*. 15:422-427.

Bussel, B., Roby-Brami, A., Neris, O. R. and Yakovleff, A. (1996). Evidence for a spinal stepping generator in man. Electrophysiological study. *Acta Neurobiologiae Experimentalis*. 56:465-468.

Calabrese, R. L. (1995a). Oscillation in motor pattern-generating networks. *Current Opinion in Neurobiology*. 5:816-823.

Calabrese, R. L., Nadim, F. and Olsen O. H. (1995b). Heartbeat control in the medicinal leech: a model system for understanding the origin, coordination, and modulation of rhyrhmic motor patterns. *Journal of Neurobiology*. 27:390-402.

Calabrese R. L. and De Schutter, E. (1992). Motor-pattern-generating networks in invertebrates: modeling our way toward understanding. *Transactions in Neurosciences*. 15(11):439-445.

Canavier, C. C., Baxter, D. A., Clark J. W. and Byrne J. H. (1993). Nonlinear dynamics in a model neuron provide a novel mechanism for transient synaptic inputs to produce long-term alterations of post-synaptic activity. *Journal of Neurophysiology*. 69:2252-2257.

Canavier, C. C., Clark J. W. and Byrne J. H. (1991) Simulation of the bursting activity of neuron R15 in Aplysia: role of ionic currents, calcium balance, and modulatory transmitters. *Journal of Neurophysiology*. 66:2107-2124.

Cazalets, J.R. Squally-Houssaini, Y. and Clarac, F. (1994). GABAergic inactivation of the central pattern generators for locomotion in isolated neonatal rat spinal cord. *Journal of Physiology*. 474:173-181.

Cohen, M. A. (1992). The Construction of Arbitrary Stable Dynamics in Nonlinear Neural Networks. *Neural Networks*. 5:83-103.

Cohen, M. A., Ermentrout, G. B., Kiemel, G. B., Kopell, N., Sigvardt, K. A. and Williams, T. L. (1992). Modeling of intersegmental coordination in the lamprey central pattern generator for locomotion. *Trends in Neurosciences*. 15:434-438.

Cohen, A. H. (1988). Evolution of the Vertebrate Central Pattern Generation for Locomotion. *Neural Control of Rhythmic Movements in Vertebrates*. Edited by Cohen, A. H., Rossignol, S., and Grillner, S. Wiley-Interscience Publication, John Wiley & Sons. ISBN 0 471-81968-9.

Cohen, A. H. and Harris-Warrick, R. (1984). Strychnine eliminates alternating motor output during fictive locomotion in the lamprey. *Brain Research*. 293:164-167.

Cohen, A. H. and Wallen, O. (1980). The neuronal correlate of locomotion in fish: "Fictive swimming" induced in an in vitro preparation of the lamprey spinal cord. *Experimental Brain Research*. 41:11-18.

Collins, J. J. (1995). Gait Transitions. *The Handbook of Brain Theory and Neural Networks*. Edited by Arbib, M. A. The Bradford Book, The MIT Press. ISBN 0-262-01148-4.

Connor, J. A. (1985). Neural Pacemakers and Rhythmicity. *Annual Review of Physiology*. 47:17-28.

Coombes, S. Doole, S. H. (1996). Neuronal population dynamics with post inhibitory rebound: A reduction to piecewise linear discontinuities circle maps. *Dynamics and Stability of Systems. Applied Ninlinear Mathematics. Report* 1996.

Cowley, K.C. and Schmidt, B.J. (1995). Effects of inhibitory amino acids antagonists on reciprocal inhibitory interactions during rhythmic motor activity in the vitro neonatal rat spinal cord. *Journal of Neurophysiology*. 74:1109-1117.

Dale, N. (1995). Experimentally derived model for the locomotor pattern generator in the *Xenopus* embrio. *Journal of Physiology*. 489(2):489-510.

Dean, J. and Cruse, H. (1995). Motor Pattern Generation. *The Handbook of Brain Theory and Neural Networks*. Edited by Arbib, M. A. The Bradford Book, The MIT Press. ISBN 0-262-01148-4.

Dekin, M. S. and Getting, P. A. (1987). In vitro characterization of neurons in the ventral part of the nucleus tractus solidarius. II. Ionic mechanisms responsible for repetitive firing activity. *Journal of Neurophysiology*. 58:215-229.

Dekin, M. S. and Getting, P. A. (1984). Firing pattern of neurons in the nucleus tractus solitarious: Modulation by membrane hyperpolarization. *Brain Research*. 324:180-184.

Delcomyn, F. (1980). Neural basis of rhythmic behavior in animals. *Science*. 210:492-498.

Destexhe, A., Mainen, Z. F., Sejnowski, T. J. (1998). Kinetic Models of Synaptic Transmission. *Methods in Neuronal Modeling. From Ions to Networks*. Edited by Koch, C. and Segev, I. The Bradford Book, The MIT Press. ISBN 0-262-11231-0.

Destexhe, A., Contreras, D., Sejnowski, T. J. and Steriade, M. (1994a). A Model of Spindle Rhythmicity in the Isolated Thalamic Reticular Nucleus. *Journal of Neurophysiology*. 72(2):803-818.

Destexhe, A., Mainen, Z. F., Sejnowski, T. J. (1994b). Synthesis of models for excitable membranes, synaptic transmission, and neuromodulation using a common kinetic framework.. *Journal of Computational Neuroscience*. 1:195-230.

Destexhe, A., Babloyantz, A. and Sejnowski, T. J. (1993). Ionic Mechanisms for Intrinsic Slow Oscillations in Thalamic Relay. *Biophysical Journal*. 65:1538-1552.

Dickinson, P. S. (1995). Neuromodulation in Invertebrate Network Systems. *The Handbook of Brain Theory and Neural Networks*. Edited by Arbib, M. A. The Bradford Book, The MIT Press. ISBN 0-262-01148-4.

Dickinson, P. S. and Nagy, F. (1983). Control of a central pattern generation by an identified modulatory interneuron in crustacea. II. Induction and modification of plateau potentials in pyloric neurons. *Journal of Experimental Biology*. 105:59-82.

Douglas, J. R., Noga, B. R., Dai, X. and Jordan, L. M. (1993). The effects of intrathecal administration of excitatory amino acid agonists and antagonists on the initiation of locomotion in the adult cat. *Journal of Neuroscience*. 13:990-1000.

Dowling, J. E. (1992). *Neurons and Networks. An Introduction to Neuroscience*. The Belknap Press of Harvard University Press. ISBN 0-674-60820-8.

Eaton, R.C. and Hackett, J.T. (1984). The role of the Mauthner cell in fast-starts involving escape in teleos fishes. *Natural Mechanisms in Startle Behavior*. Edited by Eaton. R.C. New York: Plenum.

Ekeberg, O., Wallen, P., Lansner, A., Traven, H., Brodin, L. and Grillner, S. (1991). A computer based model for realistic simulations of neural networks. *Biological Cybernetics*. 65:81-90.

Fenaux, F., Cario, M., Palisses, R., and Viala, D. (1991). Effects of a NMDA-receptor antagonist, MK-801, on central locomotor programming in the rabbit. *Experimental Brain Research*. 86:392-401.

Fetz, E. E. and Shupe, L. E. (1995). Dynamic Models of Neurophysiological Systems. *The Handbook of Brain Theory and Neural Networks*. Edited by Arbib, M. A. The Bradford Book, The MIT Press. ISBN 0-262-01148-4.

Fredman, S.M. and Jahan-Parwar, B. (1983). Command neuron for locomotion in Aplysia. *Journal of Neurophysiology*. 49:1092-1117.

Friesen, W. O. (1994). Reciprocal Inhibition: A Mechanism Underlying Oscillatory Animal Movements. *Neuroscience and Biobehavioral Reviews*. 18(4):547-553.

Friesen, W. O. and Stent, G. S. (1978). Neural circuits for generating rhythmic movements. *Annual Review of Biophysics and Bioengineering*. 7:37-61.

Friesen, W. O. and Stent, G. S. (1977). Generation of locomotion rhythm by a neural network of recurrent cyclic inhibition. *Biological Cybernetics*. 28:27-40.

Frost, W and Katz, P. (1996). Single neuron control over a complex motor program. *Journal of Neurobiology*. 93:422-426.

Getting, P. A. (1989). Emerging Principles Governing the Operation of Neural Networks. *Annual Review of Neuroscience*. 12:185-204.

Getting, P. A. (1988). Comparative Analysis of Invertebrate Central Pattern Generator. *Neural Control of Rhythmic Movements in Vertebrates*. Edited by Cohen, A. H., Rossignol, S., and Grillner, S. Wiley-Interscience Publication, John Wiley & Sons. ISBN 0 471-81968-9.

Getting, P. A. (1983). Mechanisms of Pattern Generation Underlying Swimming in Tritonia. III. Intrinsic and Synaptic Mechanisms for Delayed Excitation. *Journal of Neurophysiology*. April 1983. 49(4): 1036-1050.

Getting, P. A. (1983). Mechanisms of Pattern Generation Underlying Swimming in Tritonia. II. Network Reconstruction. *Journal of Neurophysiology*. April 1983. 49(4):1017-1035.

Getting, P. A. (1981). Mechanisms of Pattern Generation Underlying Swimming in Tritonia. I. Network Formed by Monosynaptic Connections. *Journal of Neurophysiology*. 46:65-79.

Glass, L and Young, R. E. (1980). Structure and dynamics of neural network oscillators. *Brain Research*.

Gordon, J. (1991). Spinal Mechanisms of Motor Coordination. *Princliples of Neural Science*. Third Edition. Edited by Kendel, E. R., Schwartz, J. H. and Jessell, T. M. Appleton & Lange. ISBN 0-8385-8034-3.

Graubard, K. J., Raper, J. A. and Hartline, D. K. (1983). Graded synaptic transmission between identified spiking neurons. *Journal of Neurophysiology*. 50:508-521.

Grillner, S., Wallen, P. and Brodin, L. (1991). Neuronal Network Generating Locomotor Behavior in Lamprey. Circuitry, Transmitters, Membrane Properties, and Simulation. *Annual Review of Neuroscience*. 14:169-199.

Grillner, S., Buchanan, J. T., Wallen, P. and Brodin, L. (1988). Neural Control of Locomotion in Lower Vertebrates: From Behavior to Ionic Mechanisms. *Neural Control of Rhythmic Movements in Vertebrates*. Edited by Cohen, A. H., Rossignol,

S., and Grillner, S. Wiley-Interscience Publication, John Wiley & Sons. 1988. ISBN 0 471-81968-9.

Grillner, S. and Wallen, P. (1985). Central pattern generators for locomotion, with special reference to vertebrates. *Annual Review of Neuroscience*. 8:233-261.

Grillner, S. (1981a). Control of locomotion in bipeds, tetrapods, and fish. *The Handbook of Physiology. Vol. II. Motor Control.* (Edited by Brooks, V. B.). Americal Physiological Society.

Grillner, S., McClellan, A., Sigvardt, K., Wallen, P., and Wilen, M. (1981b). Activation of NMDA-receptors elicits "fictive locomotion" in lamprey spinal cord in vitro. *Acta Physiologica Skandinavia*. 113:549:551.

Hargartner, R. D. and Cull, P. (1995). A ternary logic model for recurrent neuromine networks with delay. *Biological Cybernetics*. July 1995. 73(2):177-188,

Hamandez, P., Elbert, K. and Droge, M.H. (1991). Spontaneous and NMDA evoked motor rhythms in the neonatal mouse spinal cord: An in vitro study with comparisons to in situ activity. *Experimental Brain Research*. 85:66-74.

Harris-Warrick, R. M. (1993). Pattern generation. Current Opining in Neurobiology. 3:982-988.

Harris-Warrick, R. M. (1988). Chemical Modulation of Central Pattern Generators. *Neural Control of Rhythmic Movements in Vertebrates*. Edited by Cohen, A. H., Rossignol, S., and Grillner, S. Wiley-Interscience Publication. John Wiley & Sons. 1988. ISBN 0 471-81968-9.

Hartline, D. K. (1979). Integrative neurophysiology of the lobster cardiac ganglion. *American Zoology*. 19:53-65.

Hellgren, J., Grillner, S. and Lansner, A. (1992). Computer simulation of the segmental neural networks generating locomotion in lamprey by using populations of network interneurons. *Biological Cybernetics*. 68:1-13.

Hille, B. (1992). *Ionic Channels of Excitable Membranes*. Sinauer Associates Inc. ISBN 0-878993-323-9.

Hines, M. and Carnevale, N. T. (1997). The NEURON Simulation Environment. *Neural Computation*. 9(6): 1179-1209.

Hines, M. and Carnevale, N. T. (1995). Computer Modeling Methods for Neurons. *The Handbook of Brain Theory and Neural Networks*. Edited by Arbib, M. A. The Bradford Book, The MIT Press. ISBN 0-262-01148-4.

Hodgkin, A. L. and Huxley, A. F. (1952). A Quantitative Description of Membrane Current and its Applications to Conduction and Excitation in Nerve. *Journal of Physiology*. 117:500-544.

Hooper, S. L. (1995). Crustacean Stomatogastric System. *The Handbook of Brain Theory and Neural Networks*. Edited by Arbib, M. A. The Bradford Book, The MIT Press. ISBN 0-262-01148-4.

Hopfield, J. J. and Tank, D. W. (1986). Computing with Neural Circuits: A Model. *Science*. 8 August 1986. 233:625-633.

Hounsgaard, J., Kiehn, O. and Mintz, I. (1988). Response properties of motoneurons in a slice preparation of the turtle spinal cord. *Journal of Physiology*. 398: 575-589.

Huguenard, J. R. and McCormick, D. A. (1994). *Electrophysiology of the Neuron. An Interactive Tutorial.* Oxford University Press. ISBN 0-19-509111-6.

Huguenard, J. R. and McCormick, D. A. (1992). Simulation of the Currents Involved in Rhythmic Oscillation in Thalamic Relay Neurons. *Journal of Neurophysiology*. 68(4): 1373-1383.

Hultborn, H., Petersen, N., Browstone, R. and Nielsen. J. (1993). Evidence of fictive spinal locomotion in the marmoset (*callitrix Jacchus*). *Society Neuroscience Abstracts*. 19:539.

Hume, R. I. and Getting, P. A. (1982a). Motor organization of Tritonia swimming. II. Synaptic drive to flexion neurons from premotor interneurons. *Journal of Neurophysiology*. 47:75-90.

Hume, R. I. and Getting, P. A. (1982b). Motor organization in Tritonia swimming. III. Contribution of intrinsic membrane properties to flexion neuron burst formation. *Journal of Neurophysiology*. 47:91-102.

Jacklet, J. W. (Editor). (1989). *Neuronal and Cellular Oscillators*. Marcel Dekker, Inc. ISBN 0-8247-8030-2.

Jassar, B.S., Pennefather, P.S. and Smith, P.A. (1994). Changes in potassium activity following axonomy of B-cells in bullfrog sympathetic ganglion. Journal of Physiology. 479(3): 353-370.

Johnston, D. and Wu S. M-S. (1995). *Foundations of Cellular Neurophysiology*. A Bradford Book. The MIT Press. ISBN 0-262-10053-3.

Katz, P., S. (1995). Intrinsic and extrinsic neuromodulation of motor circuits. *Current Opinion in Neurobiology*. 5:799-808.

Katz, P. S., Getting, P. A. and Frost, W. N. (1994). Dynamic neuromodulation of synaptic strength intrinsic to a central pattern generator circuit. *Nature*. 367:729-731.

Kandel, E. R., Schwartz, J. H. and Jessell, T. M. (1991). *Princliples of Neural Science*. Third Edition. Appleton & Lange. ISBN 0-8385-8034-3.

Kiehn, O., Hounsgaard, J., and Sillar, K. T. (1997). Basic Building Blocks of Vertebrate Spinal Central Pattern Generators. *Neurons, Networks, and Motor Behavior*. Eds. Stein, P.S.G., Grillner, S., Selverston, A.I., and Stuard, D. G. A Bardford Book. MIT Press.

Koch, C. and Segev, I. (1998). *Methods in Neuronal Modeling. From Ions to Networks*. Second Edition. A Bradford Book. The MIT Press. ISBN 0-262-11231-0.

Kopell, N. (1988). Toward a Theory of Modeling Central Pattern Generators. *Neural Control of Rhythmic Movements in Vertebrates*. Edited by Cohen, A. H., Rossignol, S., and Grillner, S. Wiley-Interscience Publication, John Wiley & Sons. 1988. ISBN 0 471-81968-9.

Krasne, F.B. and Wine, J.J. (1984). The production of crayfish tailflip escape responses. *Natural Mechanisms of Startle Behavior*. Edited by Eaton, R.C. New York:Plenum.

Kristan, W. B. (1980). Generation of Rhythmic Motor Patterns. *Information Processing in the Nervous System*. Pinsker, H. M. and Willis, W. D. (Editors). Raven Press. 1980. ISBN 0-89004-422-8.

Kudo, N., Ozaki, S. and Yamada, T. (1991). Ontogeny of rhythmic activity in the spinal cord of the rat. *Neurobiological Basis for Human Locomotion*. Edited by Shimanura, M., Grillner, S. and Edgerton, V.R. Tokyo. Japan Scientific Society.

Levitan, I. B. and Kaczmarek, L. K. (1991). *The Neuron. Cell and Molecular Biology*. Oxford University Press. ISBN 0-19-507071-2.

MacGregor, R. J. (1987). *Neural and Brain Modeling*. Academic Press, Inc. San Diego. ISBN 0-12-464260-8.

Mainen, Z. F. and Sejnowski, T. J. (1998). Modeling Active Dendritic Processes in Pyramidal Neurons. *Methods in Neuronal Modeling. From Ions to Networks*. Edited by Koch, C. and Segev, I. The Bradford Book, The MIT Press. ISBN 0-262-11231-0.

Mainen, Z. F. and Sejnowski, T. J. (1996). Influence of dendritic structure on firing pattern of model neocortical neurons. *Nature*. 382:363-366.

Marder, E., Kopell, N., and Sigvardt, K. (1997). How Computation Aids in Understanding of Biological Networks. *Neurons, Networks, and Motor Behavior*. Stein, P.S.G., Grillner, S., Selverston, A.I., and Stuart, D.G. (Editors). A Bradford Book. The MIT Press. ISBN: 0-262-19390-6.

Marder, E. and Abbott, L. F. (1995). Theory in motion. *Current Opinion in Neurobiology*. 5:832-840.

Marder, E. (1993). Modulating membrane properties of neurons: Role in information processing. *Exploring Brain Functions: Models in Neuroscience*. Poggio, T. A. and Glaser, D. A. (Editors). Chichester Eng. Wiley.

McClellan, A. D. and Jang, W. (1993). Mechanosensory Inputs to the Central Pattern Generators for Locomotion in the Lamprey Spinal Cord: Resetting, Entrainment, and Computer Modeling. *Journal of Neurophysiology*. December 1993. 70(6):2442-2454.

McCormick, D. A. and Huguenard, J. R. (1992). A Model of the Electrophysiological Properties of Thalamocortical Relay Neurons. *Journal of Neurophysiology*. 68(4): 1384-1400.

McCormick, D.A. and Pape, H.-C. (1990). Properties of a hyperpolarization-activated cation current and its role in rhythmic oscillation in thalamic relay neurons. *Journal of Physiology*. 431: 291-318.

Miller, J. P. and Selverston, A. I. (1982). Mechanisms underlying pattern generation in lobster stomatogastric ganglion as determined by selective inactivation of identified neurons. II. Oscillatory properties of pyloric neurons. *Journal of Neurophysiology*. 48:1378-1391.

Mulloney, B. and Perkel, D. H. (1988). The Roles of Synthetic Models in the Study of Central Pattern Generators. *Neural Control of Rhythmic Movements in Vertebrates*. Edited by Cohen, A. H., Rossignol, S., and Grillner, S. Wiley-Interscience Publication, John Wiley & Sons. 1988. ISBN 0 471-81968-9.

Murray, J. D. (1991). *Mathematical Biology*. Springer-Verlag. ISBN 3-540-57204-X.

Nakamura, Y. and Kakakura, N. (1995). Generation of masticatory rhythm in the brainstem. *Neuroscience Research*. 23:1-19.

Nishii, J., Uno, Y. and Suzuki, R. (1994). Modeling of Movement of the Lamprey: Control of Oscillators. *Neuroscience and Biobehavioral Reviews*. 18(4):585-590.

Noga, B.R., Cowley, K.C., Huang, A., Jordan, L.M. and Schmidt, B.J. (1993). Effects of inhibitory amino acids antagonists on locomotor rhythm in the decerebrate cat. *Society of Neuroscience Abstracts*. 19:540.

Patla, A. E. (1988). Analytic Approach to the Study of Outputs from Central Pattern Generators. *Neural Control of Rhythmic Movements in Vertebrates*. Edited by Cohen, A. H., Rossignol, S., and Grillner, S. Wiley-Interscience Publication, John Wiley & Sons. 1988. ISBN 0 471-81968-9.

Pearson, K. G. (1993). Common principles of motor control in vertebrates and invertebrates. *Annual Review of Neuroscience*. 16:265-297.

Pearson, K. (1976). The control of walking. *Scientific American*. 235(6):72-86.

Perkel, D. H. and Mulloney, B. (1974). Motor pattern production in reciprocally inhibitory neurons exhibiting post-inhibitory rebound. *Science*. 185:181-183.

Pinsker, H. M. and Willis, W. D. (Editors) (1980). *Information Processing in the Nervous System*. Raven Press. 1980. ISBN 0-89004-422-8.

Plonsey, R. and Barr, R. C. (1988). *Bioelectricity: A Quantitative Approach*. Plenum Press. ISBN 0-306-42894-6.

Prentice, S. D., Patla, A. E. and Stacey, D. E. (1994). Modeling the time-keeping function of the central pattern generator for locomotion using artificial sequential neural networks. *Medical & Biological Engineering and Computing*. May 1995. 33(3):317–322.

Rall, W. (1967). Distinguishing theoretical synaptic potentials computed from different soma-dendritic distributions of synaptic inputs. *Journal of Neurophysiology*. 30: 1138-1168.

Rand, R. H., Cohen, A. H. and Holmes, P. J. (1988). Systems of coupled oscillators as models of central pattern generators. *Neural Control of Rhythmic Movements in Vertebrates*. Edited by Cohen, A. H., Rossignol, S., and Grillner, S. Wiley-Interscience Publication, John Wiley & Sons. 1988. ISBN 0 471-81968-9.

Robertson, R. M. (1995). Locust Flight: Components and Mechanisms of the Motor. *The Handbook of Brain Theory and Neural Networks*. Edited by Arbib, M. A. The Bradford Book, The MIT Press. ISBN 0-262-01148-4.

Rowat, P. F. and Selverston, A. I. (1993). Modeling the Gastric Mill Central Pattern Generator of the Lobster with a Relaxation-Oscillator Network. Journal of Neurophysiology. September 1993. 70(3):1030-1053.

Rowat, P. and Selverston, A. I. (1997a). Oscillatory mechanisms in Pairs of Neurons Connected with Fast Inhibitory Synapses. *Journal of Computational Neurosciences*. 4:103-127.

Rowat, P. and Selverston, A. I. (1997b). Synchronous Bursting Can Arise from Mutual Excitation, Even When Individual Cells are not Endogenous Bursters. 4:129-139.

Russell, D. F. and Hartline, D. K. (1978). Bursting neural networks: A reexamination. *Science*. 200: 453-456.

Satterlie, R. A. (1985a). Reciprocal inhibition and post-inhibitory rebound produce reverberation in locomotion pattern generation. *Science*. 229:402-404.

Satterlie, R. A. (1989). Reciprocal Inhibition and Rhythmicity: Swimming in a Pteropod Mollusk. *Neuronal and Cellular Oscillators*. Edited by Jacklet, J. W. Marcel Dekker, Inc. ISDN: 0-8247-8030-2.

Satterlie, R. A..LaBarbara, M. and Spencer, A. N. (1985b). Swimming in the pteropod mollusc Clione limacina. Behavior and morphology. *Journal of Experimental Biology*. 116:189-204.

Segev, I. And Burke, R. (1998). Compartmental Models of Complex Neurons. *Methods in Neuronal Modeling. From Ions to Networks*. Edited by Koch, C. and Segev, I. The Bradford Book, The MIT Press. ISBN 0-262-11231-0.

Selverston, A. I. and Moulins, M. (1985). Oscillatory Neural Networks. *Annual Review of Physiology*. 47:29-48.

Sherman, S. M. and Koch, C. (1998). Thalamus. *The Synaptic Organization of the Brain*. Edited by Shepherd, G. M. Oxford University Press. ISBN 0-19-511824-3.

Shik, M. L. and Orlovski, G. N. (1976). Neurophysiology of locomotor automatism. *Physiology Review*. 56:465-501.

Sillar, K. T. (1991). Spinal pattern generation and sensory gating mechanisms. *Current Opinion in Neurobiology*. 1:583-589.

Smith J.C. and Feldman, J.L. (1987). In vitro brainstem-spinal cord preparations for study of motor systems for mammalian respiration and locomotion. *Journal of Neuroscience Methods*. 21: 321-333.

Soffe, S.R. (1989). Roles of glycinergic inhibition and N-methyl-D-aspartate receptor mediated excitation in the locomotor rhythmicity of one half of the Xenopus embryo central nervous system. *European Journal of Neuroscience*. 1:561-571.

Taga, G. (1995). A model of the neuro-musculo-skeletal system for human locomotion. *Biological Cybernetics*. July 1995. 73(2):113-121.

Tauck, D.L., Frosh, M.P. and Lipton, S.A. (1988). Characterization of GABA- and glycine-induced currents of solitary rodent retinal ganglion cells in culture. *Neuroscience*. 27:193-203.

Tegner, J., Matsushima, T., El Manira, A., and Grillner, S. (1993). The spinal GABA system modulates burst frequency and intersegmental coordination in the lamprey: Differential effects of $GABA_A$ and $GABA_B$ receptors. *Journal of Neurophysiology*. 69:647-657.

Traven H. G. C., Brodin, L., Lansner, A. and Ekeberg, O. (1993). Computer Simulations of NMDA and non_NMDA Receptor-Mediated Synaptic Drive: Sensory and Supraspinal Modulation of Neurons and Small Networks. *Journal of Neurophysiology*. August 1993. 7(2): 695-709.

Yamada, W.M., Koch, C. and Adams, P.R. (1998). Multiple Channels and Calcium Dynamics. *Methods in Neuronal Modeling. From Ions to Networks. Second Edition.* Edited by Koch, C. and Segev, I. A Bradford Book. The MIT Press. ISBN 0-262-11231-0.

Yeoman, M. S., Vehovszky, A., Kemenes, G., Elliott, C. J., and Benjamin, P. R. (1995). Novel interneuron having hybrid modulatory-central pattern generator properties in the feeding system of the snail, *Lymnaea stagnalis*. *Journal of Neurophysiology*. 73:112-124.

Wallen, P. Ekeberg, O. Lasner, A., Brodin, L., Traven, H. and Grillner, S. (1992). A Computer-Based Model for Realistic Simulations of Neural Networks. II. The Segmental Network Generating Locomotion Rhythmicity in the Lamprey. *Journal of Neurophysiology*. 68(8):1939-1950.

Wang, X-J. and Rinzel, J. Oscillatory and Bursting Properties of Neurons. *The Handbook of Brain Theory and Neural Networks*. Edited by Arbib, M. A. The Bradford Book, The MIT Press. ISBN 0-262-01148-4.

Wang, X-J. and Rinzel, J. (1992) Alternating and synchronous rhythms reciprocally inhibitory model neurons. *Neural Computation*. 4:84-97.

Weeks, J.C. and Kristian, W.B. (1978). Initiation, maintenance and modulation of swimming in medicinal leech by activity of a single neuron. *Journal of Experimental Biology*. 77:71-88.

Wiersma, C.A. and Ikeda, K. (1964). Interneurons commending swimmeret movements in the crayfish *Procambarus clarki*. *Comprehensive Biochemistry and Physiology*. 12:509-525.

Williams, T. L. and Sigvardt, K. A. (1995). Spinal Cord of Lamprey: Generation of Locomotion Patterns. *The Handbook of Brain Theory and Neural Networks*. Edited by Arbib, M. A. The Bradford Book, The MIT Press. ISBN 0-262-01148-4.

Wilson, D. M. and Waldron, I. M. (1968). Models for the generation of the motor output pattern in flying locusts. *Proceedings of IEEE*. 56:1058-1064.

Windhorst, U. (1988). How Brain-like is the Spinal Cord? Interacting Cell Assemblies in the Nervous System. Studies of Brain Function, Vol. 15. Springer-Verlag, 1988, ISBN 3-540-18405-8.

Wyman, R. J. (1977). Models for the generation of the breathing rhythm. *Annual Review of Physiology*. 39:417-488.

Ziv, I., Baxter, D. A. and Byrne, J. H. (1994). Simulator for Neural Networks and Action Potentials: Description and Application. *Journal of Neurophysiology*. January 1994. 71(1): 294-308.

Zuker, R. S., Kennedy, D. and Selverston, A. I. (1971). Neuronal circuit mediating escape responses in crayfish. *Science*. 173:645-649.